NSF Grant ATM-9015485
National Science Foundation

An Observational and Modelling Study of the June 26-27, 1985 Pre-Storm Mesoscale Convective System

by
Kevin W. Manning

Department of Atmospheric Science
Colorado State University
Fort Collins, Colorado

Steven A. Rutledge, P.I.

Colorado State University

Department of Atmospheric Science

Paper No. 501

AN OBSERVATIONAL AND MODELLING STUDY OF THE JUNE 26-27, 1985 PRE-STORM MESOSCALE CONVECTIVE SYSTEM

by

Kevin W. Manning

Department of Atmospheric Science

Colorado State University

Fort Collins, CO 80523

Research Supported by

National Science Foundation

under Grant ATM-9015485

May 29, 1992

Atmospheric Science Paper No. 501

ABSTRACT OF THESIS

AN OBSERVATIONAL AND MODELLING STUDY OF THE 26 - 27 JUNE PRE-STORM MESOSCALE CONVECTIVE SYSTEM

A case study of the 26 - 27 June 1985 PRE-STORM Mesoscale Convective System (MCS) is presented. The system was analyzed using the dense surface and upper-air observations available from the PRE-STORM field program. The system formed along and ahead of a cold front, beneath the right entrance region of a jet streak, in a weak-to-moderate shear and weak-to-moderate CAPE environment. The system was not well organized in a leading-line/trailing-stratiform pattern, but exhibited a number of short, weak, and short-lived bands of convection. These bands were followed by a poorly-defined stratiform region. However, in vertical cross sections of Doppler radar data taken normal to the front, the familiar layered flow structure including a rear inflow jet was evident, along with some of the reflectivity characteristics of a typical stratiform region.

Analysis of the surface data revealed that the convective system produced a thunderstorm outflow boundary which soon became the dominant feature in the surface observations. As this outflow boundary developed, the front itself weakened considerably, almost to the point of dissipating in some areas.

Nested-grid simulations were performed with the Regional Atmospheric Modelling System (RAMS). A coarse-grid simulation, with a grid spacing of 75 km and convective parameterization, simulated the synoptic scale evolution well, and developed convection along the front in the PRE-STORM area. A fine-grid simulation, with a grid spacing of 25 km, simulated several characteristics of the observed convective system, including a prefrontal boundary and the general prefrontal nature of the convection. A fine-grid

simulation with the convective parameterization deactivated, along with unsuccessful two-dimensional simulations, suggest that large-scale lifting from circulations associated with a jet streak may have been important in sustaining the convective system.

Kevin Webster Manning
Department of Atmospheric Science
Colorado State University
Fort Collins, CO 80523
Spring 1992

ACKNOWLEDGEMENTS

I would like to thank my advisors, Drs. Steven A. Rutledge and William R. Cotton, for their assistance in this research. In addition, I would like to thank Dr. Jerome M. Schmidt for his assistance with the Colorado State University - Regional Atmospheric Modelling System.

This research was funded by the National Science Foundation under grants ATM-9015485 and ATM-8814913. The simulations and analyses of model output were done on the National Center for Atmospheric Research's Cray Y-MP computer. NCAR is supported in part by the National Science Foundation.

TABLE OF CONTENTS

LIST OF FIGURES

Chapter One

INTRODUCTION

In recent years, many meteorologists have put much time and effort into researching the broad category of weather phenomena known as Mesoscale Convective Systems. A Mesoscale Convective System (MCS) is a precipitation system with a horizontal length scale of 10 - 500 km and which includes some significant convection during part of its lifetime (NCAR, 1984). This broad definition includes such systems as Mesoscale Convective Complexes (MCCs; Maddox, 1980), midlatitude prefrontal squall lines, large convective rainbands, groups of individual thunderstorms, tropical squall lines, and tropical cloud clusters. Lifetimes of MCSs are usually about 6 - 12 h, but on some occasions MCSs may last as long as several days (*e.g.* Wetzel *et al.*, 1983).

The study of MCSs is one of the major research focuses in mesoscale meteorology today. There are several reasons for this intense interest. First, MCSs produce much precipitation in the United States as well as other parts of the world. Fritsch *et al.* (1986) determined that for the year 1982 (which they judged to be a normal year in terms of precipitation for the United States), 30 - 70% of the warm season precipitation and up to 50% of the annual precipitation in many parts of the central plains of the United States was associated with the passage of MCSs. They concluded that MCSs are "the dominant warm-season rain producing weather systems over much of the Midwest." Thus, a better understanding of MCSs may lead to a better understanding of precipitation budgets and other hydrological concerns on the central plains. Second, MCSs frequently produce severe weather in the form of floods, damaging winds, damaging hail, tornadoes, and lightning (Houze *et al.*, 1990). Better forecasting of MCSs may thus lead to an improved

ability to forecast severe weather, which in turn would save many lives and prevent much property damage. Third, MCSs pose an interesting problem in weather analysis and forecasting. Although the systems as a whole usually have horizontal scales of hundreds of kilometers and time scales of 6 - 12 h or more, the convective cells and other important substructures of MCSs may have horizontal scales of less than 10 km and time scales of less than an hour. Synoptic-scale observational networks and operational forecast models cannot resolve features on these scales.

Because of the inability of the standard observational networks to adequately resolve MCSs, the meteorological community has in recent years launched a number of field programs designed specifically to collect data on the mesoscale. Examples of these programs, conducted in various parts of the world, include GATE (GARP Atlantic Tropical Experiment), PRE-STORM (Preliminary Regional Experiment - Stormscale Operational Meteorological Program), and TAMEX (Taiwan Area Mesoscale Experiment). These field programs, which used Doppler radars, instrumented aircraft, surface and upper-air mesoscale networks, and other mesoscale observational instruments and techniques, have given meteorologists an unprecedented view of MCSs, which in turn has sparked a large number of observational and modelling studies of Mesoscale Convective Systems. Some of the results of these studies are discussed in the following section.

1.1 Previous studies

In this section is a discussion of some of the observational studies of MCSs and related topics, followed by a discussion of some modelling studies.

1.1.1 Observational studies

Mesoscale convective systems come in a variety of forms, from the "random convection" of the 3 - 4 June, 1985 PRE-STORM case (McAnelly and Cotton, 1990) to the highly organized, linear structure of the 10 - 11 June 1985 PRE-STORM case (Rutledge *et al.*, 1988; Johnson and Hamilton, 1988). The strongest and most severe squall lines often form along or ahead of a cold front, in the warm sector of a strong cyclonic storm system (Cotton and Anthes, 1989). These lines usually propagate faster than and ahead of the front and are thus called *prefrontal squall lines* (*e.g.* Newton, 1950; Srivastava *et al.*, 1986). *Ordinary squall lines*, on the other hand, tend to be weaker and more common than the prefrontal squall lines, and may or may not be associated with weak frontal systems (Cotton and Anthes, 1989). *Frontal squall lines* form along a front, but need the sustained frontal lifting to maintain convection.

Bluestein and Jain (1985), in a study of severe Oklahoma squall lines, categorized convective lines by the pattern of development seen on low-level scans of radar reflectivity. Their four categories are: *broken line*, in which discrete cells form nearly simultaneously in a line and then develop into a more solid line; *back building*, in which a new cell develops upstream from an old cell; *broken-areal*, in which a disorganized area of cells develops into a solid line; and finally, *embedded-areal*, in which a convective line appears embedded in a larger area of stratiform precipitation.

Houze *et al.* (1990) similarly classified Oklahoma MCSs based on radar reflectivity patterns. Although they did not restrict themselves to linearly-organized storms as did Bluestein and Jain (1985), they did use a linearly-organized archetype to categorize systems based on their resemblance to a leading line of convection followed by a trailing region of stratiform precipitation. They classified storm organization and symmetry along two spectra: from *strongly classifiable* to *weakly classifiable* and from *symmetric* through *intermediate* to *asymmetric*. They used the leading-line/trailing-stratiform pattern as their

model because it seemed to be a commonly occurring pattern. A variety of both observational and modelling studies of squall lines has led to a detailed conceptual model of this type of system.

Houze *et al.* (1989) present a detailed description of this conceptual model, which reflects the work of many meteorologists over the past five decades. Fig. 1.1 shows the main features of this model as seen in a middle tropospheric level horizontal slice and in a vertical cross section taken perpendicular to the convective line. The figure shows the idealized system in its mature stage. The primary features of the conceptual model to note in the horizontal slice are:

• The *leading line*, which consists of a line of mature convective cells, as seen, for example, in Smull and Houze (1987a). These cells have high reflectivities and produce intense convective rainfall.

• The *trailing stratiform region*, a large, relatively homogeneous area of moderate reflectivity and steady, moderate rainfall. The stratiform rainfall most likely results from a combination of two processes: 1) *in-situ* production of condensate and precipitation by the mesoscale updraft in the stratiform region (Gamache and Houze, 1983; Rutledge, 1986); and 2) the rearward advection by the ascending front-to-rear flow of particles produced in the convective line. These particles then grow by deposition as they fall through the stratiform cloud to become the snow and rain of the stratiform precipitation (Rutledge and Houze, 1987). This process is called the "seeder-feeder" process (Rutledge and Hobbs, 1983).

• The *transition zone*, a local minimum of reflectivity located between the leading line and the trailing stratiform region (*e.g.* Smull and Houze, 1987a).

In the vertical cross section, the primary features to note are:

• The *progression of cells* from the new cell, followed by the mature cell, followed by the old cell (*e.g.* Smull and Houze, 1987a). The new cell forms at middle levels due to convective updrafts above the gust front. Just behind the new cell is the older, mature cell,

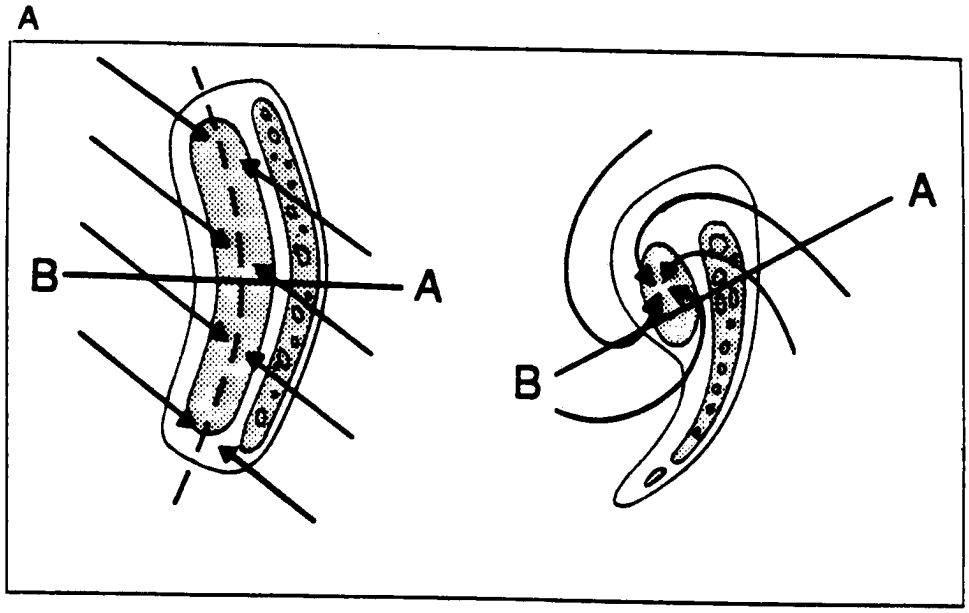

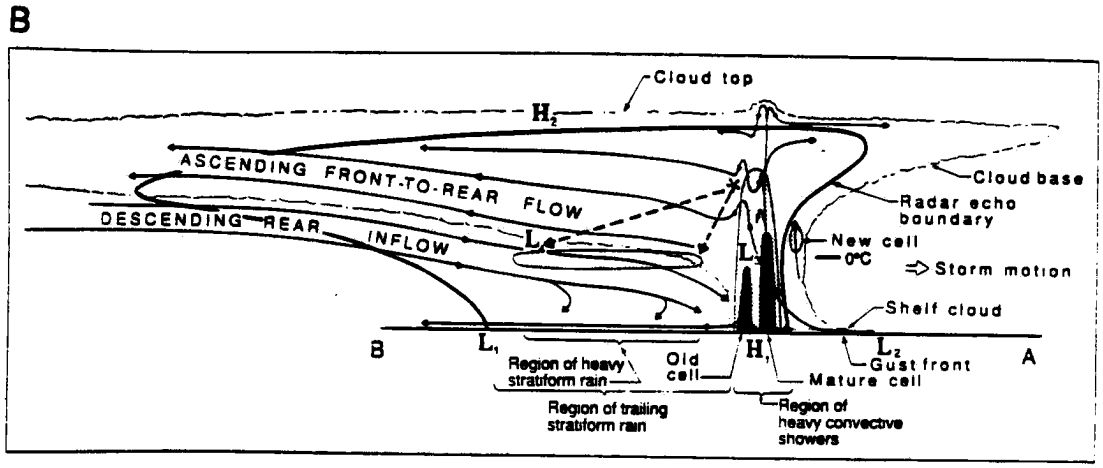

Fig. 1.1: A conceptual model of a midlatitude squall line as seen by radar a) in horizontal cross sections of two differently organized systems taken at middle tropospheric levels; and b) in a vertical cross section taken along line AB. Stippling represents areas of higher reflectivity. Arrows represent storm-relative flow. From Houze *et al.* (1989).

characterized by intense convective updrafts and downdrafts and producing heavy convective showers. Behind the mature cell is the older, dissipating cell. As time passes, the front-to-rear flow advects the older, dissipating cells over the rear inflow. This progression of cells accounts for a discrete component of the system's propagation (Srivastava *et al.*, 1986).

• The *bright band*, a narrow layer of enhanced reflectivity found near the melting level in the stratiform region (*e.g.* Rutledge *et al.*, 1988). The bright band occurs as an effect of changes in the size, dielectric constant, and fallspeed of the hydrometeors as they change from ice particles to raindrops (Battan, 1973).

• *Low-level inflow* into convective cells, beginning in the boundary layer ahead of the gust front (*e.g.* Smull and Houze, 1985).

• The *mesoscale updraft and downdraft* in the stratiform precipitation region, which have been inferred from upper-air mesonetwork analyses (*e.g.* Ogura and Liou, 1980) and Doppler radar measurements of divergence (*e.g.* Srivastava *et al.*, 1986), and measured more directly with vertically-pointing Doppler radar (*e.g.* Rutledge *et al.*, 1988). These studies and others suggest that the upper portion of the stratiform region is characterized by mean ascending motion (mesoscale updraft), while the lower part is characterized by mean descending motion (mesoscale downdraft). The mesoscale updraft may be a result of the latent heating due to freezing and vapor deposition. The mesoscale downdraft may be a result of the cooling due to the evaporation, sublimation, and melting of precipitation in the dry rear inflow.

• *Upper level divergence*, as the convective updrafts reach the tropopause and spread out (*e.g.* Smull and Houze, 1985).

• *The gust front*, created as the convective downdrafts, caused by precipitation loading and evaporational cooling, spread out upon reaching the ground (Fujita, 1955; Wakimoto, 1982).

• The *front-to-rear flow*, which ascends from middle tropospheric levels just behind the convective line to the upper troposphere in the rear portion of the system. This front to rear flow has been documented with both sounding analyses (*e.g.* Ogura and Liou, 1980) and Doppler radar (*e.g.* Smull and Houze, 1987a). The front-to-rear flow helps to generate and maintain the stratiform region by advecting hydrometeors from the convective line (see discussion of the trailing stratiform region, above). The front-to-rear flow also advects water vapor, which can later condense in the mesoscale updraft; as well as heat, which helps to maintain the ascent and therefore the stratiform cloud.

• The *rear inflow*, which descends from middle levels near the rear of the stratiform region to the convective line, and sometimes extends through the convective line to merge with the gust front (Newton, 1966; Zipser, 1969; Ogura and Liou, 1980; Leary and Rappaport, 1987; Smull and Houze, 1987; Rutledge *et al.*, 1988). Newton (1950) was among the first to identify the rear inflow in midlatitude squall lines. In composite sounding analyses of a prefrontal squall line case, he identified what he described as a "tongue of minimum θ_w descending from above the polar front and forward to the squall front." Other researchers, using soundings, wind profilers, and Doppler radars, have also observed the rear inflow. Smull and Houze (1987b) suggest that two separate mechanisms may work together to produce the rear inflow. They argue that near the convective line, the inflow is related to a perturbation pressure minimum just behind the convective updrafts. Toward the rear of the system, they suggest that the inflow is due to the development of a middle level mesolow (see discussion of pressure features, below).

• *Pressure features*, which include at the surface (Johnson and Hamilton, 1988; Fujita, 1955): a wake low near the back edge of the stratiform region (L_1), a mesohigh beneath the convective line (H_1), and a mesolow ahead of the convective line (L_2); and at upper levels: mesolows just behind the convective line (L_3) and in the stratiform region (L_4), and a mesohigh in the upper troposphere above the system (H_2).

This model is idealized and no system should be expected to exhibit all of the above features. However, there have been a number of detailed studies of cases (both midlatitude and tropical MCSs) which have fairly closely fit the leading-line/trailing-stratiform model (*e.g.* Ogura and Liou, 1980; Gamache and Houze, 1982; Heymsfield and Schotz, 1985; Smull and Houze, 1985, 1987a; Srivastava *et al.*, 1986; Rutledge *et al.*, 1988; many others). There have been fewer studies of less organized cases (*e.g.* Schmidt and Cotton, 1988; McAnelly and Cotton, 1990).

Jet-streak circulations may have been an important feature in the case described in this study, as discussed in the following chapters. The circulations which are associated with upper-level jet streaks have been described by Uccellini and Johnson (1979), Keyser and Shapiro (1986), and others, and are depicted in Fig. 1.2.

1.1.2 Modelling studies

There have been a number of modelling studies of MCSs, making use of a variety of models in both two-dimensional and three-dimensional simulations. Some of these modelling studies as well as several theoretical studies of convection are discussed below.

In a series of simulations with a three-dimensional cloud model, Weisman and Klemp (1982) studied the effects of varying amounts of shear and buoyancy on storm evolution and organization. They found that with no shear, the simulated storms developed in much the same manner as short-lived single-cell thunderstorms. When unidirectional shear was included, the simulated storms experienced periodic redevelopment along the outflow boundaries, similar to multicellular storms. With even more unidirectional shear, the storms developed in a manner similar to observed right-moving and left-moving supercells. With more realistic directional shear, Weisman and Klemp suggest that right-moving supercells would develop in the simulations.

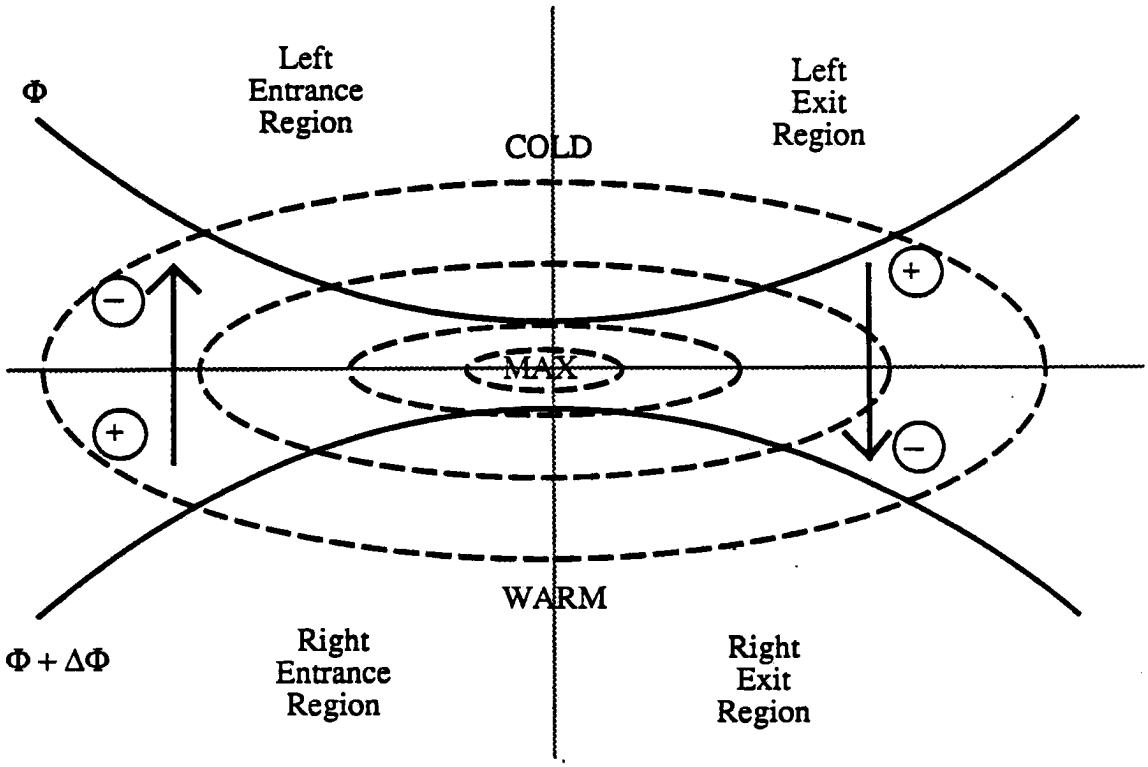

Fig. 1.2: Schematic illustration on a constant pressure surface of jet-streak circulations for a straight upper-tropospheric jet maximum. Heavy solid lines are geopotential height contours. Dashed lines are isotachs. Arrows show the sense of cross-front ageostrophic wind component at level of maximum wind. Plus and minus signs show the sense of midtropospheric vertical velocity (w). Adapted from Keyser and Shapiro (1986).

convective line by the front-to-rear flow aloft, but did note some *in-situ* condensate production.

Chen and Cotton (1988), using two-dimensional simulations, performed a number of sensitivity experiments which suggested some important effects which radiation, melting, and ice-phase heating have on convective and stratiform circulations in MCSs. Their model, which included parameterizations of microphysical processes of water vapor, cloud water, rain water, ice crystals, graupel, and aggregates, had a horizontal resolution of 1.5 km. They successfully simulated an MCS in two dimensions, including such features as a stratiform region and mesoscale updrafts and downdrafts. Their sensitivity experiments suggested that the primary conditions affecting the rear inflow were radiative heating in the upper troposphere and convective-scale downdrafts in the convective line. The mesoscale downdraft was found to be of only secondary importance.

Schmidt and Cotton (1990), in a two-dimensional modelling study with 2 km horizontal resolution, examined squall-line longevity and propagation from the point of view of gravity waves. In a case with strong shear throughout most of the troposphere, they found that the presence of strong tropospheric shear caused the lower-level and upper-level gravity waves excited by the convection to align vertically and thereby create a deep layer of upward motion, thus enabling sustained, deep convection. They noted (as did Lafore and Moncrieff, 1989) that the effects of the convection could easily alter the ambient shear conditions. They further noted that in their simulations, the upper-level gravity waves seemed to be instrumental in developing a rear inflow in the system. The waves displaced isentropes and blocked the flow aloft, which channelled the flow to lower levels as a rear-to-front jet.

Moving up in scale, Orlanski and Ross (1984) simulated the meso-α-scale (about 250 - 2500 km) characteristics of an observed frontal squall line with 61.5 km horizontal resolution, but with explicit prediction of cloud water and the associated heating, not a convective parameterization scheme. Despite the coarse resolution, their simulations

produced a squall line similar in many respects to the analysis (by Ogura and Liou, 1980) of a similar system.

The modelling studies by Zhang *et al.* (1989) are particularly interesting because they suggest that the important forcing mechanisms for MCS initiation may at times be contained in the synoptic-scale observations. Zhang *et al.* proposed that the meso-β-scale (about 25 to 250 km) structure and evolution of MCSs may be successfully simulated from conventional meteorological observations (*e.g.* the standard NMC upper-air and surface observations). They tested this hypothesis with a version of the Pennsylvania State University/NCAR three-dimensional mesoscale hydrostatic model with nested grids, a modified Fritsch-Chappell (1980) convective parameterization for the fine grid, the Anthes-Kuo parameterization (Anthes and Keyser, 1979) for the coarse grid, and an explicit convective scheme. The coarse grid (75 km resolution) included most of the continental United States, and the fine grid (25 km resolution) covered a 1500 x 1200 km area including the PRE-STORM region. They initialized the model with the 1200 UTC conditions on 10 June 1985 from the NMC operational analyses. They then compared their results to the detailed analyses (by Augustine and Zipser, 1987; Johnson and Hamilton, 1988; Rutledge *et al.*, 1988; and others) of the 10 - 11 June PRE-STORM squall line. They reported that on the 25 km scale the model simulated "quite well" the observed MCS, including convective bands, surface pressure features, a rear-inflow jet, and the leading-line/trailing-stratiform structure with a transition zone.

Cram *et al.* (1991a,b) similarly performed a nested-grid simulation of a prefrontal squall line, part of which was analyzed by Srivastava *et al.* (1986). They performed simulations with various combinations of microphysics and cumulus parameterization. The coarse grid for these simulations was 80 km, while the fine grid was 20 km. The observed squall line was initiated by convergence along the front and propagated faster than the front. The squall line propagated discretely: new convection, thought to be initiated by gravity waves, formed up to 100 km ahead of the front and gust front. The results of the

Thorpe *et al.* (1982), using a two-dimensional cloud model, performed a theoretical study of cumulonimbus evolution in a variety of shear environments. They concluded that steady convection results if middle to upper levels have weak shear, and low levels have a large shear to prevent the gust front from propagating away from the convection. With these conditions, a single, long-lived cell developed in the simulations. With stronger shear at upper levels, the results were unsteady, multicellular convection or convection which decayed completely. These conclusions follow those of Takeda (1971), who suggested that a low-level jet is necessary for long-lived convection, as well as those of Hane (1973).

In a study using cloud simulations in two and three dimensions, Rotunno *et al.* (1988) reached a similar conclusion that low-level shear was needed to sustain deep, long-lived convection. They based their argument on the vorticity balance between the cold pool and the ambient low-level shear which would be necessary to produce vertical updrafts. The simulated systems experienced periodic redevelopment at the outflow boundary, and late in their evolution tended to develop flow structures similar to observed midlatitude squall lines. This development occurred even though the trailing stratiform region was not simulated; thus Rotunno *et al.* suggest that these flow structures may be a response to the convection.

Lafore and Moncrieff (1989), using a series of two-dimensional simulations, also demonstrated that low-level shear is an important factor in the structure and evolution of convection, but argued that the dynamics of the system as a whole determine the structure and organization of the systems. Their simulations, on a larger scale than those of Rotunno *et al.*, included the stratiform region. In these simulations, a descending rear-inflow jet developed, which they attributed to the direct effect of the convection. They cautioned that the squall line itself can modify the ambient shear, making the assumptions of their own and similar modelling studies questionable.

In a modelling study of tropical convection, Dudhia and Moncrieff (1987) imposed varying amounts of large-scale ascent on a simulation of convective bands. With no large-scale forced ascent, persistent convective activity could not be maintained. It was only when large-scale ascent of 1 - 2 mb s^{-1} was imposed (which Dudhia and Moncrieff described as typical of the ITCZ region) that the development of new convective cells was maintained.

A number of researchers, using a variety of models in both two and three dimensions, have attempted to simulate various aspects of observed midlatitude squall lines. For example, Dudhia and Moncrieff (1989) simulated a PRE-STORM case with a three-dimensional model with 2 km horizontal resolution. Their model included parameterized cloud and rain processes, but no ice-phase processes. Although the observed squall line did not develop supercells, the modelled system developed three supercellular storms on the right flank of the squall line. This development may have been due to the horizontally homogeneous initialization used in their study. However, other features were well represented, such as the general storm alignment, the multicellular structure of the convection, and a deep mesovortex.

Fovell and Ogura (1988) simulated a squall line in two dimensions with a 1 km horizontal grid spacing. They used a two-dimensional anelastic cloud model with parameterized microphysics, which included cloud water, rain, ice crystals, snow, and hail. They initialized the model with a prestorm sounding from the 22 May 1976 Oklahoma squall line (analyzed by Ogura and Liou, 1980; and Smull and Houze; 1985, 1987b). The simulated system developed into a long-lasting multicellular storm with characteristics similar to the conceptual model of a squall line in a vertical cross section (Fig. 1.1b) and to the observations of the 22 May 1976 case. They were able to simulate many of the features of observed squall lines, such as the leading-line/trailing-stratiform structure, a rear inflow, and the multicellular progression of cells. They concluded that the trailing stratiform region in the simulations was primarily a result of hydrometeors transported rearward from the

simulations compared reasonably well with the observations in terms of the locations of the front and squall line, and locations and magnitudes of the mesohigh and presquall mesolow. These simulations also provided evidence that the squall line did propagate as a gravity wave. However, the simulations produced no gust front, and no wake low or rear inflow jet, as the model did not adequately resolve the stratiform precipitation.

1.2 The present study

The 26 - 27 June 1985 PRE-STORM case was a weak squall line with weakly organized bands of moderate convection. It occurred in an environment of weak-to-moderate shear and weak-to-moderate CAPE (convective available potential energy). It formed along and ahead of a shallow cold front, in the right-entrance region of an upper-tropospheric jet streak, but did not propagate well ahead of the front, in contrast to the cases of Newton (1950) and Cram *et al.* (1991a,b). The system produced much rain; local accumulations were greater than 75 mm. In the classification scheme of Houze *et al.* (1990), this case would probably fall into the *moderately classifiable* category, with *intermediate symmetry*.

The objectives of this study were to explore an MCS which was not as strong or well organized as (but probably more typical than) many of those previously examined, and to explore the interactions between the convection and the front. To achieve those objectives, observations from the PRE-STORM field program and numerical simulations with the Regional Atmospheric Modelling System (RAMS), developed at Colorado State University, were used. In Chapter 2, the PRE-STORM experiment, the data collected during the field program, and the data analysis procedures used in this case study are described. In Chapter 3, the observations from the PRE-STORM data set of the 26 - 27 June 1985 MCS are presented. In Chapter 4, the model used and the simulations

performed are described. Finally, Chapter 5 contains a summary of the study as well as some suggestions for future research.

Chapter Two

THE PRE-STORM FIELD PROGRAM

In May and June of 1985, the data-collection phase of the PRE-STORM program was conducted. The PRE-STORM program was designed specifically to collect data on the mesoscale, in order to examine in greater detail than previously possible the mesoscale structure of MCSs. Investigators collected data in the Kansas and Oklahoma region using a variety of techniques and instruments, including surface and upper-air mesonetworks, Doppler radars, Doppler wind profilers, instrumented aircraft, and a lightning location network. The main objectives of the field program were to "1) achieve a reliable and coordinated observing system for investigating MCSs, and 2) collect the data necessary to begin preliminary investigations of the origin, development, dissipation, and structure of MCSs" (Cunning, 1986).

The PRE-STORM program was developed as a preliminary experiment to the STORM-Central program. Therefore, two further objectives of PRE-STORM related to refining the instrumentation and goals of STORM-Central. These objectives were: 3) "to test and evaluate these new sensing systems [*e.g.* wind profilers, airborne Doppler radars] in order to help optimize their implementation" in the STORM program, and 4) to collect data that could be used "to sharpen and focus the scientific objectives of the STORM-Central program" (Cunning, 1986).

2.1. The PRE-STORM observational data set

The various sources of data collected in PRE-STORM are described in this section, with emphasis on the data used in the present case study. For further details of the PRE-STORM program, see Cunning (1986).

2.1.1. Surface mesonetwork

The surface network consisted of eighty-four automated observation stations. Forty-two NCAR/FOF PAM-II (Portable Automated Mesonetwork) stations, located mainly in Kansas, and forty-two NSSL SAM (Surface Automated Mesonetwork) stations, located primarily in Oklahoma, were deployed on a grid about 350 x 450 km, with approximately 50 km between stations (Fig. 2.1). The stations reported 5 min averages of temperature, pressure, wet-bulb temperature, and wind, as well as maximum wind gusts and accumulated rainfall.

In this study, the surface data were plotted in two ways: 1) as surface maps, which were then subjectively analyzed; and 2) as time series.

2.1.2. Upper-air mesonetwork

The upper-air network consisted of 14 National Weather Service sounding sites in the PRE-STORM area and twelve supplemental rawinsonde sites in Kansas and Oklahoma (Fig. 2.1). These 26 sites took soundings at either 1.5 or 3 h intervals during operational periods. The average spacing in Kansas and Oklahoma between sounding sites was approximately 150 km. For this study, the sounding data were plotted on skew-T log-P diagrams.

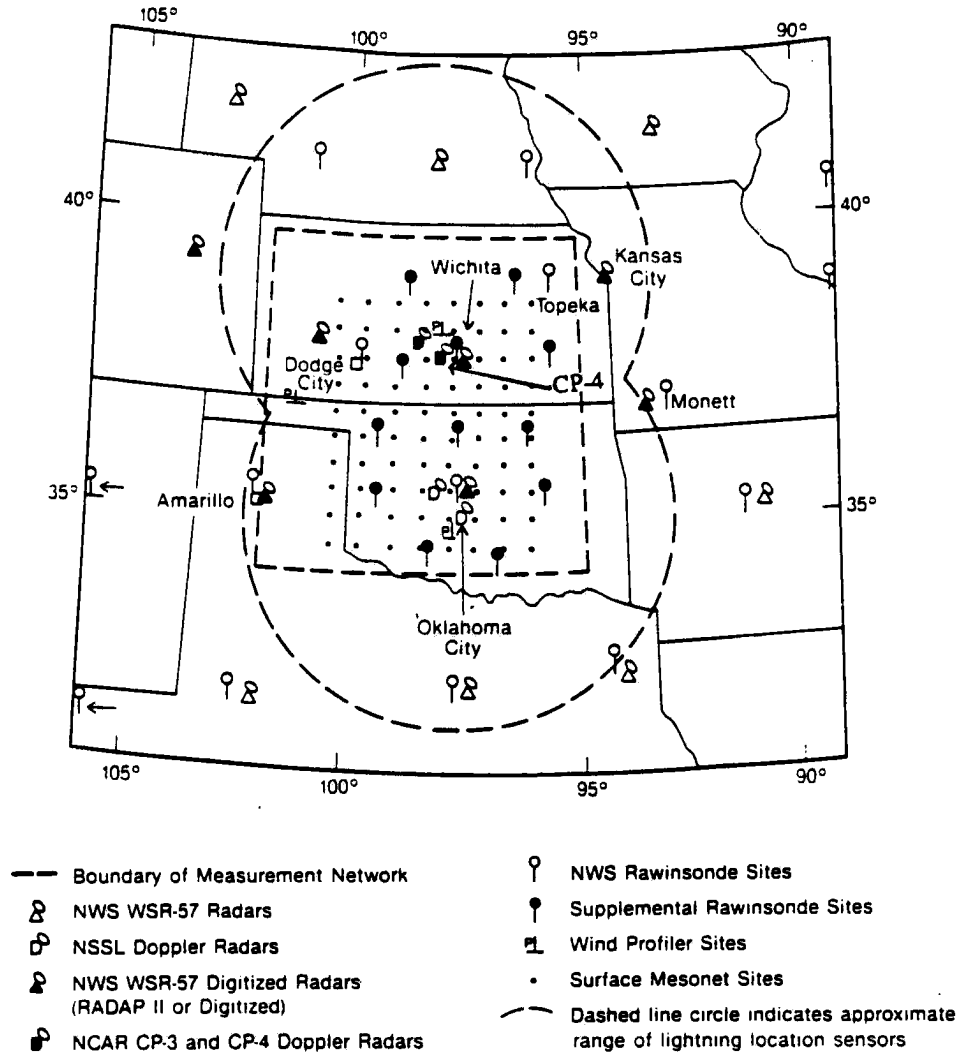

Fig. 2.1: The OK PRE-STORM observational mesonetwork. From Cunning (1986).

2.1.3. Radars

Six WSR-57 radar sites in the PRE-STORM area (Fig. 2.1) recorded digitized volume-scan radar data. The present case study used the WSR-57 data from Wichita, Kansas and Oklahoma City, Oklahoma, which were plotted as composites of low-level scans of radar reflectivity.

Four ground-based Doppler radars operated in two dual-Doppler pairs (Fig. 2.1). One pair, consisting of the NSSL 10 cm Doppler radars, was located in Norman and Cimarron, Oklahoma. The other pair, NCAR's CP-3 and CP-4 5 cm Doppler radars, were located at Nickerson, Kansas and Cheney Reservoir near Wichita. This case study used the data from the NCAR CP-4 radar at Cheney Reservoir.

The CP-4 radar operated with an azimuthal resolution of 0.8°, a gate spacing of 260 m, and a maximum range of 135 km. The Nyquist velocity was 15.24 m s^{-1}. Hence, the radar velocity data were often aliased, and so the data from CP-4 were unfolded using the RDSS (Research Data Support System) software package (Oye and Carbone, 1981). The data were then transferred to a Cartesian grid with 1 km resolution in the horizontal and 0.5 km resolution in the vertical using the SPRINT (Sorted Position Radar Interpolation) software package (Mohr *et al.*, 1979), and plotted in horizontal slices. The Cartesian grids were then rotated using the CEDRIC (Cartesian Editing and Display of Radar data under Interactive Control) software package (Mohr and Miller, 1983) to produce Cartesian grids oriented orthogonal to the front. The data were then plotted in vertical cross sections oriented normal to the front.

2.1.4. Other data

In addition to the above data sources, several other types of data were collected and archived. These data types included data from instrumented aircraft, airborne Doppler

radars, wind-profiling systems, and a lightning-detection system. These data were not used in the present case study.

Chapter Three

OBSERVATIONS OF THE 26 - 27 JUNE 1985 PRE-STORM MCS

In this chapter, selected observations of the 26 - 27 June 1985 PRE-STORM MCS are presented. In the first section, observations of the system from the synoptic scale are discussed, using satellite images, surface analyses, and upper-air analyses from the National Meteorological Center (NMC). In the second section, the MCS is discussed as seen with the more detailed observations available from the PRE-STORM data set: data from the WSR-57 radars, the surface mesonetwork, the upper-air mesonetwork, and the CP-4 Doppler radar. In the third and final section of this chapter, the observations are summarized.

3.1 Synoptic overview

The dominant feature in the NMC surface analyses (Fig. 3.1) was a surface cold front. This front, which at 0600 (all times are UTC unless otherwise specified) extended from an area of weak low pressure north of Minnesota southeastward into Arizona, first entered the PRE-STORM network during the morning hours of 26 June, shortly before 1200 (not shown). Although it was almost stationary in the northern part of the United States, in the area of Kansas and Oklahoma the front had been moving at a rate between about 2.5 and 6 m s^{-1}. By 1800 (not shown), there were reports of thunderstorms ahead of the front in Kansas. By 2100, the NMC surface analyses included a squall line (indicated by the double-dotted line in Fig. 3.1b) situated approximately 100 - 150 km ahead of the front. The frontal speed at this time was about 4 - 8 m s^{-1}. By 0600, the

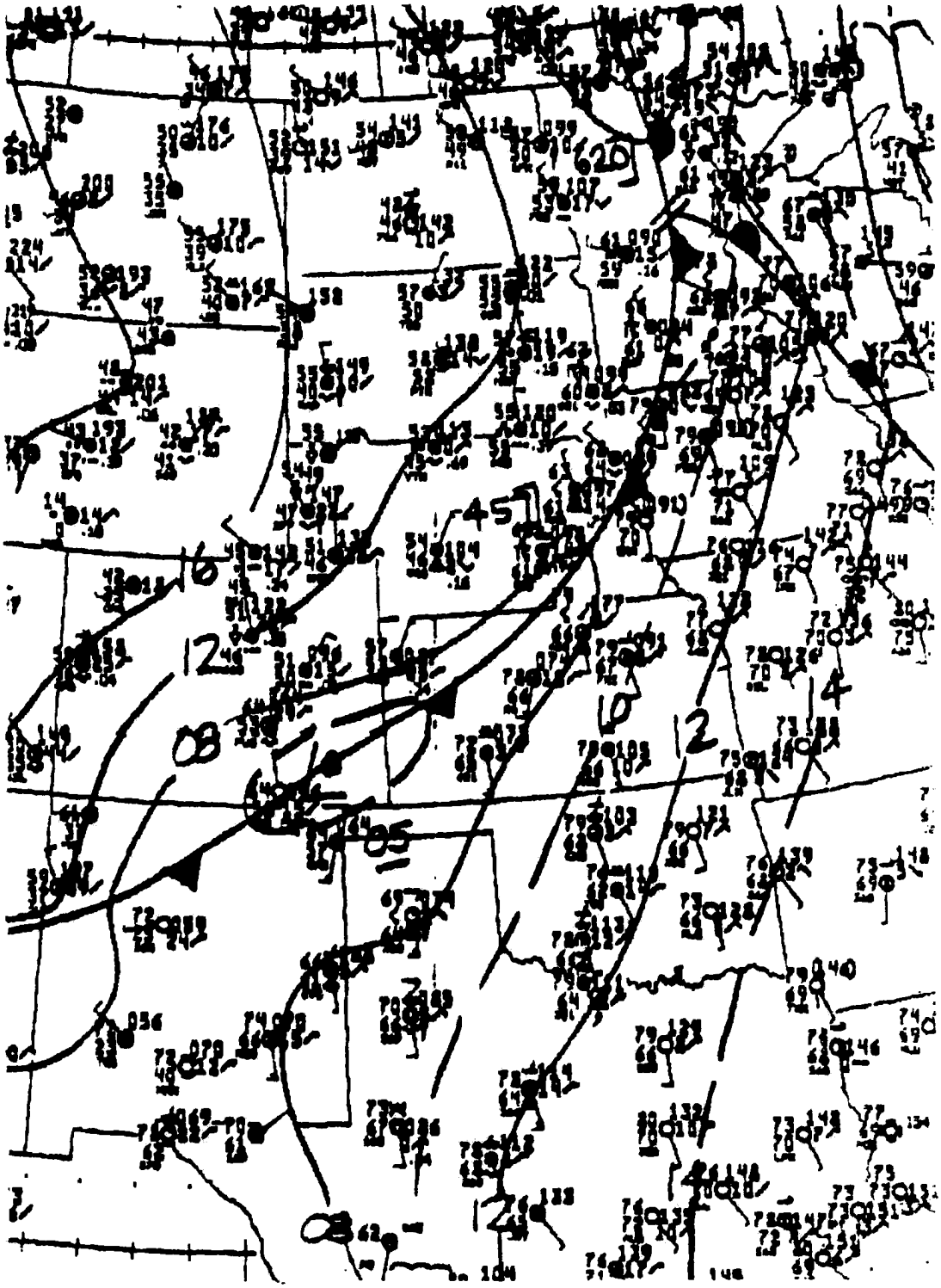

a) 0600 UTC, 26 June

Fig. 3.1: NMC surface analyses from 26 - 27 June, 1985, at a) 0600 UTC, 26 June; b) 2100 UTC, 26 June; c) 0600 UTC, 27 June; and d) 0900 UTC, 27 June.

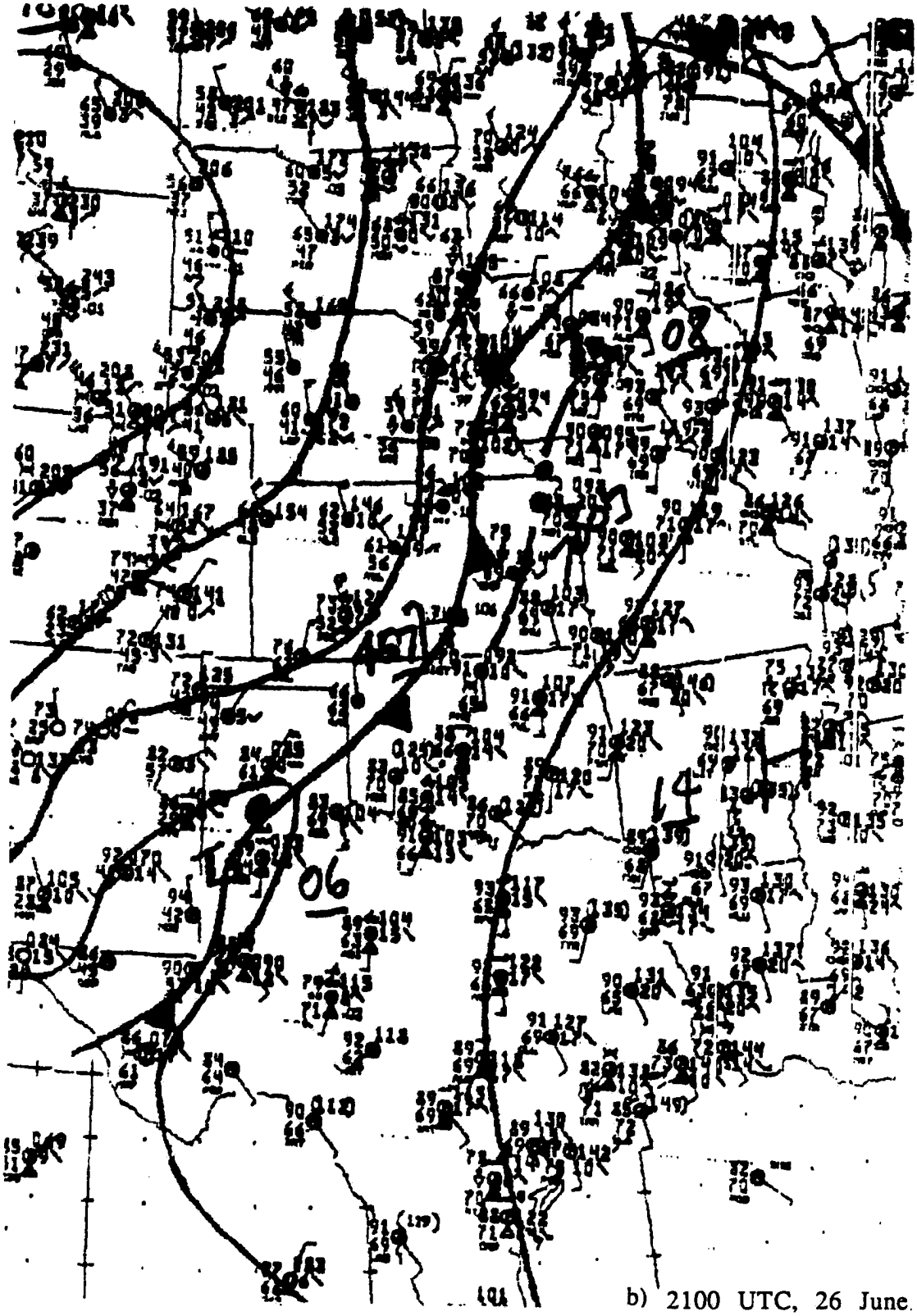

Fig. 3.1: Continued.

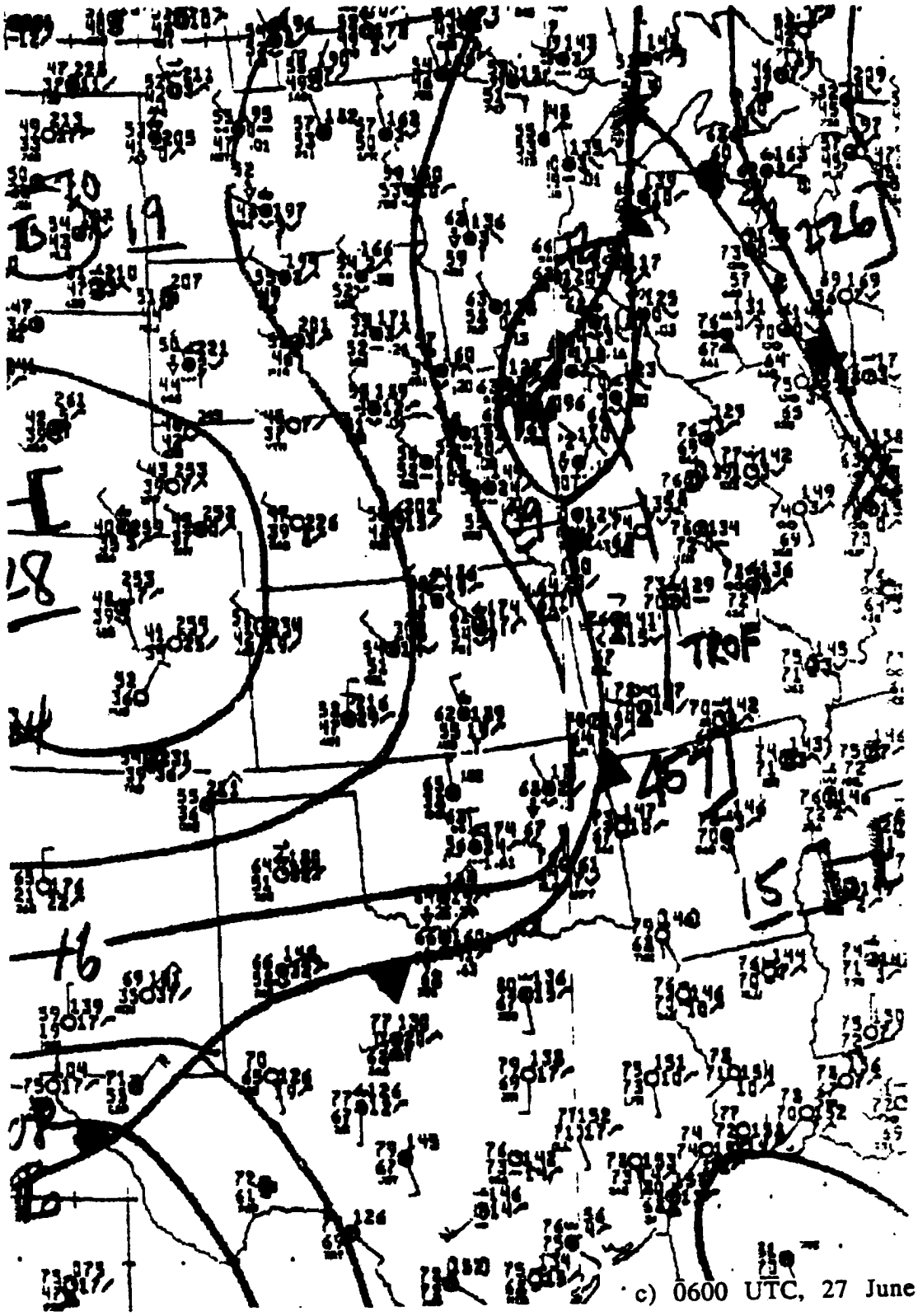

Fig. 3.1: Continued.

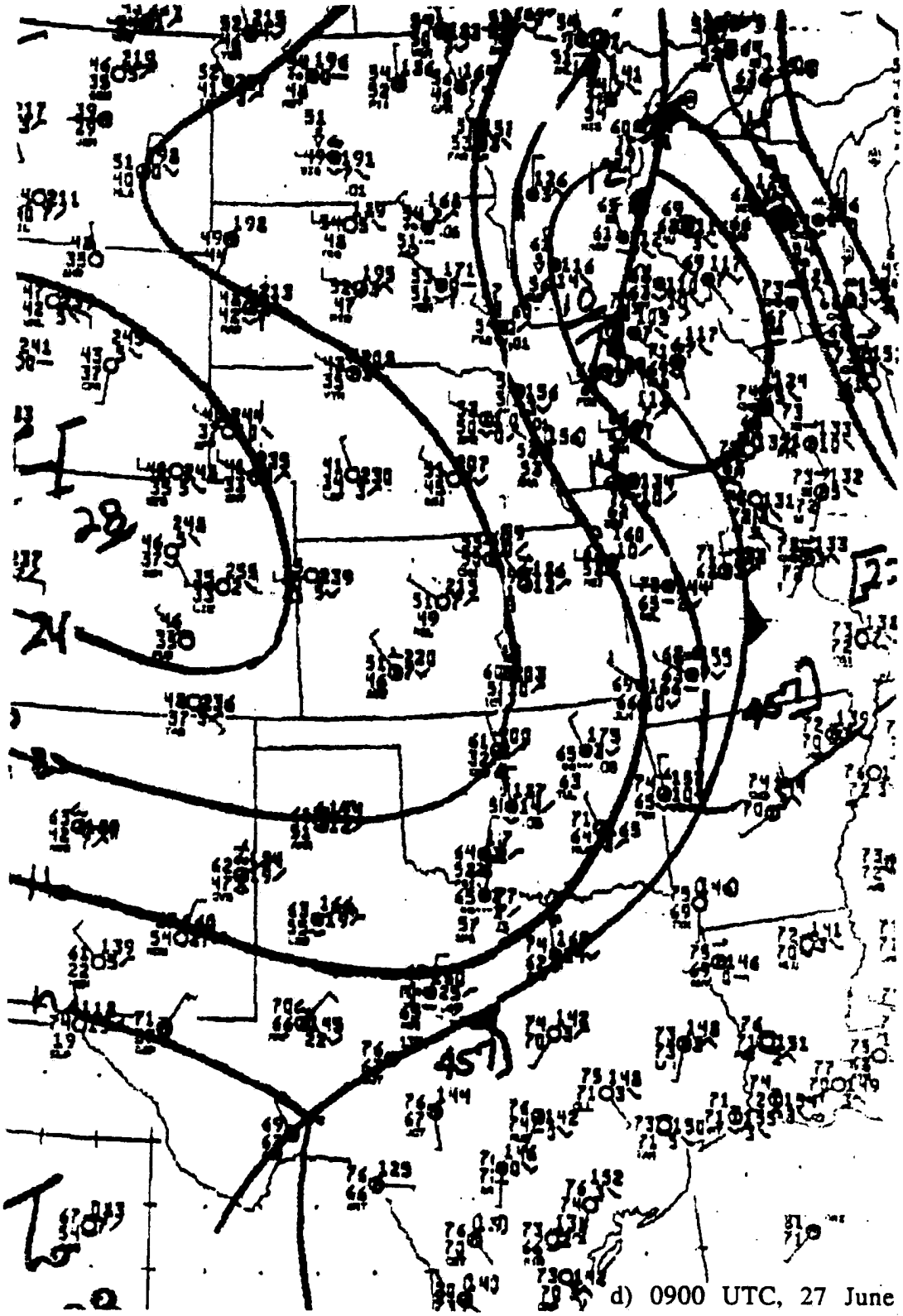

d) 0900 UTC, 27 June

Fig. 3.1: Continued.

squall line was downgraded in the analyses to a pressure trough, still approximately 150 km ahead of the front. By 0900, the trough line was analyzed as a cold front. Thus, from the synoptic-scale analyses, the front seems to have propagated discretely. However, these analyses must be viewed with caution, as the NMC has been known to analyze some unusual frontal behavior (Mass, 1991).

The NMC upper-air analyses at 500 and 200 mb (Fig. 3.2) featured a high-amplitude blocking pattern off the east coast of the United States and a deep trough over the western part of the country. The 500 mb charts for 1200 on the 26th and 0000 on the 27th indicate that the cutoff low over New England and the ridge over the eastern half of the United States were nearly stationary during the period, while the trough in the west had moved slowly eastward. The surface pressure trough and front were in the usual position with respect to the upper-level trough: on the eastern side of the 500 mb trough.

Another significant upper-air feature was a jet streak to the west of the PRE-STORM area. In the 200 mb chart from 1200, 26 June (Fig. 3.5c), the jet streak on the western side of the trough was located about 200 km behind the surface front and had wind speeds up to about 45 m s^{-1} (90 kts). The 200 mb chart from 12 h later (Fig. 3.5d) shows that the right entrance region of the streak was moving over the PRE-STORM area. The location of the jet streak was favorable to enhance convection in the PRE-STORM area because of upper-level upward motion induced by jet streak circulations.

Satellite images (Fig. 3.3) provide an overview of the system. Early in the day (1200), a 200 - 300 km wide band of clouds was located, for the most part, ahead of the cold front. Earlier satellite images (not shown) suggest that these clouds were the remains of previous convection. Embedded in these clouds, near the Kansas-Oklahoma border at 1200, was a small area of convection, as revealed by a spot of colder cloud tops about 5000 km^2 in area. The upper-level cloud shield continued to grow until about 2200, when it extended from northern Wisconsin into Oklahoma. After about 0000, the cloud shield

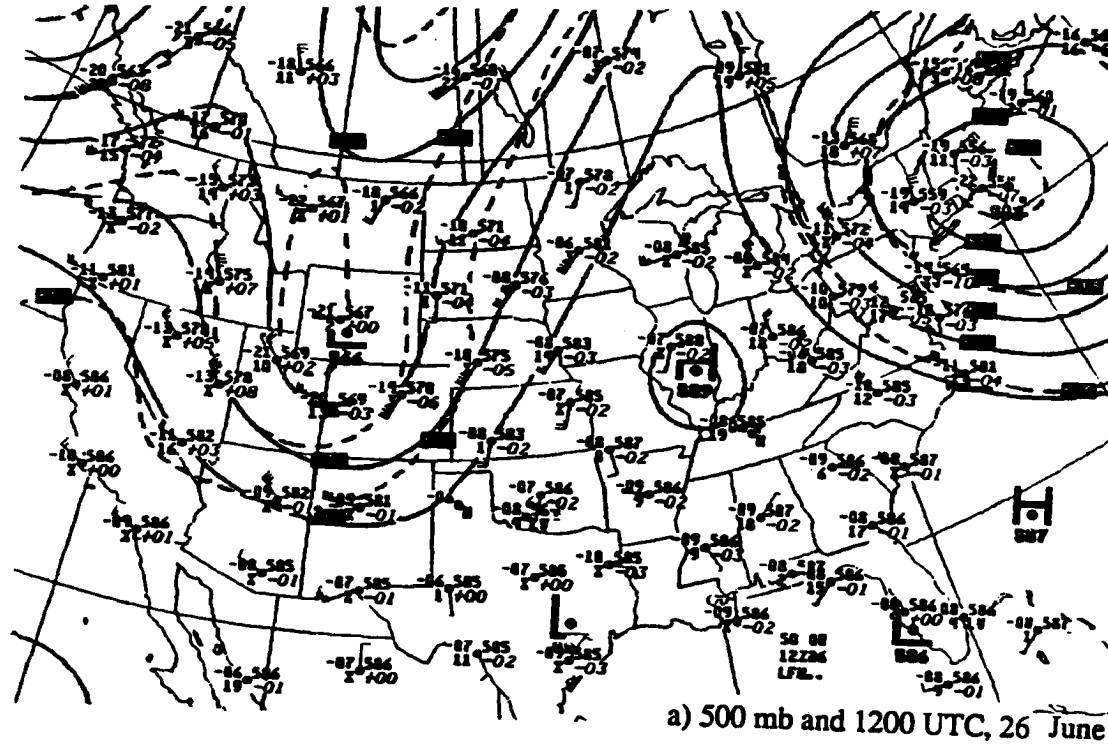

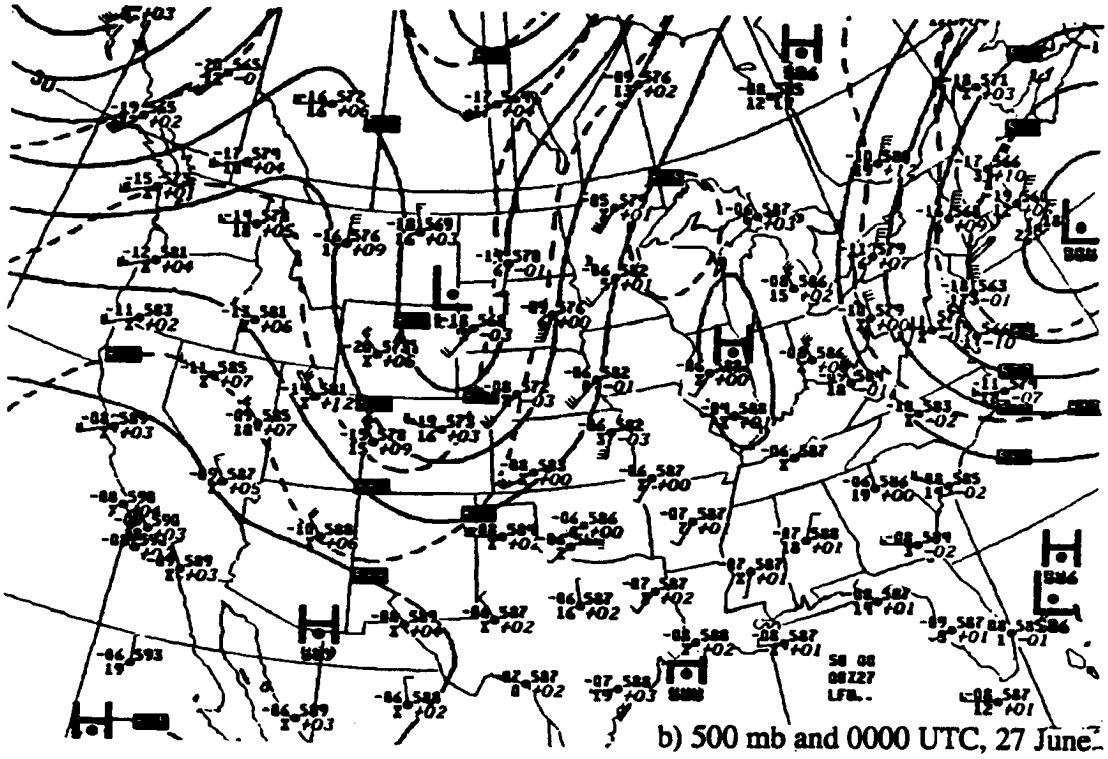

Fig. 3.2: NMC upper air analyses for 26 - 27 June, 1985, at a) 500 mb and 1200 UTC, 26 June; b) 500 mb and 0000 UTC, 27 June; c) 200 mb 1200 UTC, 26 June; and d) 200 mb and 0000 UTC, 27 June.

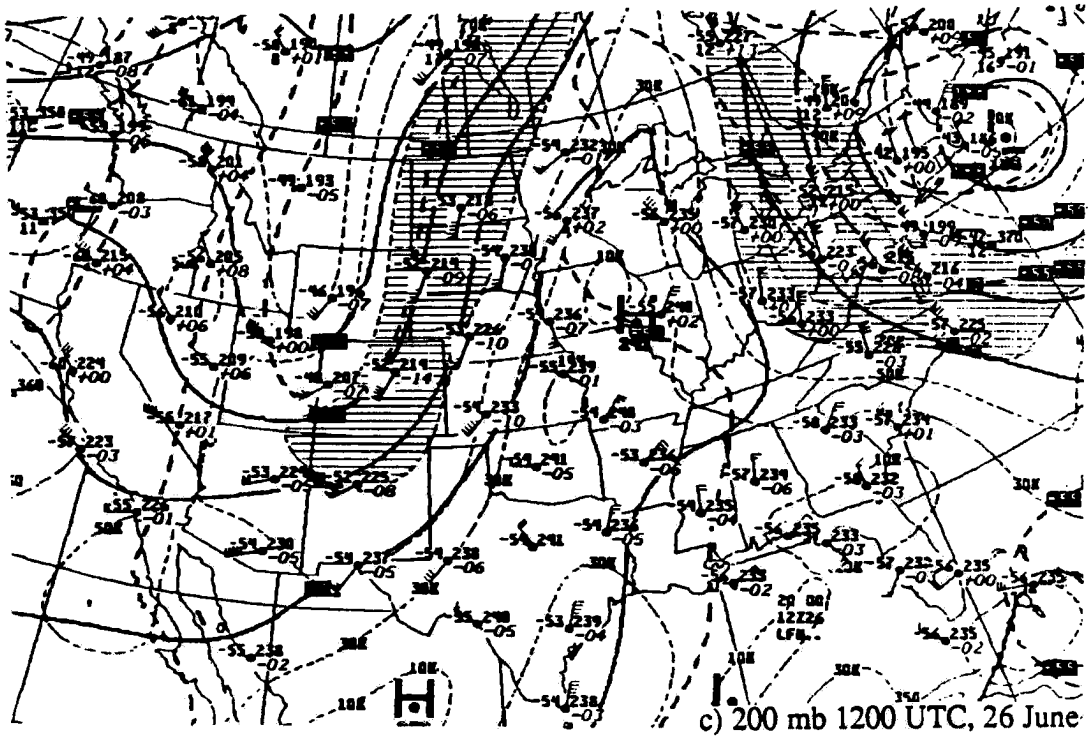

c) 200 mb 1200 UTC, 26 June

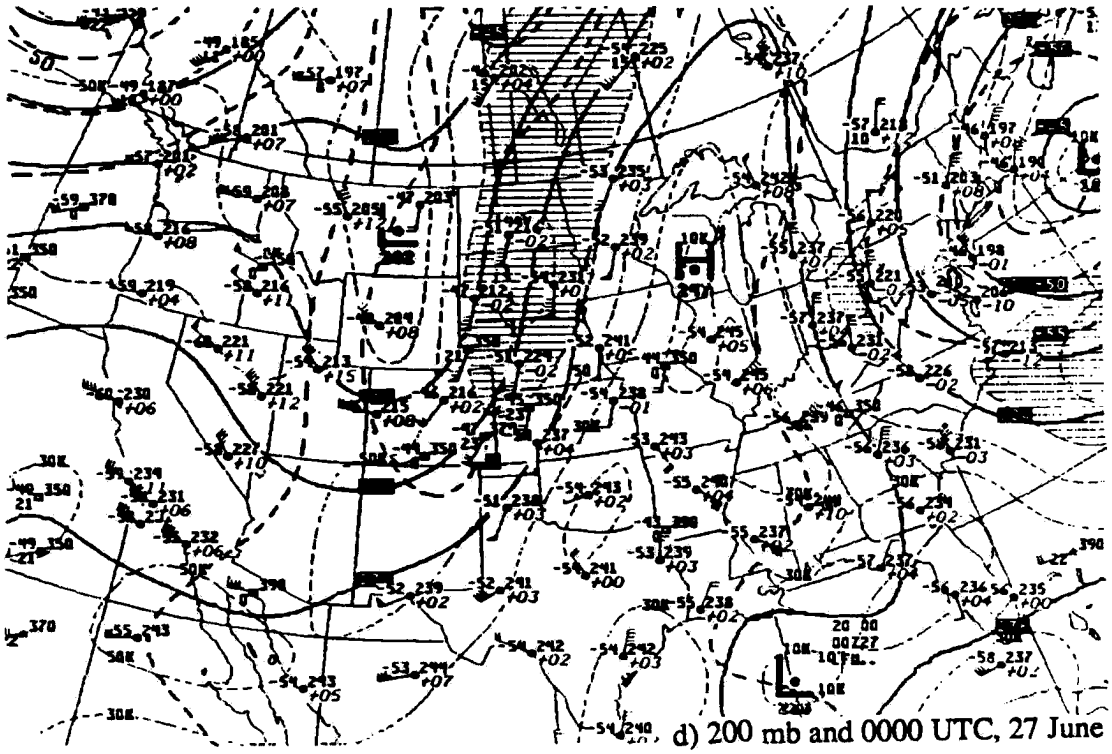

d) 200 mb and 0000 UTC, 27 June

Fig. 3.2: Continued.

a) 1200 UTC, 26 June

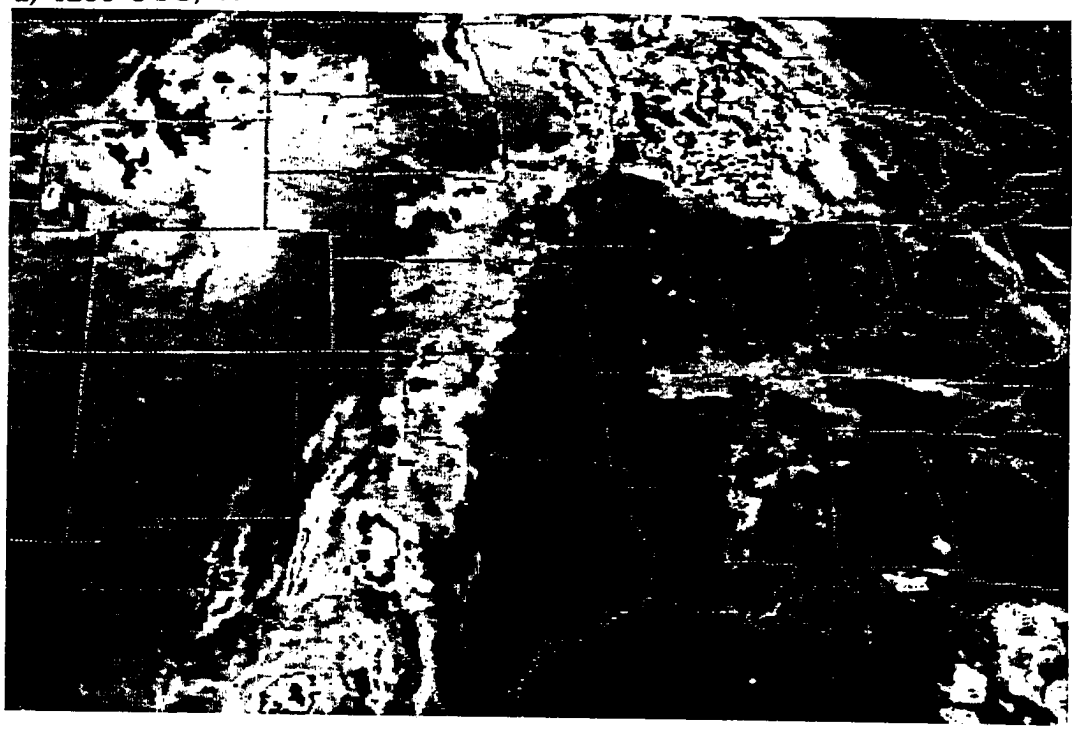

b) 2200 UTC, 26 June

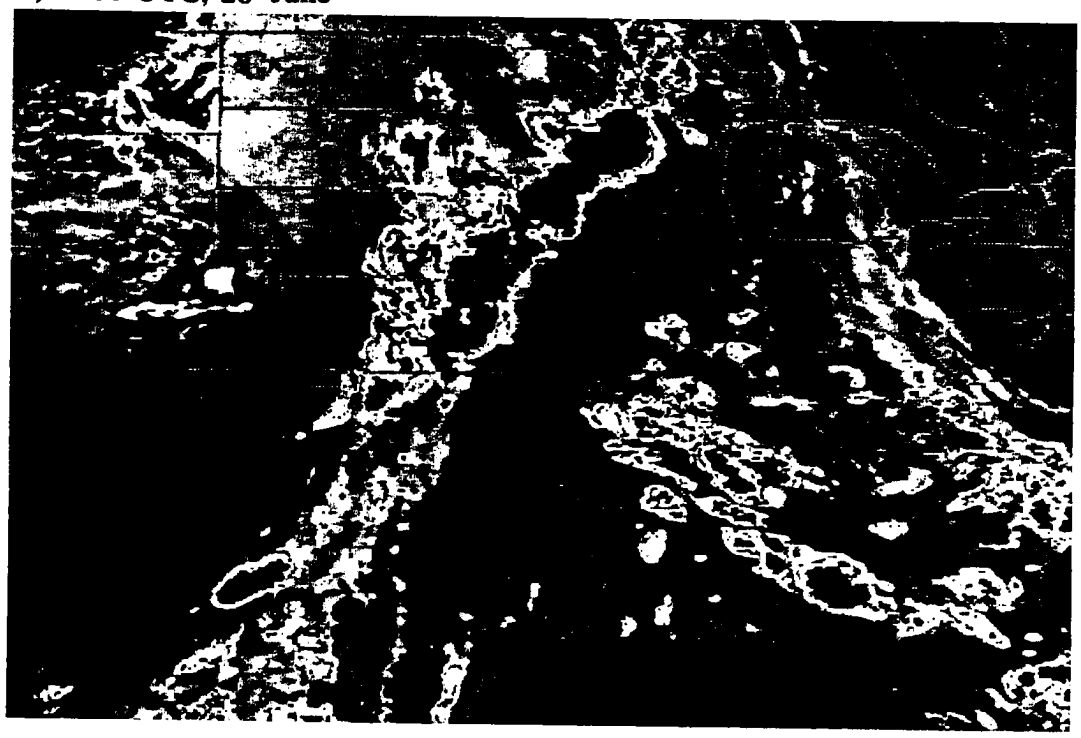

Fig. 3.3: IR-enhanced satellite images from a) 1200 UTC, 26 June; b) 2200 UTC, 26 June; c) 0000 UTC, 27 June; and d) 0800 UTC, 27 June.

c) 0000 UTC, 27 June

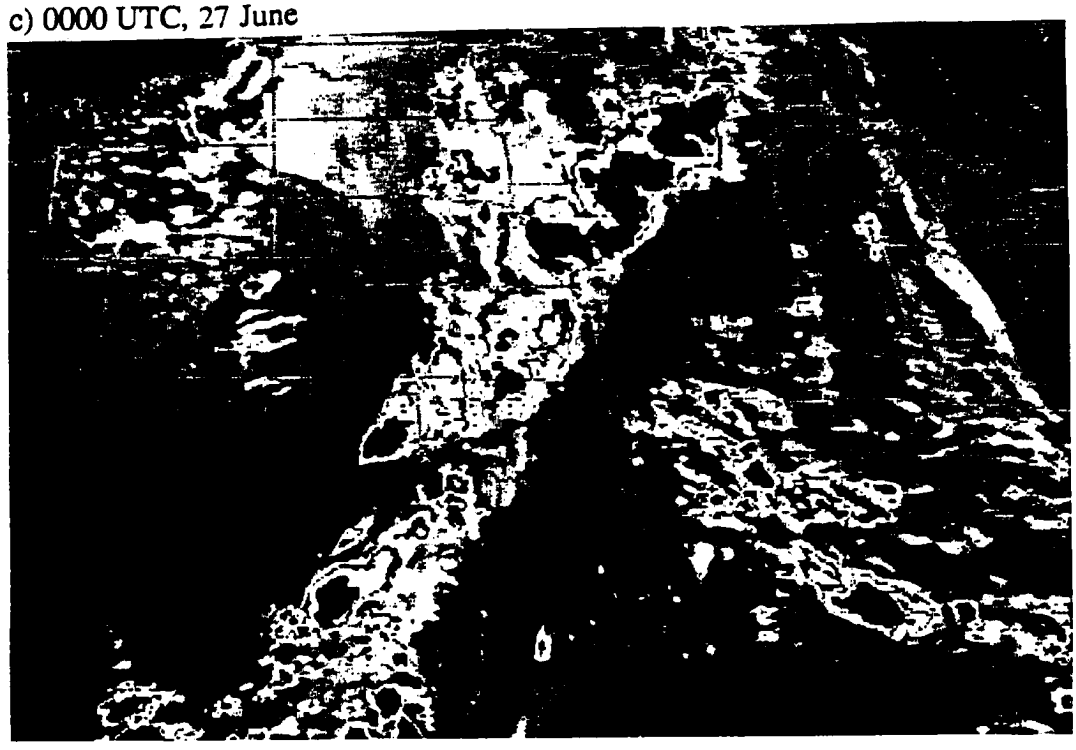

d) 0800 UTC, 27 June

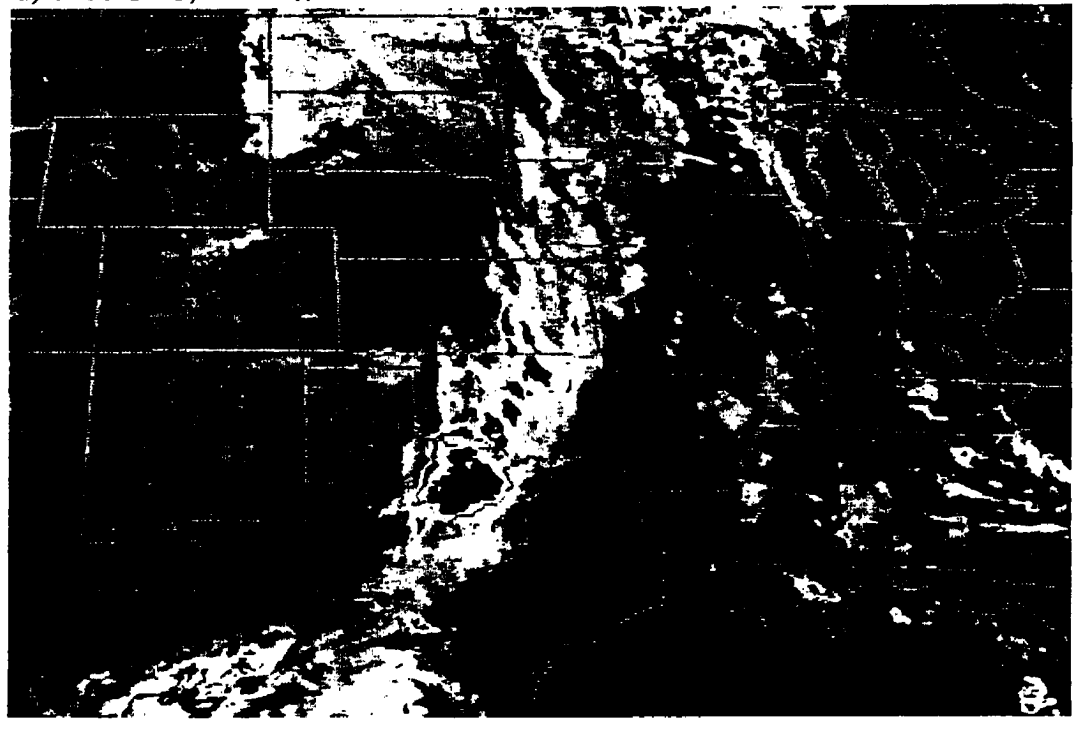

Fig. 3.3: Continued.

began to decrease in areal coverage and break up. By 0800, the only deep convection in the area was located in north central Texas.

The synoptic-scale observations did to some extent resolve the MCS, but their usefulness in analyzing MCSs is limited because significant structures and motions of these systems occur on much smaller scales not effectively resolved by the synoptic-scale data. The PRE-STORM program, designed in part to address this limitation, collected data on scales smaller than the synoptic-scale observations. It is these smaller-scale observations that are used in the next section to further explore this particular MCS.

3.2 PRE-STORM observations

In this section, selected portions of the PRE-STORM data set are used to discuss the 26 - 27 June 1985 MCS. In the following four subsections are discussed the prestorm environment (before about 1400) and three stages in the system's evolution, similar to those discussed by Ogura and Liou (1980). Although the evolution of the MCS in this study does not quite fit the breakdown in Ogura and Liou, their categories are still useful and approximately applicable. The three stages in this system's evolution (with their approximate times) were: the *intensifying stage* (about 1400 - 2000), when convection began to be widespread; the *mature stage* (about 2000 - 0000), during which the convection reached its peak intensity; and the *dissipating stage* (after about 0000), during which the convection weakened and the system eventually dissipated.

3.2.1 The prestorm environment and early convection

The front first entered the surface mesonetwork shortly before 1200 (0700 CDT), 26 June. During the morning hours (*e.g.* 1200 and 1400, Fig. 3.4) the location of the front was clearly marked by a sudden veering of the wind and by gradients of surface

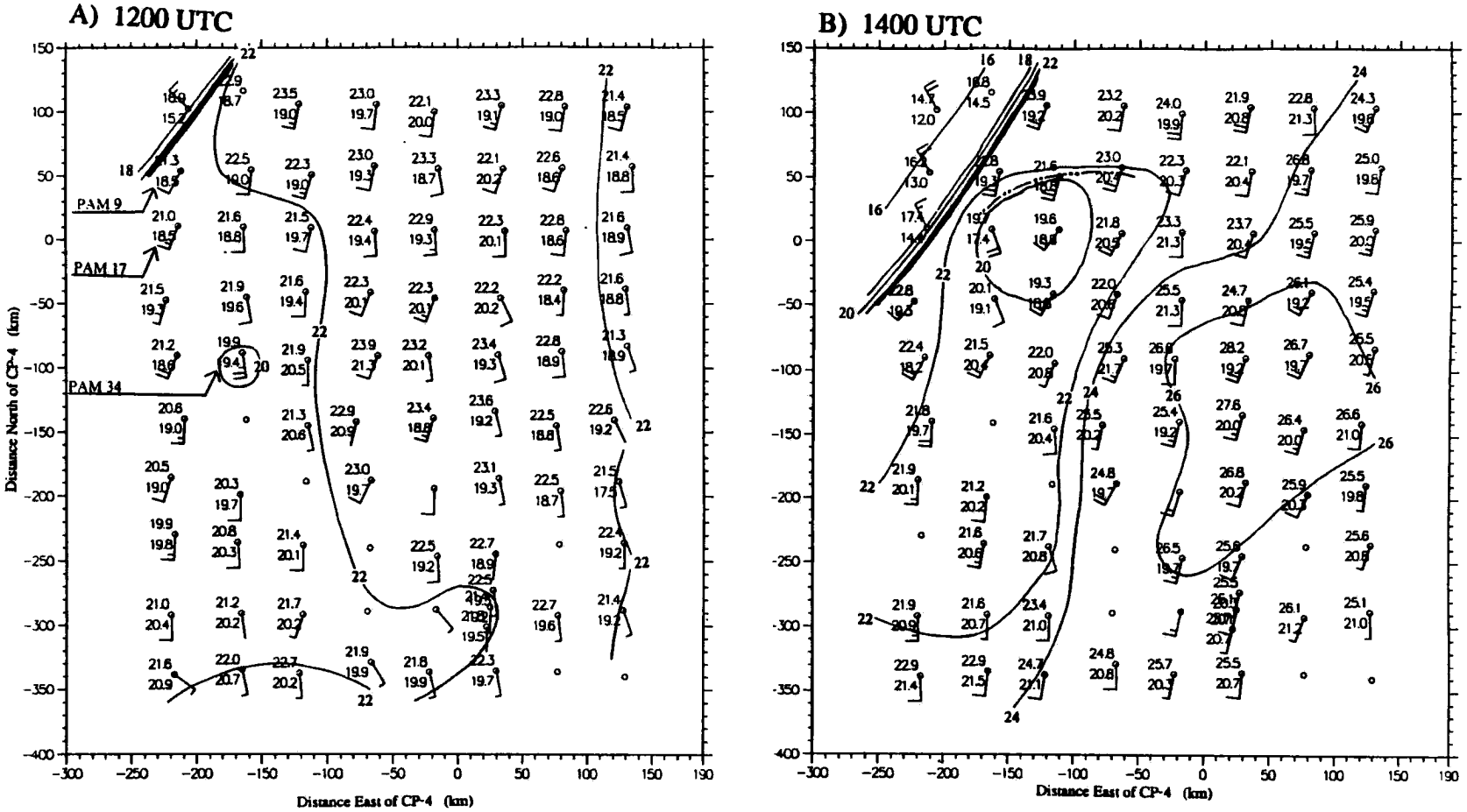

Fig. 3.4: Surface analysis of PAM/SAM data from a) 1200 UTC and b) 1400 UTC, 26 June 1985. Data plotted are temperature (°C), dewpoint (°C), and wind (full barb = 5 m s^{-1}). Temperature contoured at 2°C intervals. Heavy line indicates position of surface front. Double-dotted line indicates position of a surface gust front.

temperature and dewpoint. Time series from two PAM stations (Fig. 3.5), for example, clearly show the passage of the front. Temperature and dewpoint dropped by 3 - 5°C and the wind veered by 120° over a period of 15 - 20 min. The surface plots and time series clearly show that before the convective system began, the front was a distinct feature in the surface observations.

Certain features visible in the satellite images (discussed in section 3.1) can be identified in the surface data. The broad band of clouds noted in Fig. 3.3a, for instance, reduced solar heating of the surface in a band 200 - 300 km wide ahead of the front (Fig. 3.4b). In the clear area, temperatures had risen to 25 - 28°C by 1400, while in the cloudy area, surface temperatures were still about 20 - 23°C. This differential surface heating resulted in a second temperature gradient, about 200 km ahead of the frontal gradient.

The effects of the small area of early convection noted in Fig. 3.3a were also recorded by the surface network. By 1200 (Fig. 3.4a), this convection had caused some slight but noticeable cooling at PAM 34. In the time series from that station (Fig. 3.6), the passage of the convective cell at about 1200 was marked by a drop in temperature and dewpoint, a brief period of stronger winds, some turning of the wind, a brief pressure rise, and rainfall of about 15 mm in a 40 min period. These changes have been analyzed as a thunderstorm outflow in Fig. 3.4. By 1400, the outflow had moved north, and several other PAM stations had experienced similar changes with the passage of the cell.

The environment into which the front was moving was characterized by weak shear and weak to moderate CAPE. The 1200 sounding from Omaha (Fig. 3.7a) had only about 560 J kg^{-1} of CAPE. The 1200 sounding from Dodge City (Fig. 3.7b) had somewhat more CAPE, about 1100 J kg^{-1}. These numbers are significantly less than the average values of CAPE generally above 2000 J kg^{-1} which Bluestein and Jain (1985) found for severe Oklahoma squall lines. However, these numbers are comparable to the CAPE values of all but the "Strongly Classifiable" cases of Houze *et al.* (1990). All three soundings show that there was almost no directional shear throughout the troposphere, and

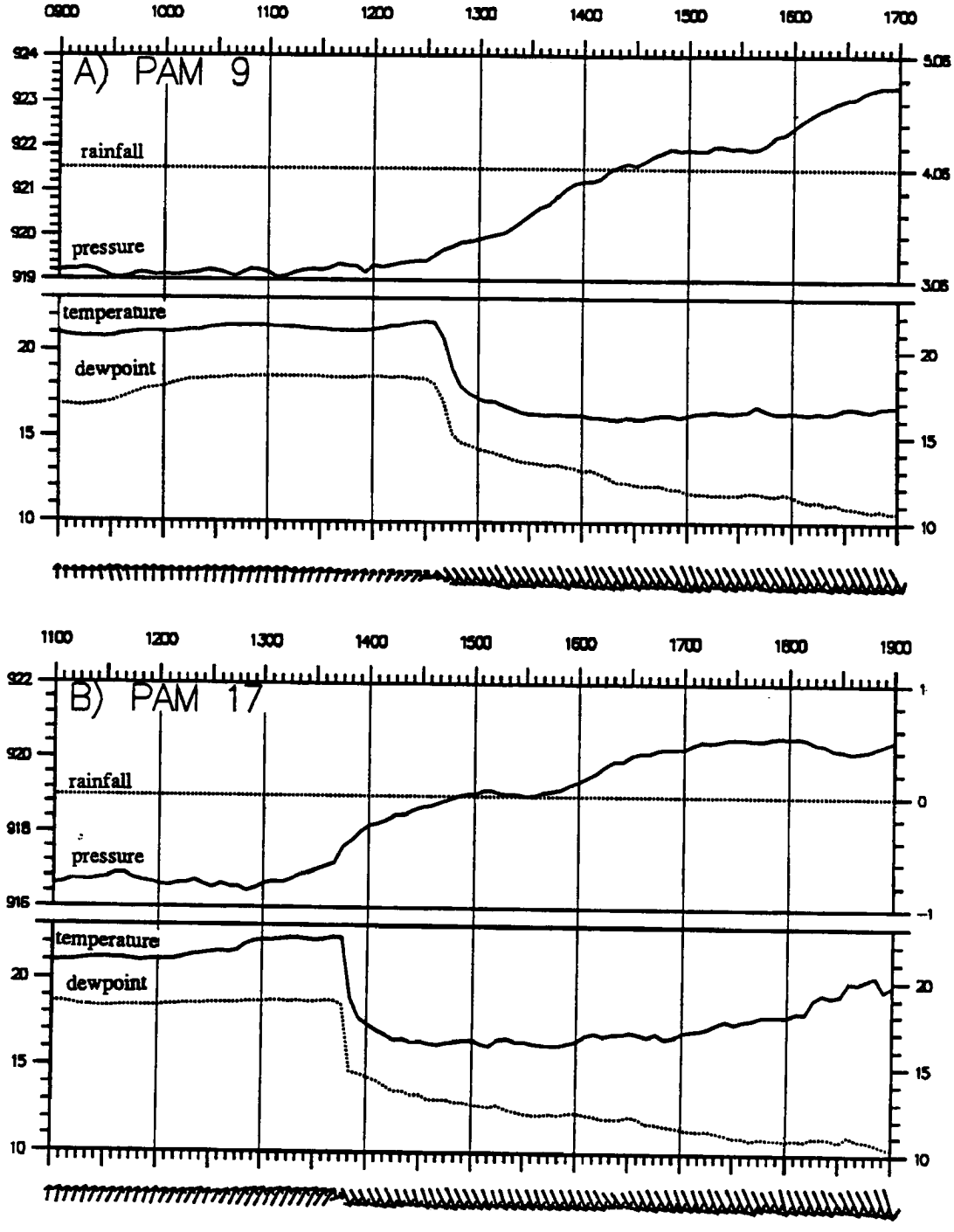

Fig. 3.5: Time series from PAM stations. Data plotted are temperature (°C), dewpoint (°C), pressure (mb), rainfall (mm), and wind vectors. Data displayed are from the 8 hours following a) 0900 UTC at PAM 9; and b) 1100 UTC at PAM 17.

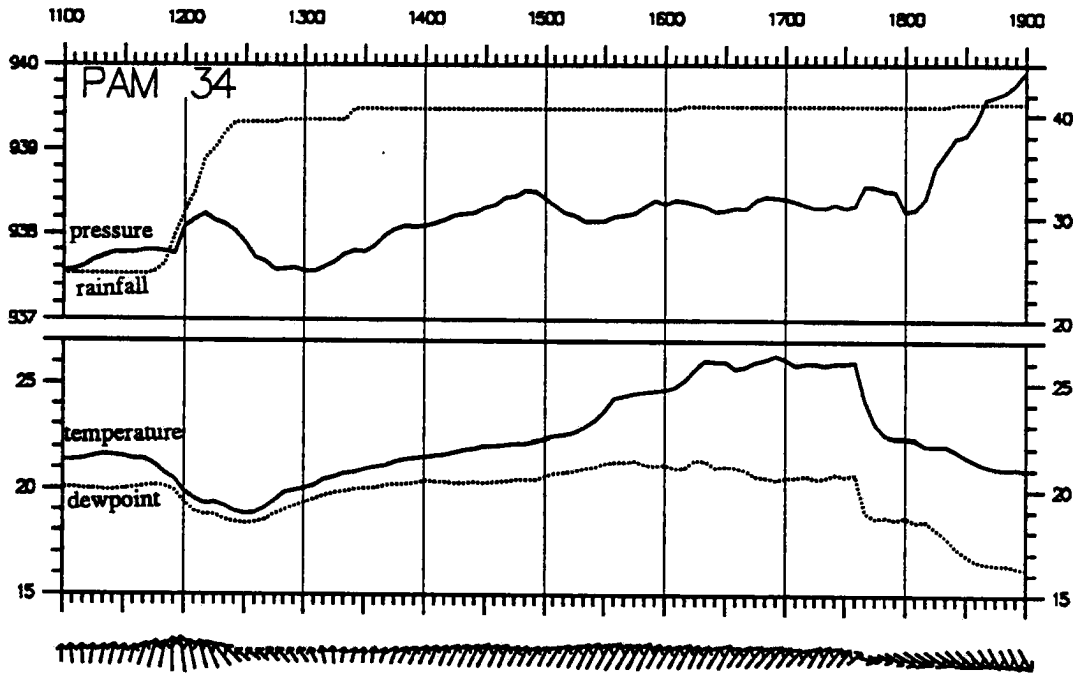

Fig. 3.6: Same as Fig. 3.5, except for PAM 34, for the 12 h following 0900 UTC.

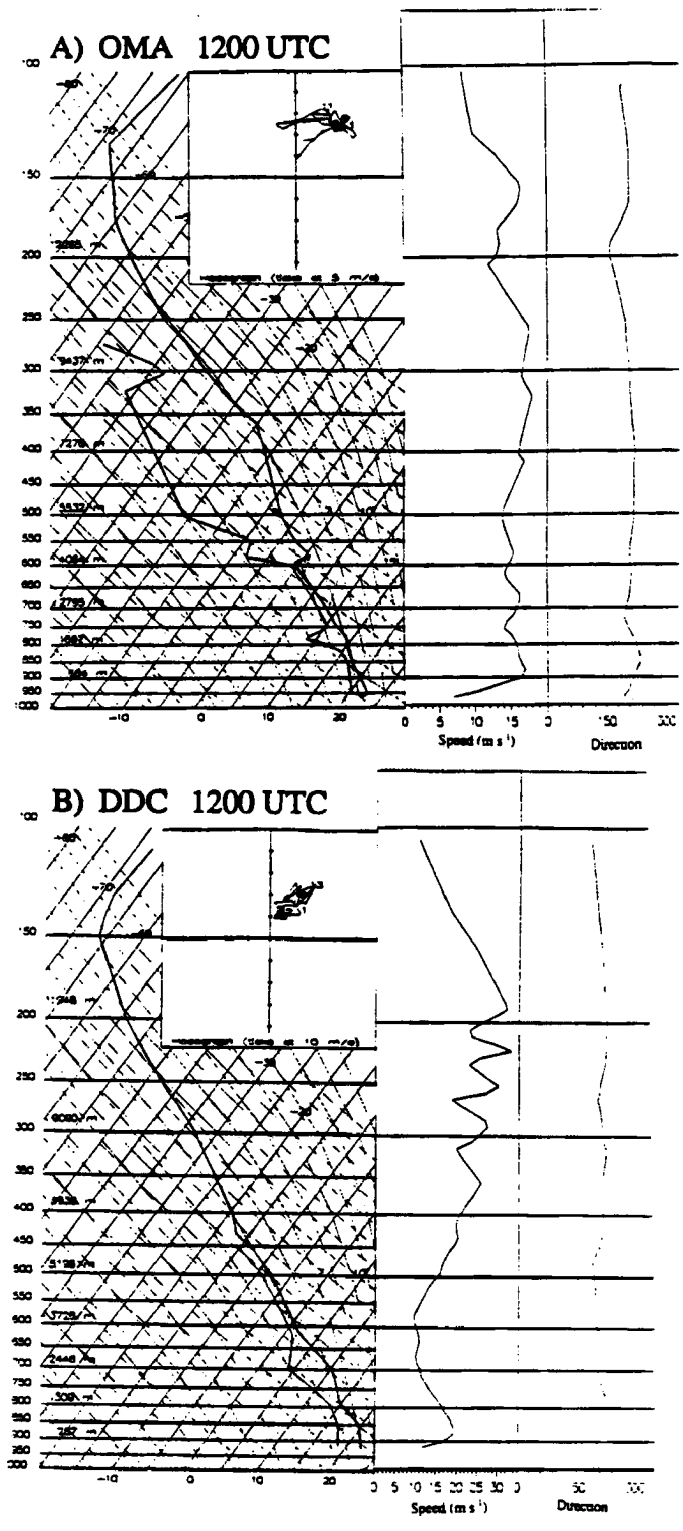

Fig. 3.7: Soundings taken at 1200 26 June from a) Omaha, Nebraska (OMA); b) Dodge City, Kansas (DDC); and c) Oklahoma City, Oklahoma (OKC).

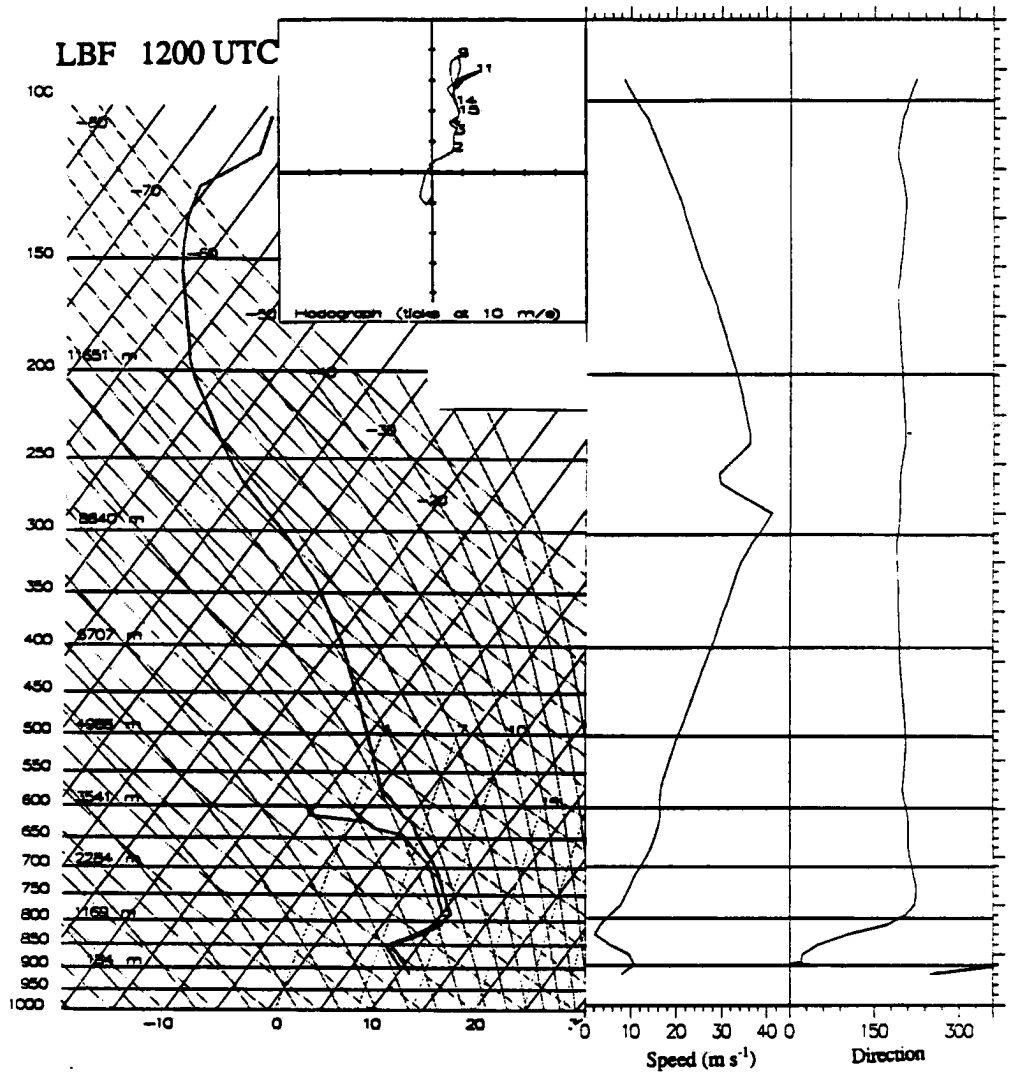

Fig. 3.8: Same as Fig. 3.7, except from North Platte, Nebraska (LBF).

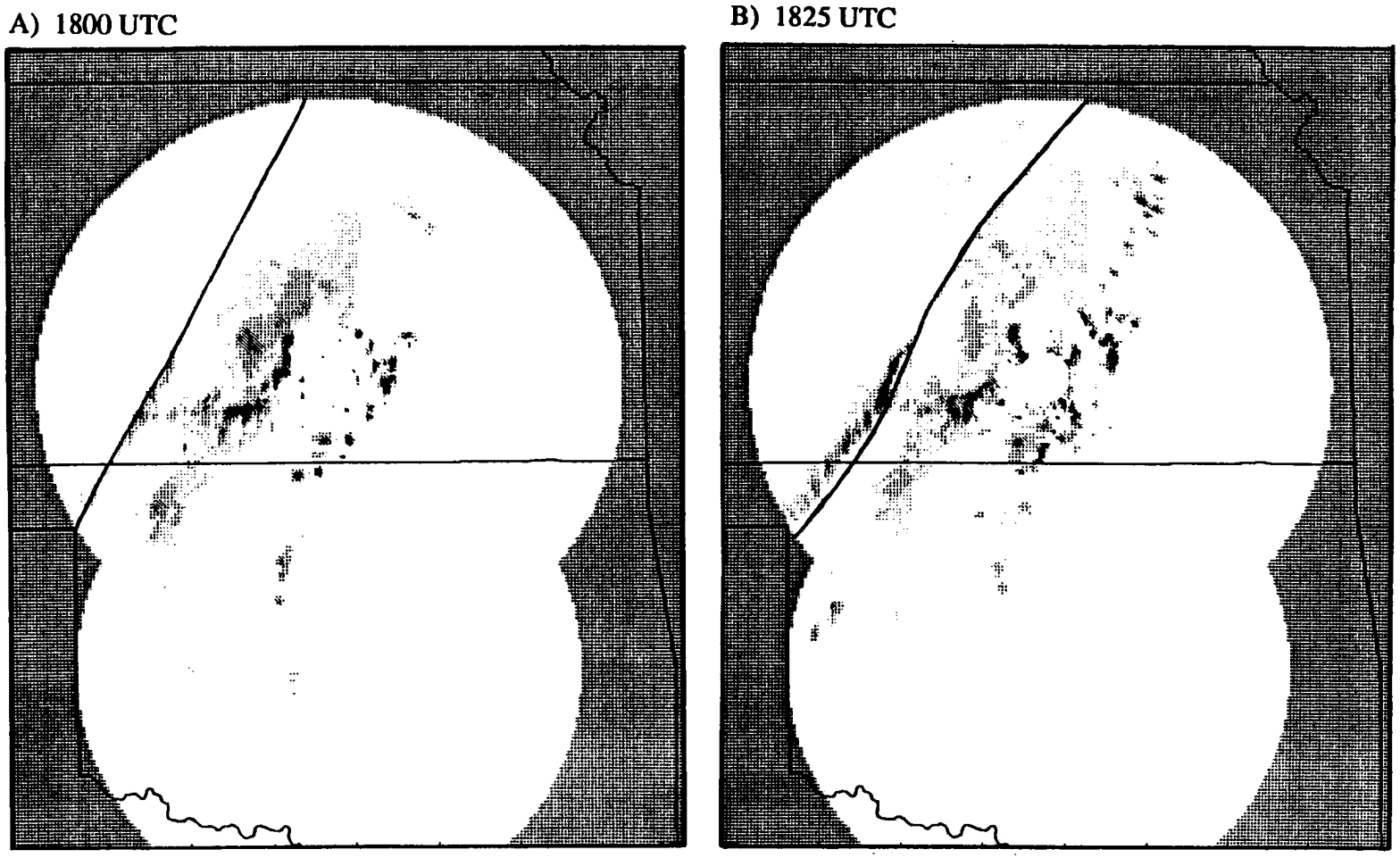

Fig. 3.9: Composite of low-level PPIs from Wichita, Kansas and Oklahoma City, Oklahoma. Shading levels are 15, 30, 40, 45, 50, and 55 dBZ. Heavy solid line indicates approximate frontal location. a) at 1800 UTC, 26 June; b) at 1825 UTC, 26 June; c) at 1905 UTC, 26 June; and d) at 1945 UTC, 26 June.

C) 1905 UTC

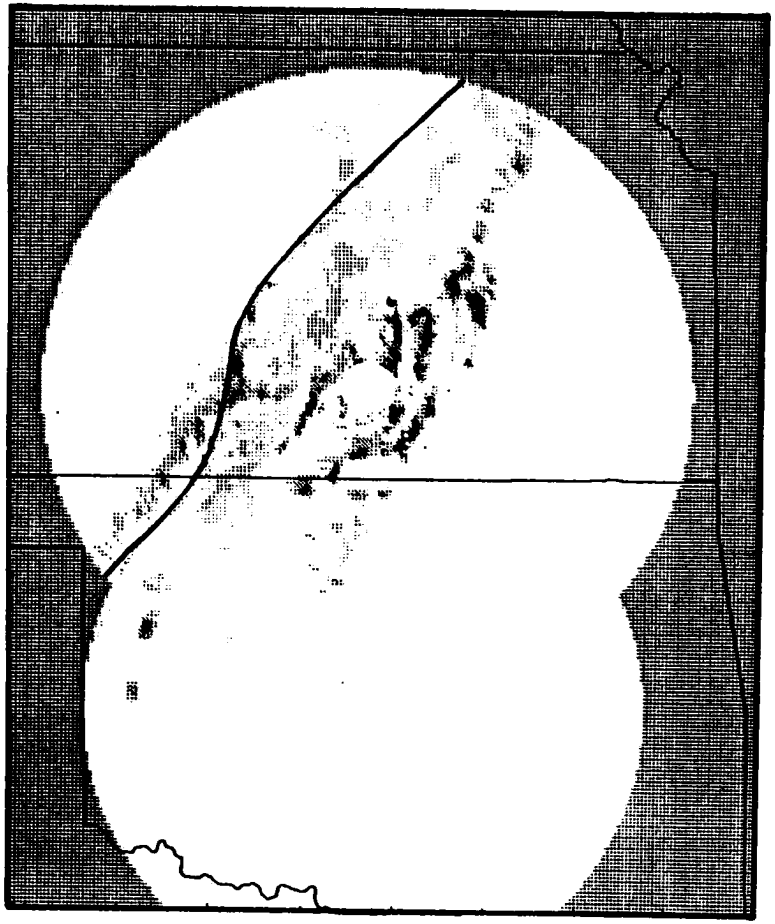

D) 1945 UTC

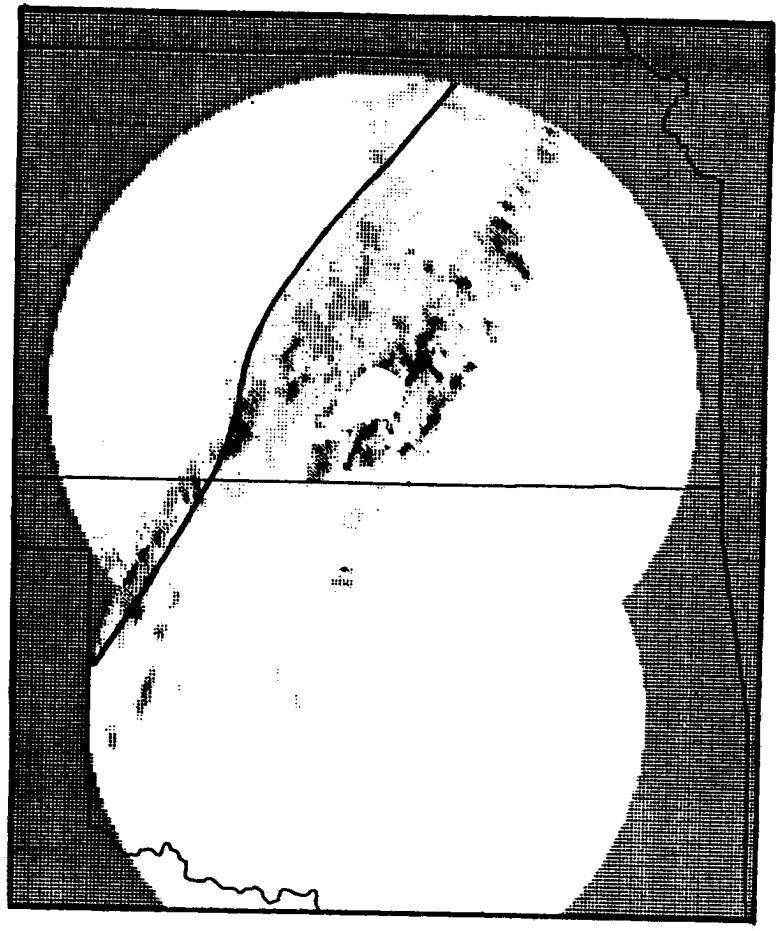

Fig. 3.9: Continued.

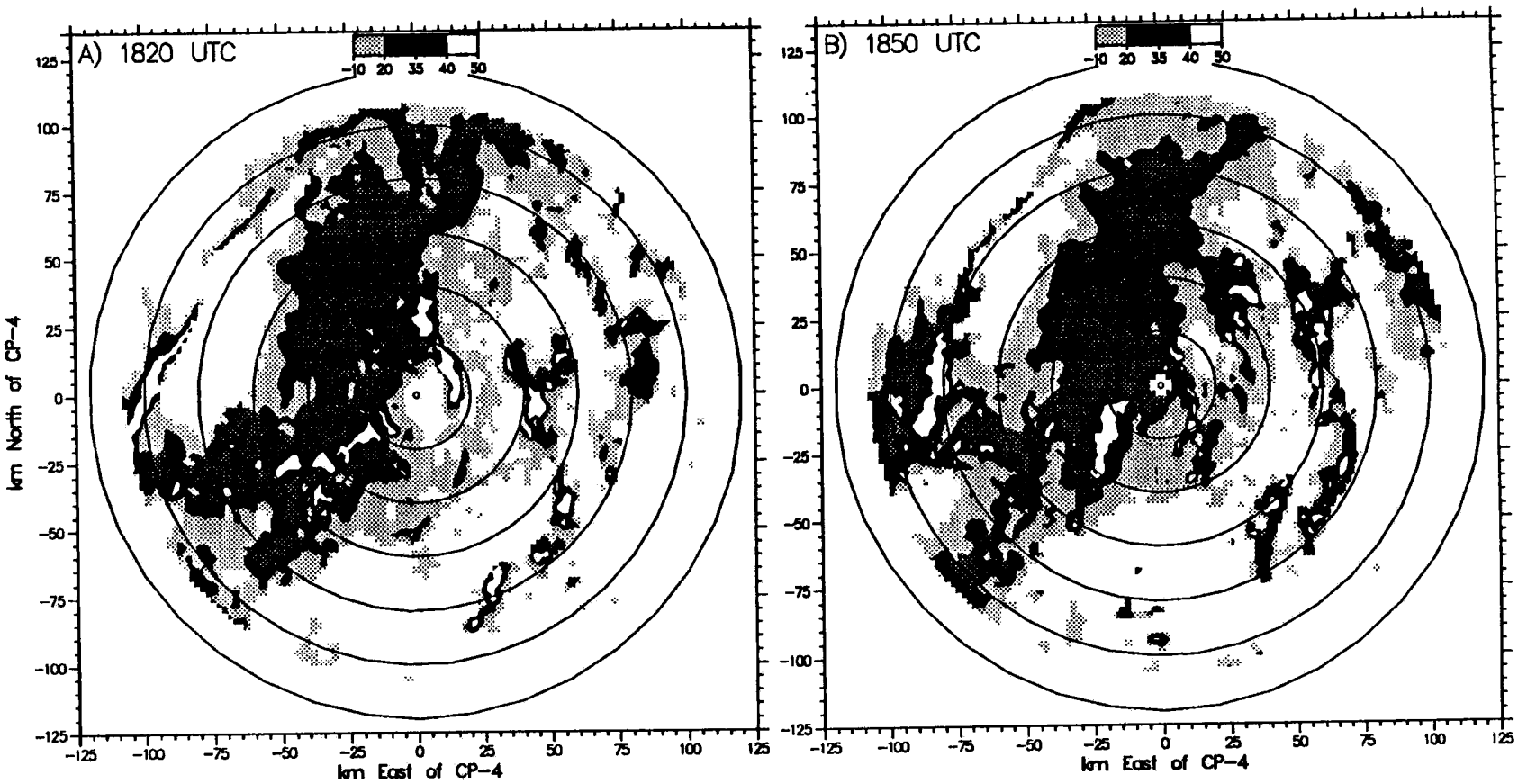

Fig. 3.10: Horizontal cross sections of reflectivity (dBZ) from the NCAR CP-4 radar at a) 1820 UTC, b) 1850 UTC, c) 1920 UTC, and d) 2000 UTC, 26 June. Cross sections are at 1.5 km AGL. Shading levels are: light gray, -10 to 20 dBZ; dark gray, 20 to 35 dBZ; black, 35 to 40 dBZ; and white, 40 to 50 dBZ.

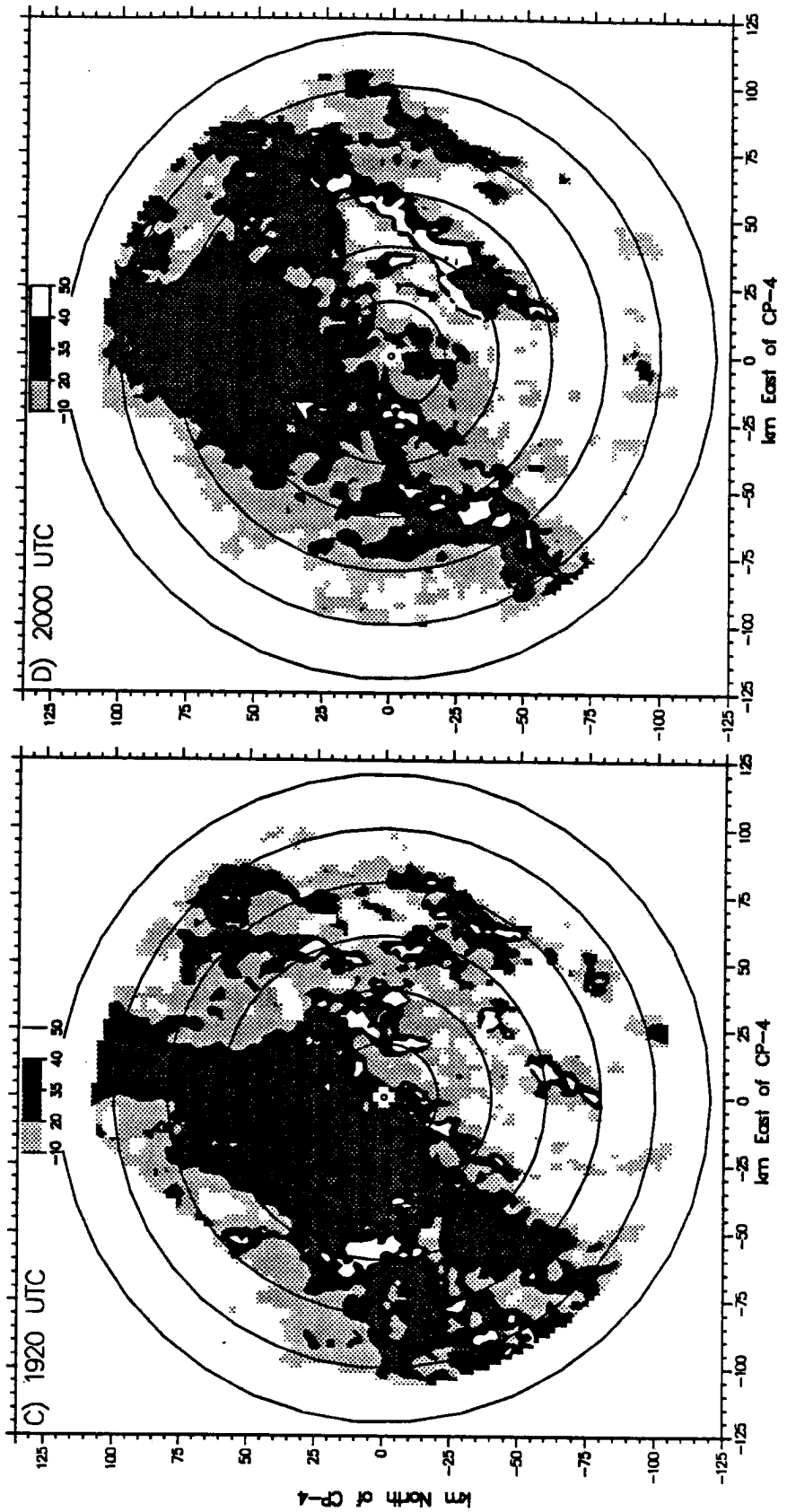

Fig. 3.10: Continued.

overall convection was not strong. Although maximum reflectivities as recorded by CP-4 during this period were greater than 55 dBZ, only a small area of the horizontal cross sections had reflectivities greater than about 40 dBZ. Vertical cross sections (Fig. 3.11) and horizontal cross sections taken at higher altitudes (not shown) indicate that reflectivity cores greater than about 35 dBZ occasionally extended up to about 12 km.

Although the overall organization was weak, the convection was consistently organized into short (50 - 100 km) bands roughly paralleling the front. Each band was short lived, as were the cells which made up the bands. The horizontal cross sections thus show little continuity from one time to another. The horizontal cross sections from 1850 and 1920 (Figs. 3.10b and 3.10c), for example, were taken about 0.5 h apart. Although each cross section exhibits several short bands, it is difficult to track most of the lines between 1850 and 1920 with any confidence.

There was a slight indication of a stratiform region between about 1800 and 2000 (*e.g.* Fig. 3.10b), but the region was narrow and not strictly stratiform, as convective echoes appeared in the region (*e.g.* 20 km west and 40 km northwest of the radar at 1919, Fig. 3.10c). The vertical cross sections (Fig. 3.11), however, show that this area did have the characteristics of a stratiform region, including a marked bright band and an overhanging anvil echo structure. The front (marked by the narrow line of echoes northwest of CP-4 during this period) seemed to catch up with the main body of echoes by 2000.

Even though the convection was not strong or long-lived, and the system was not organized as a "classic" squall line, the line-normal flow structure of the system was typical to that of many other squall lines. The vertical cross sections of Doppler velocity (Fig. 3.12) clearly show three of the four flow regimes of the conceptual model of chapter 1: 1) the inflow into the front of the storm rising and extending to the rear of the system, 2) the middle level descending rear inflow, and 3) the low-level front to rear return flow near the surface. This pattern persisted for much of the lifetime of the system.

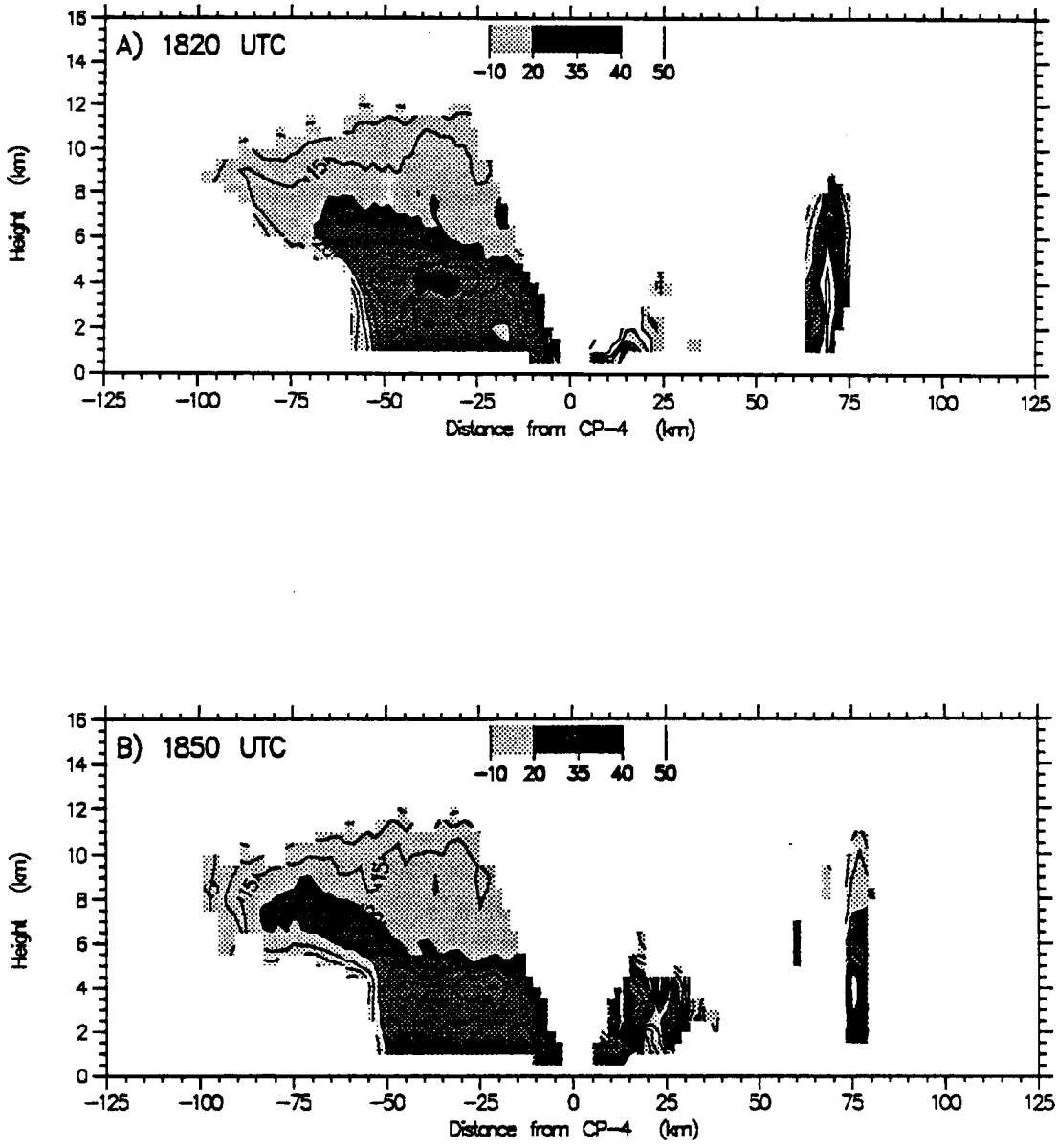

Fig. 3.11: Vertical cross section of reflectivity from the NCAR CP-4 radar at a) 1820 UTC, 26 June; b) 1850 UTC, 26 June; c) 1920 UTC, 26 June; and d) 2000 UTC, 26 June. Cross section is approximately normal to the front.

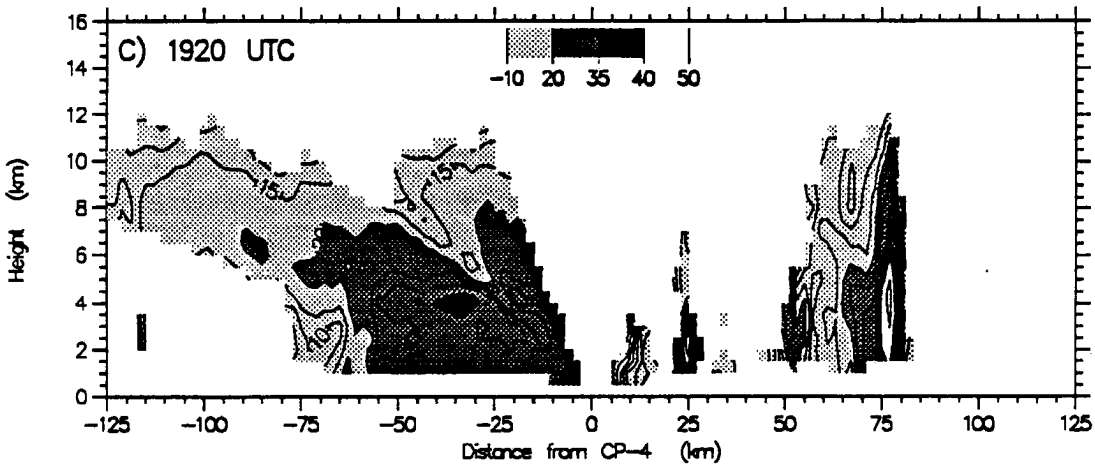

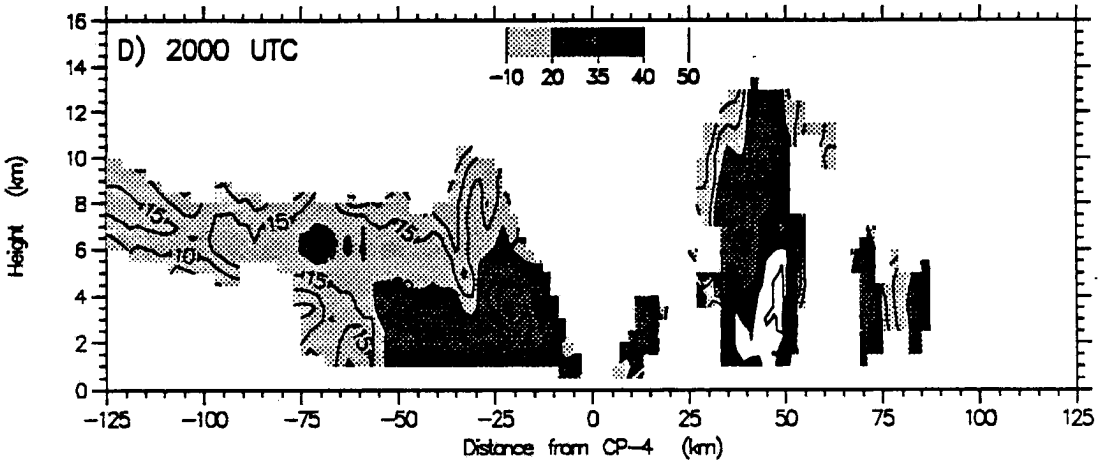

Fig. 3.11: Continued

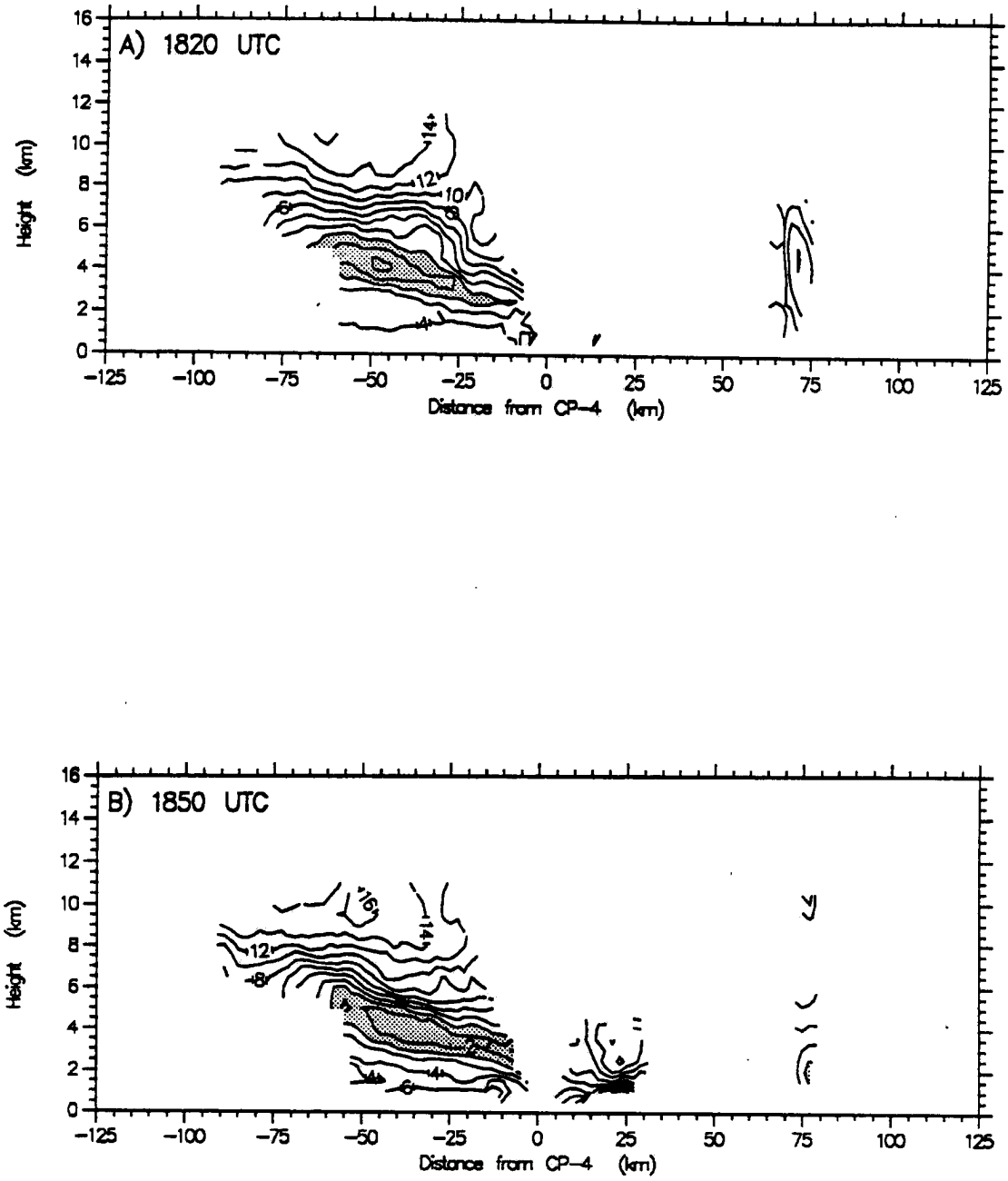

Fig. 3.12: Same as Fig. 3.11, except of Doppler velocity. Contour interval is 2 m s^{-1}. Shading indicates areas of positive (*i.e.*, left to right) velocity.

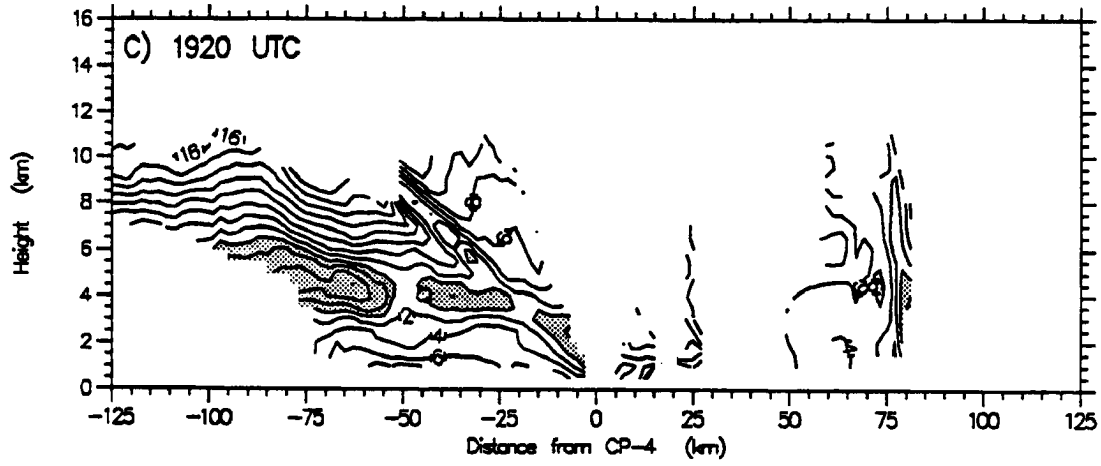

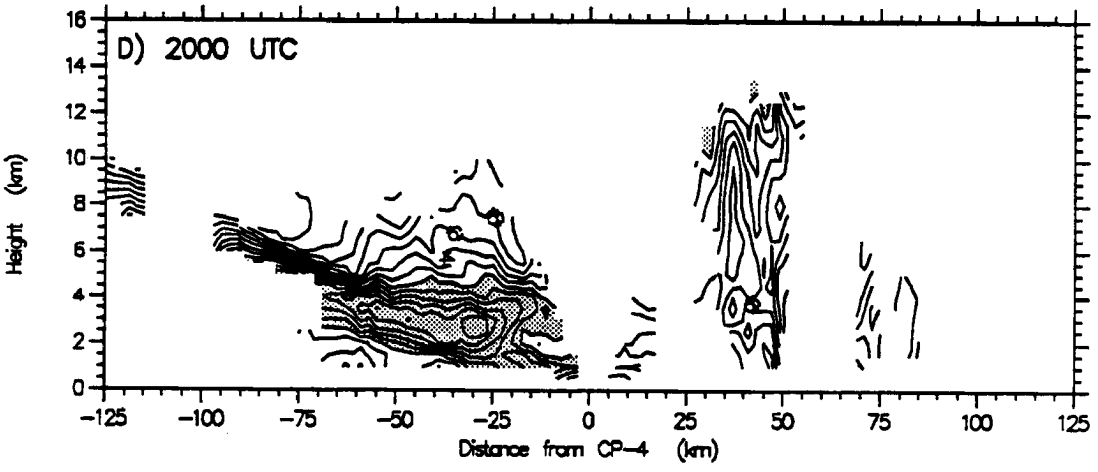

Fig. 3.12: Continued

The rear inflow strengthened during this stage. In the vertical cross sections prior to 2000, the maximum speed in the inflow was less than 6 m s^{-1}. By 1200, however, the inflow had reached speeds of greater than 12 m s^{-1}.

The convection began to have more of an effect on the surface conditions after about 1800, as thunderstorm outflows began to complicate the surface analyses. By 1820 (Fig. 3.13a), several outflow boundaries had passed some of the PAM stations east of CP-4. The convection which caused these boundaries can be seen in the 1820 horizontal cross section (Fig. 3.10a) at about 15, 45, and 85 km east of CP-4. The analyses must be viewed with caution, however: because the data were not continuous in space, the boundaries were better resolved and could be more accurately located when they were near a surface station. For this reason, the strongest and most obvious boundaries in the analyses seem to occur close to PAM and SAM stations.

At 1900 (Fig. 3.13b), there were again several outflow boundaries. Some of these boundaries were possibly the same ones analyzed at 1820, while some of them were new boundaries. By 2000 (Fig. 3.13d), the effect of the numerous boundaries was to intensify prefrontal temperature gradients. The temperature drop at the front was by this time 2 - 3°C or less, whereas at the outflow boundaries, the temperature had dropped by as much as 8 - 10°C. From the surface plots alone, it was not always clear where the front was.

However, it was still easy to distinguish between the front and the outflow boundaries in the time series. At the outflow boundaries, the wind shift at this time tended to be smaller than and not as long-lasting as that at the front. Additionally, the dewpoint tended to drop to about the same extent as the temperature at the front while it generally did not drop significantly at the outflow boundary.

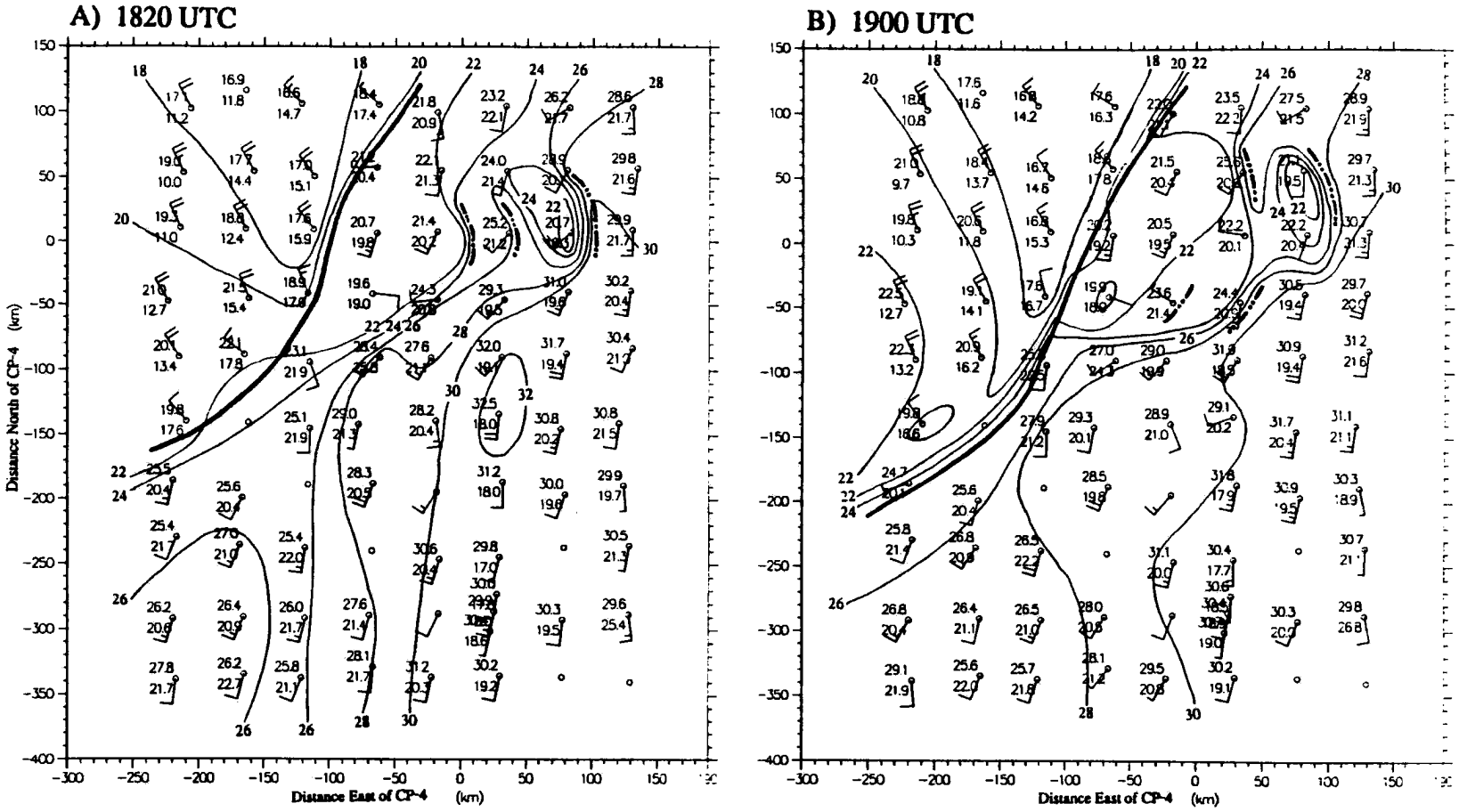

Fig. 3.13: Same as Fig. 3.4, except at a) 1820 UTC, 26 June; b) 1900 UTC, 26 June; c) 1930 UTC, 26 June; and d) 2000 UTC, 26 June.

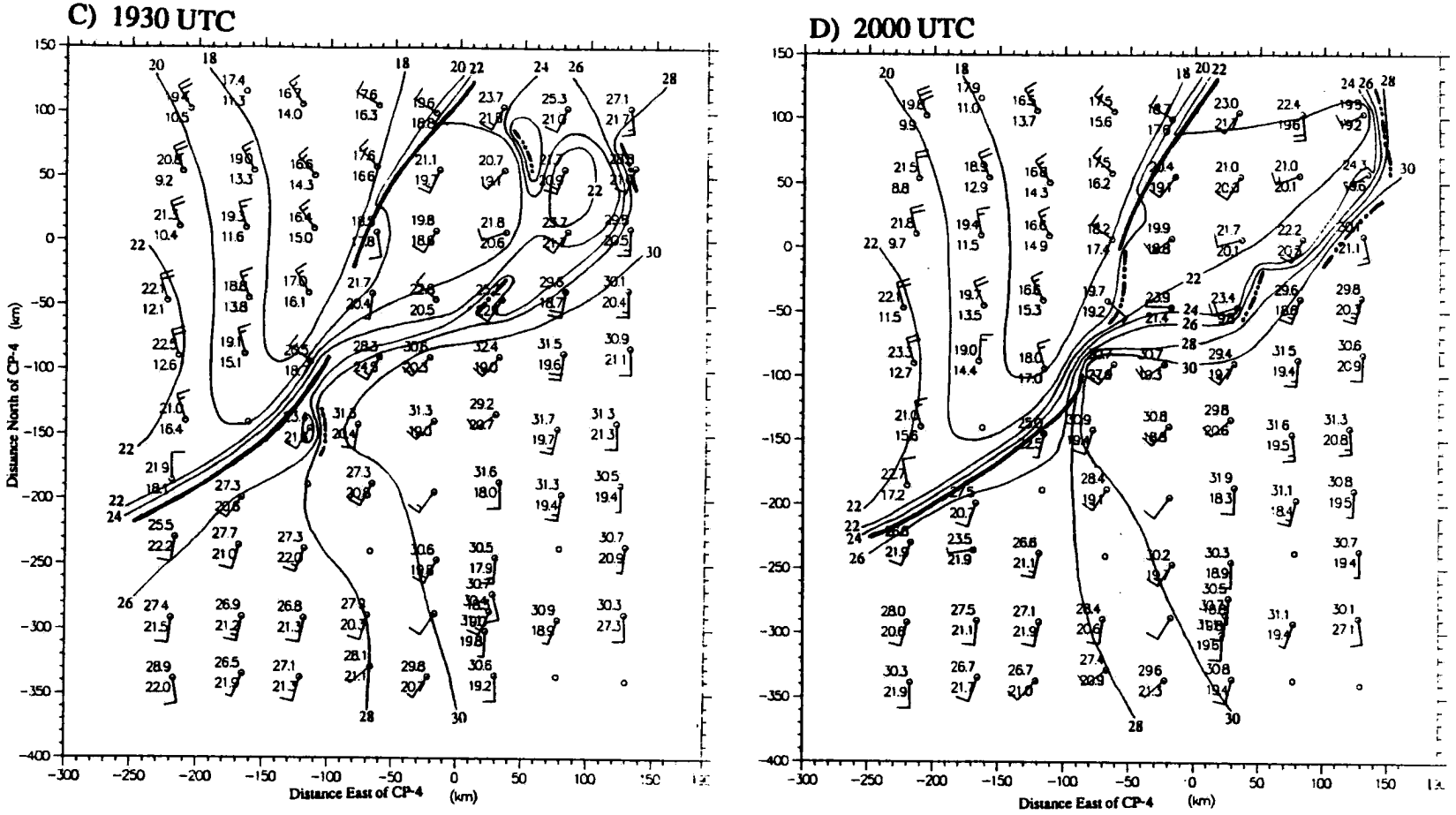

Fig. 3.13: Continued.

3.2.3 Mature stage

During the mature stage, (from about 2000 to 0000) the system seemed to reach its peak convective activity; however, such activity was never strong. The system was again characterized by weakly-organized moderate convection. WSR-57 composites (Fig. 3.14) again show only short bands of small convective cells. The last significant convection in Kansas (near the end of the mature stage) seems to be representative of the convectively active portion of the system's life. At 2330 (Fig. 3.14c), a short band of convective echoes oriented approximately north-south was located approximately 100 km east of Wichita. But by 0010 (Fig. 3.14d), there was no trace of this band, which appears to have lasted less than 2 h.

On the smaller scale shown in the horizontal cross sections from CP-4 (Fig. 3.15), bands and individual cells formed and dissipated quickly. For example the several pre-frontal bands in existence at 2055 had become much more disorganized by 2125, and by about 2145 several new bands appear to have formed out of the remains of the old ones. Traces of these newer bands were difficult to find by 2205.

The organization (or lack thereof) of this system was clearly dissimilar to that of the "classic" model of a squall line. Where the model has one long-lived line of strong convection (although the individual cells may be short-lived), this case produced a number of short-lived lines of only moderate intensity. Where the model has a well-developed stratiform region, this case had only a weakly-developed stratiform region. But as mentioned before, the structure of the line-normal velocity field (Fig. 3.16) was similar to that of the conceptual model for a squall line: the three flow regimes mentioned in Section 3.2.2 were still quite evident.

One of the soundings taken during this period also showed the rear inflow. The 2100 sounding from FRI (Fig. 3.17), in the stratiform region, showed a well-defined layer in

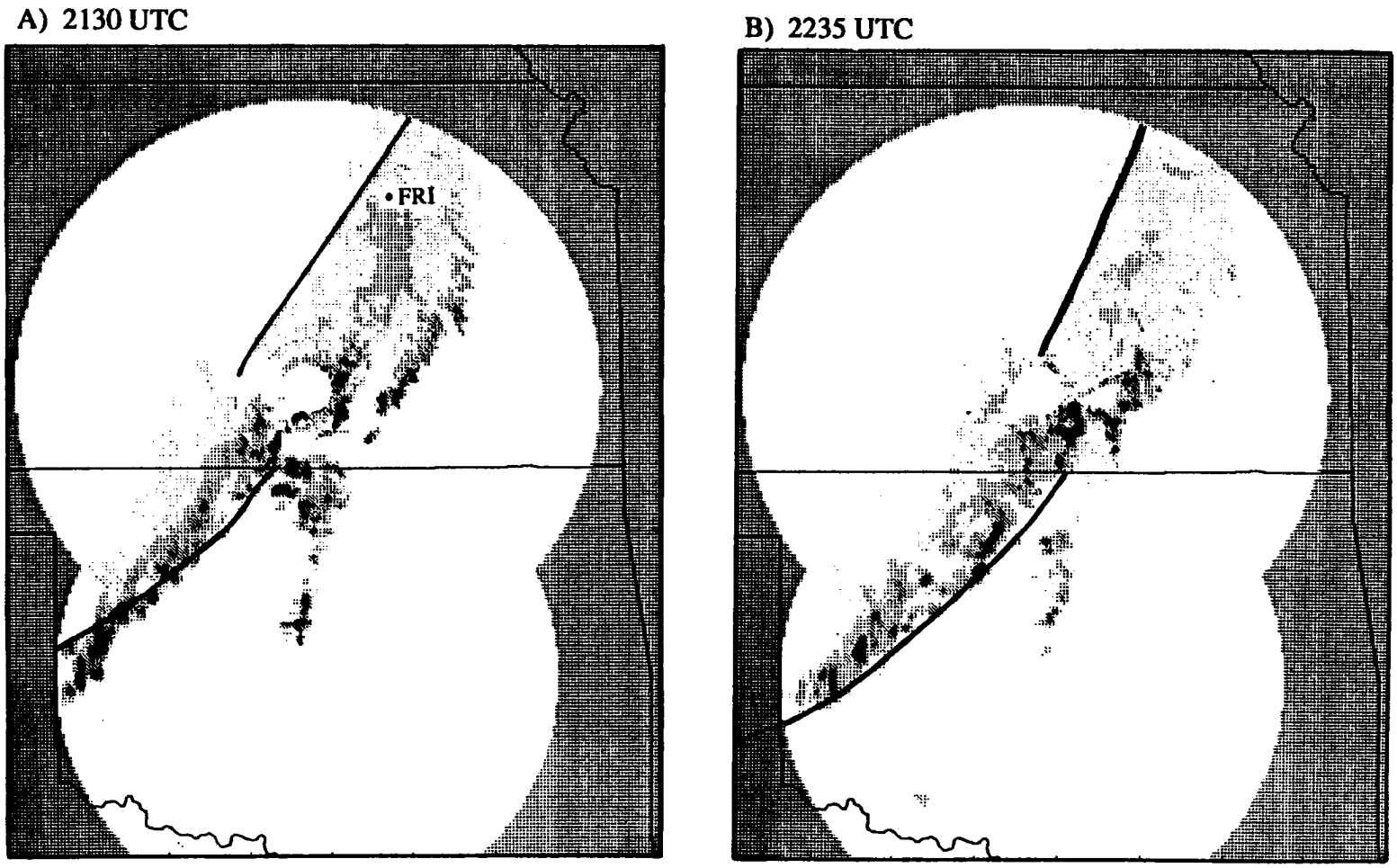

Fig. 3.14: Same as 3.9, except at a) 2130 UTC, 26 June; b) 2235 UTC, 26 June; c) 2330 UTC, 26 June; and d) 0010 UTC, 27 June.

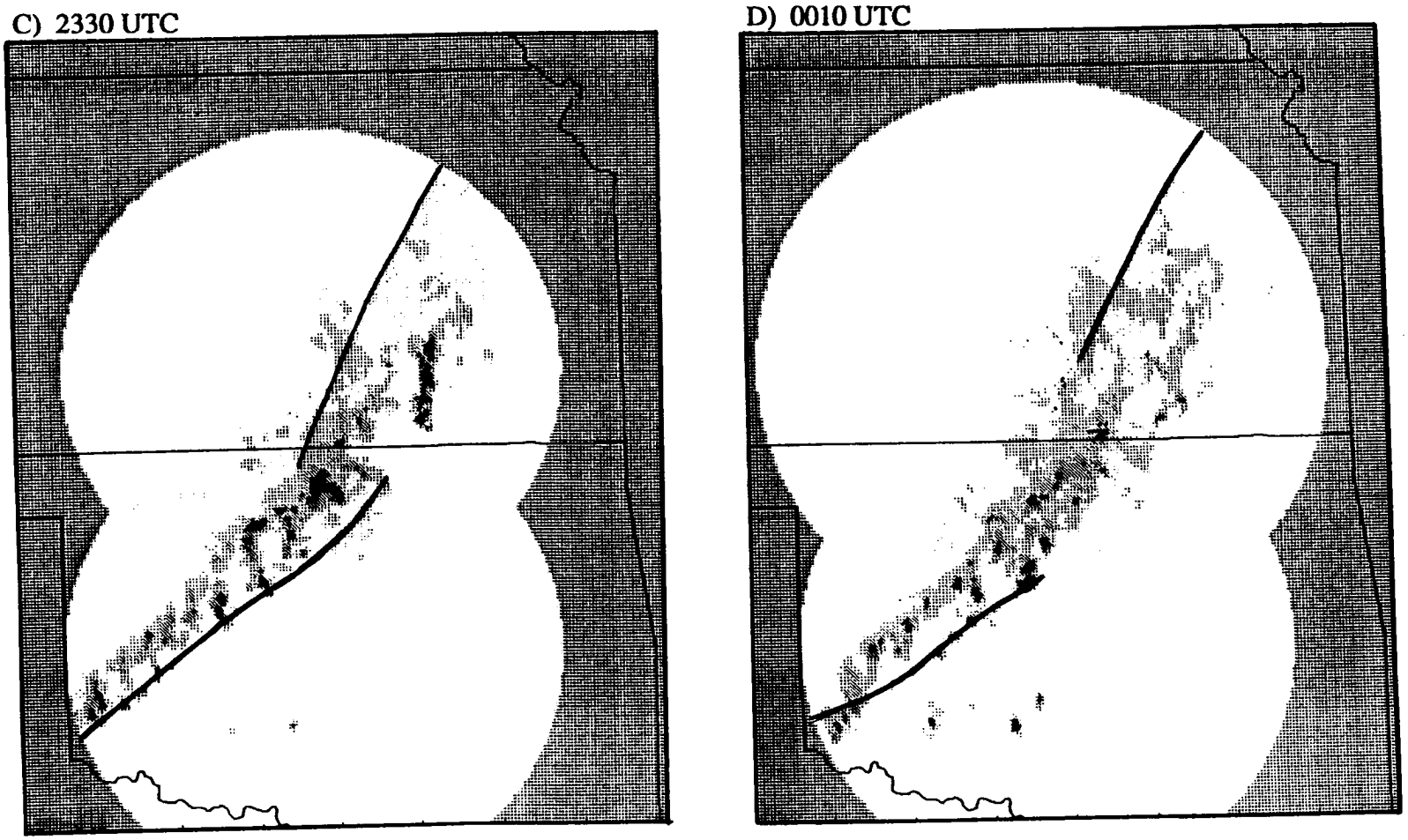

Fig. 3.14: Continued.

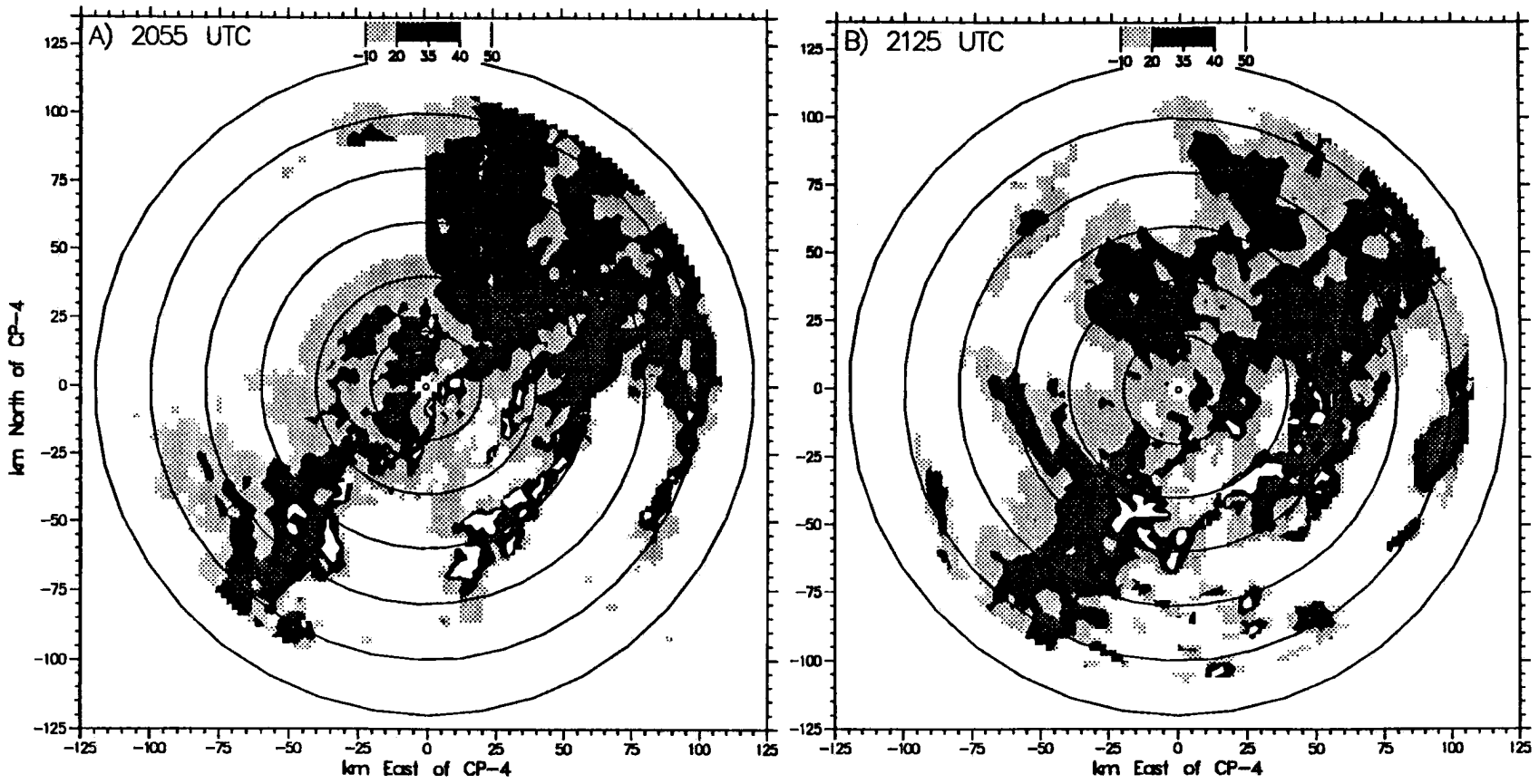

Fig. 3.15: Same as Fig. 3.10, except at a) 2055 UTC; b) 2125 UTC; c) 2145 UTC; and d) 2205 UTC, 26 June.

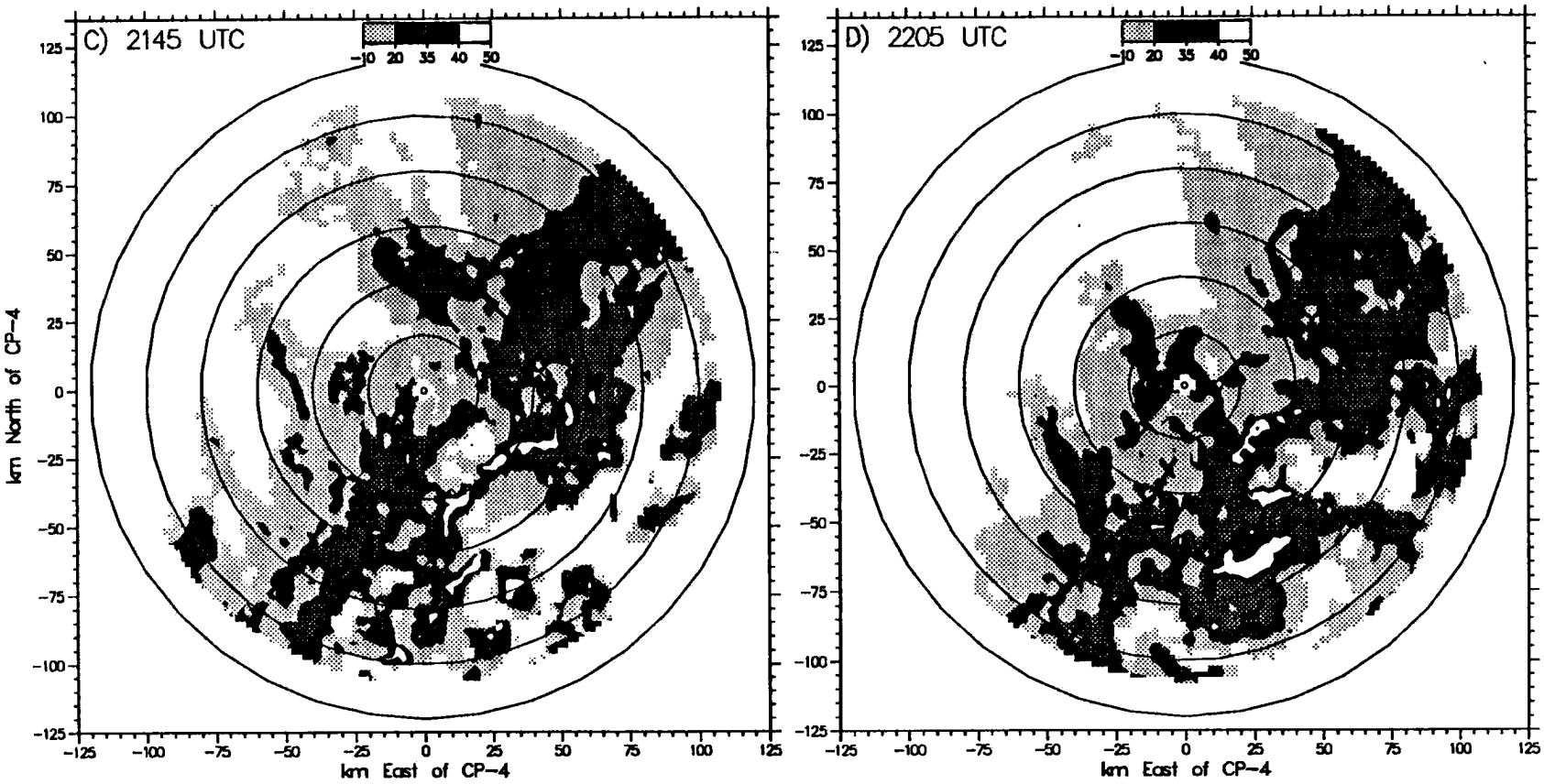

Fig. 3.15: Continued.

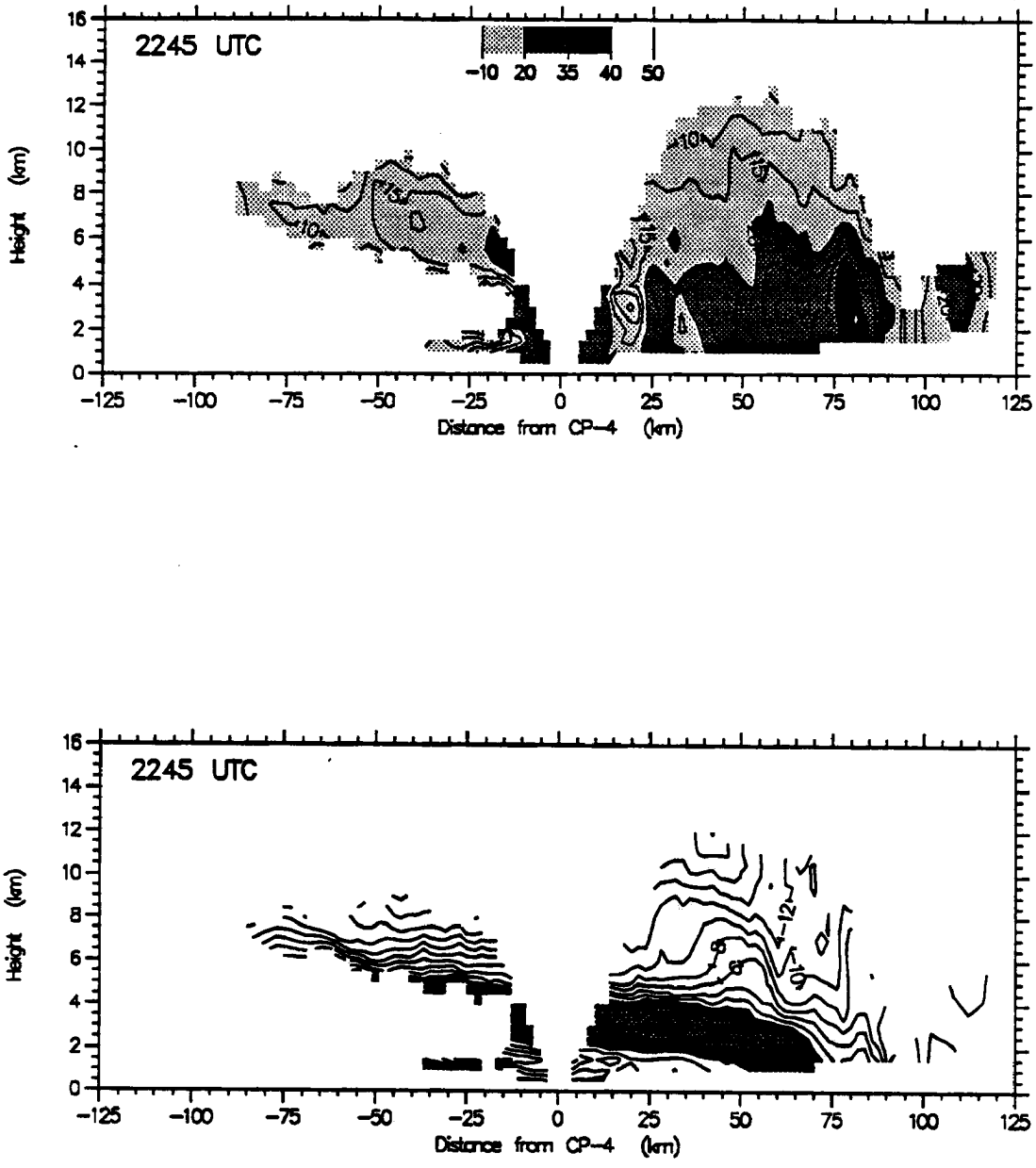

Fig. 3.16: Same as Fig. 3.12, except at 2245 UTC .

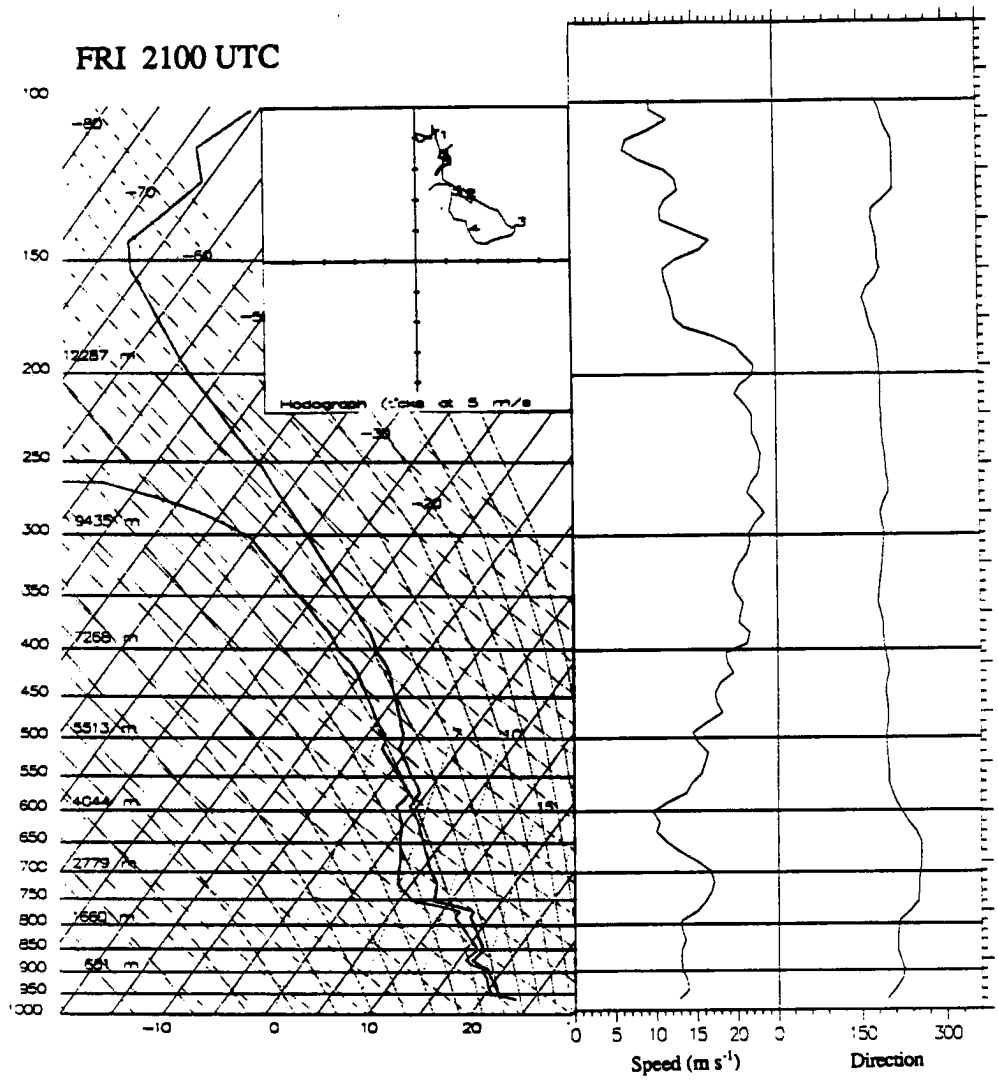

Fig. 3.17: Same as Fig. 3.7, except from FRI at 2100 UTC.

which westerly flow was maximized. Also, temperature and dewpoint curves indicate the cooling and drying of the mesoscale inflow.

The surface plots (Fig. 3.18) and time series (Fig. 3.19) during the mature stage documented some interesting behavior of the front and the outflow boundaries. In the northern and central part of the surface network, the outflow boundaries were characterized by temperature drops of up to 10°C, the beginning of a pressure rise, and a sudden, obvious wind shift (*e.g.* PAMs 14 and 37). The front, however, was characterized by a temperature drop of only about 2°C. At PAM 37, for example, the outflow boundary passed the station at about 2100, while the front did not pass until about 2310. By 0000, the front had become distinctly discontinuous as the outflow boundary strengthened. In the southern part of the network (*e.g.* SAMs 10 and 12), the convection was closely linked to the front such that there was no outflow boundary independent of the front. However, about 200 km to the north and west (*e.g.* SAMs 31, and 40), the outflow had apparently propagated 150 km or farther ahead of the front. Time series show two boundaries passing, followed after 3 - 4 h by the front.

3.2.4 Dissipating stage

During the dissipating stage (after about 0000), the MCS moved from the PRE-STORM observational network and dissipated. As the convection weakened, the upper-level cloud shield broke up and decreased in area (see the satellite images, Fig 3.3). The WSR-57 composites (Fig. 3.20) show the weakening of the system after about 0000. Convection had virtually ceased in Kansas by 0030; only a few echoes had reflectivities greater than 40 dBZ. The large scale reflectivity pattern began to resemble a stratiform region, with relatively uniform radar echoes. In Oklahoma, however, the convection continued in a few wave-like bands until about 0230, after which weak convection continued in a small area until about 0530, when nothing but stratiform echoes were

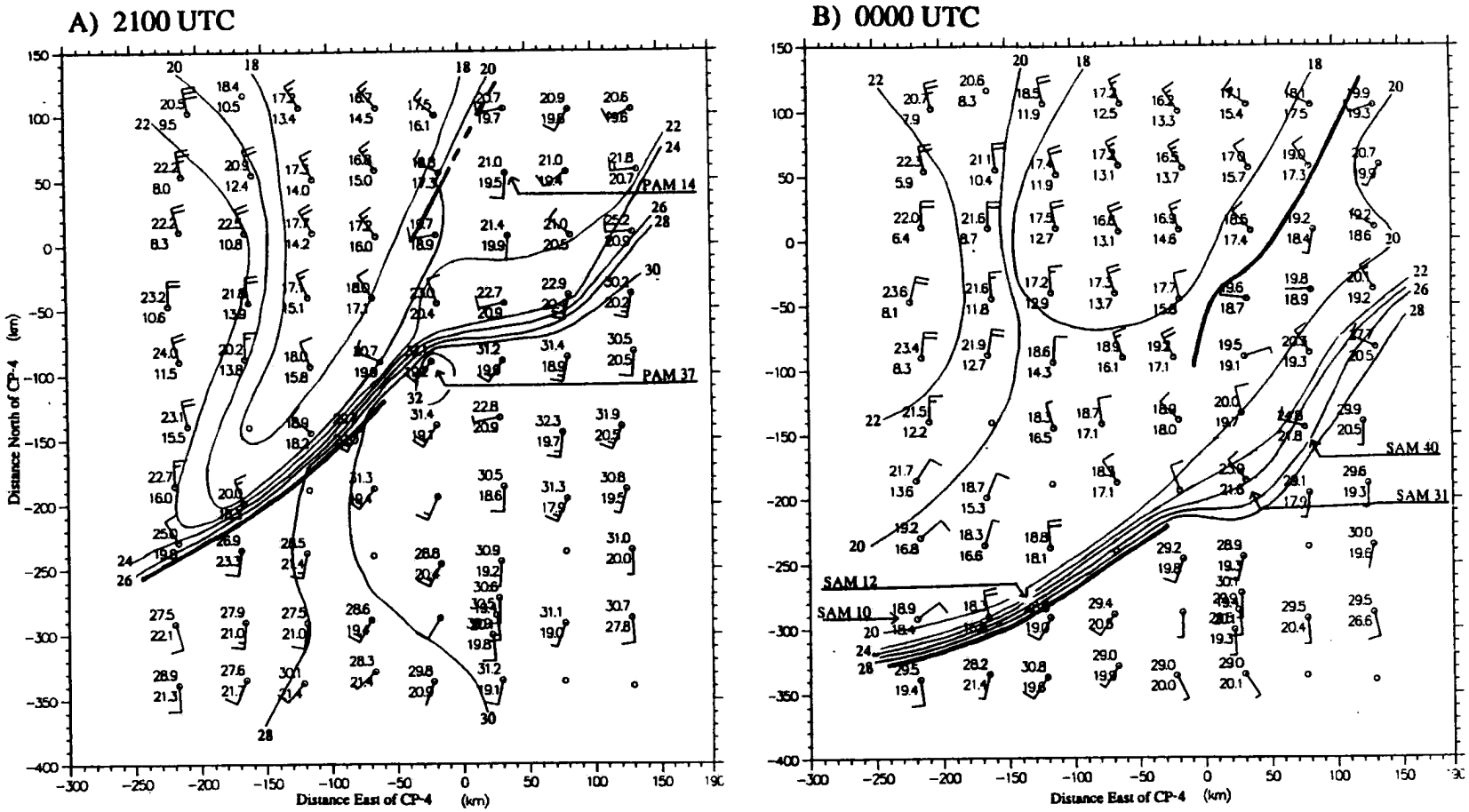

Fig. 3.18: Same as Fig. 3.4, except at a) 2100 UTC, 26 June; and b) 0000 UTC, 27 June.

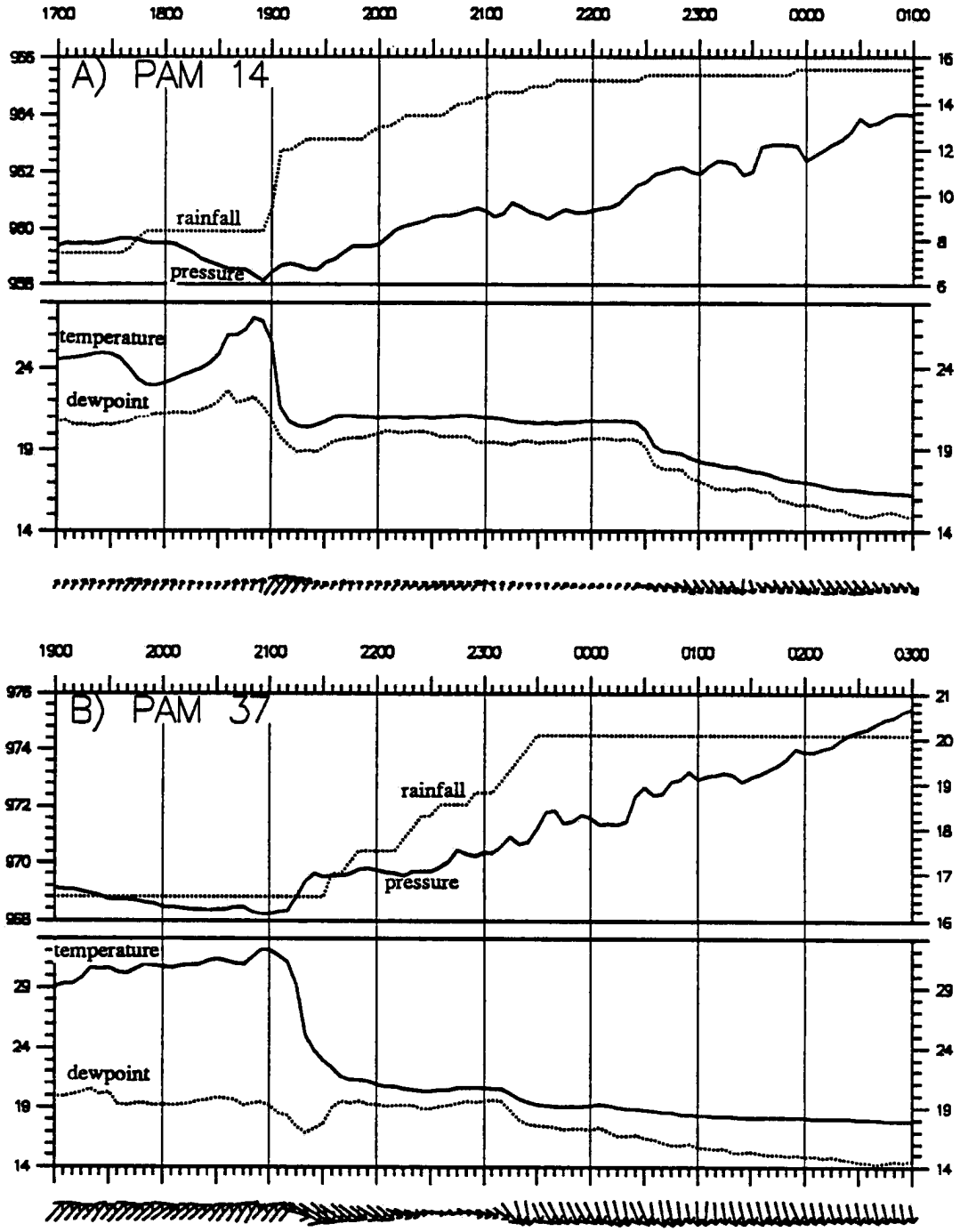

Fig. 3.19: Same as Fig. 3.5, except at a) PAM 14, for the 8 h following 1700 UTC; b) PAM 37, for the 8 h following 1900 UTC c) SAM 10, for the 8 h following 2100 UTC; d) SAM 12, for the 8 h following 2100 UTC; e) SAM 31, for the 8 h following 2100 UTC; f) SAM 40, for the 8 h following 2200 UTC.

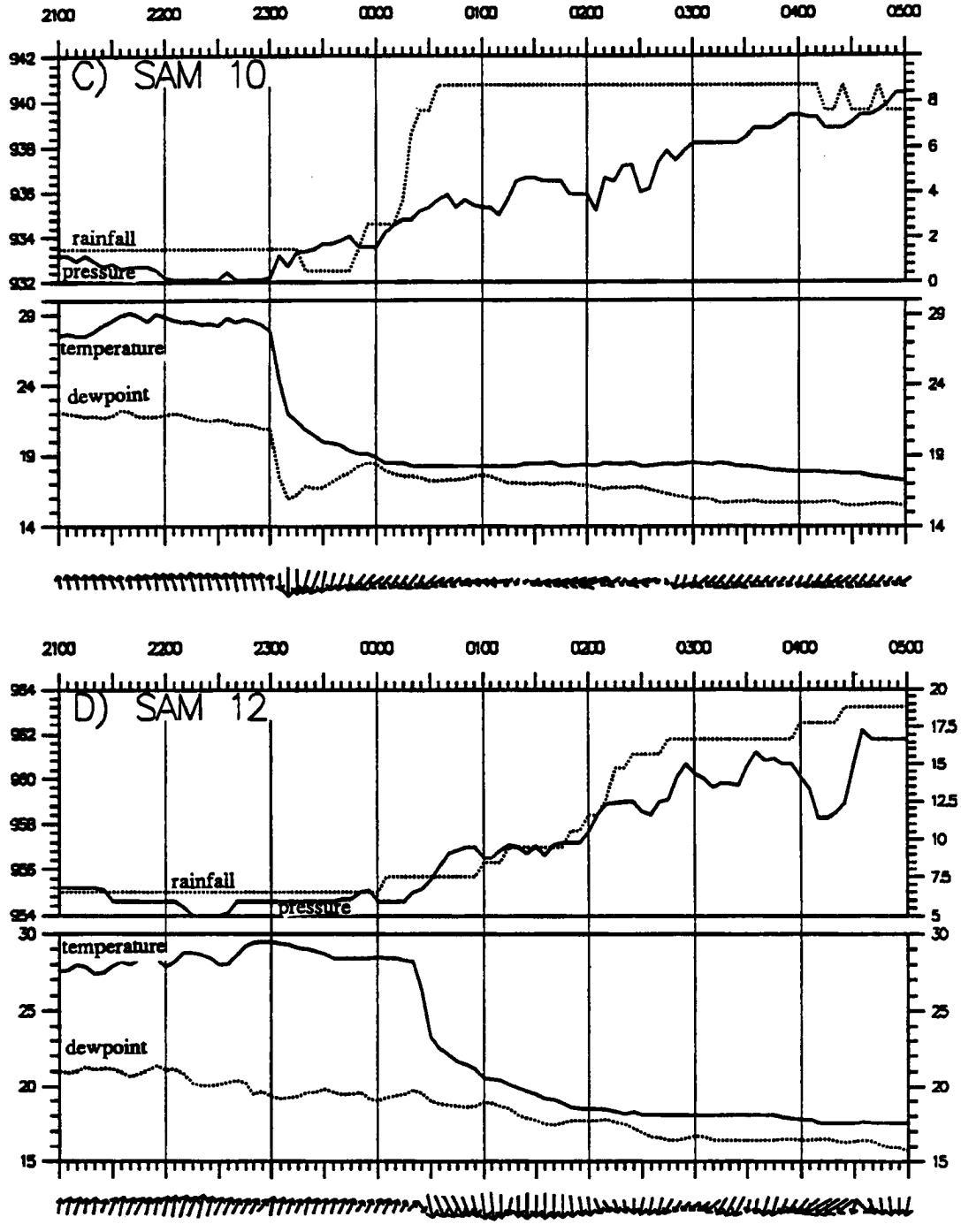

Fig.3.19: Continued.

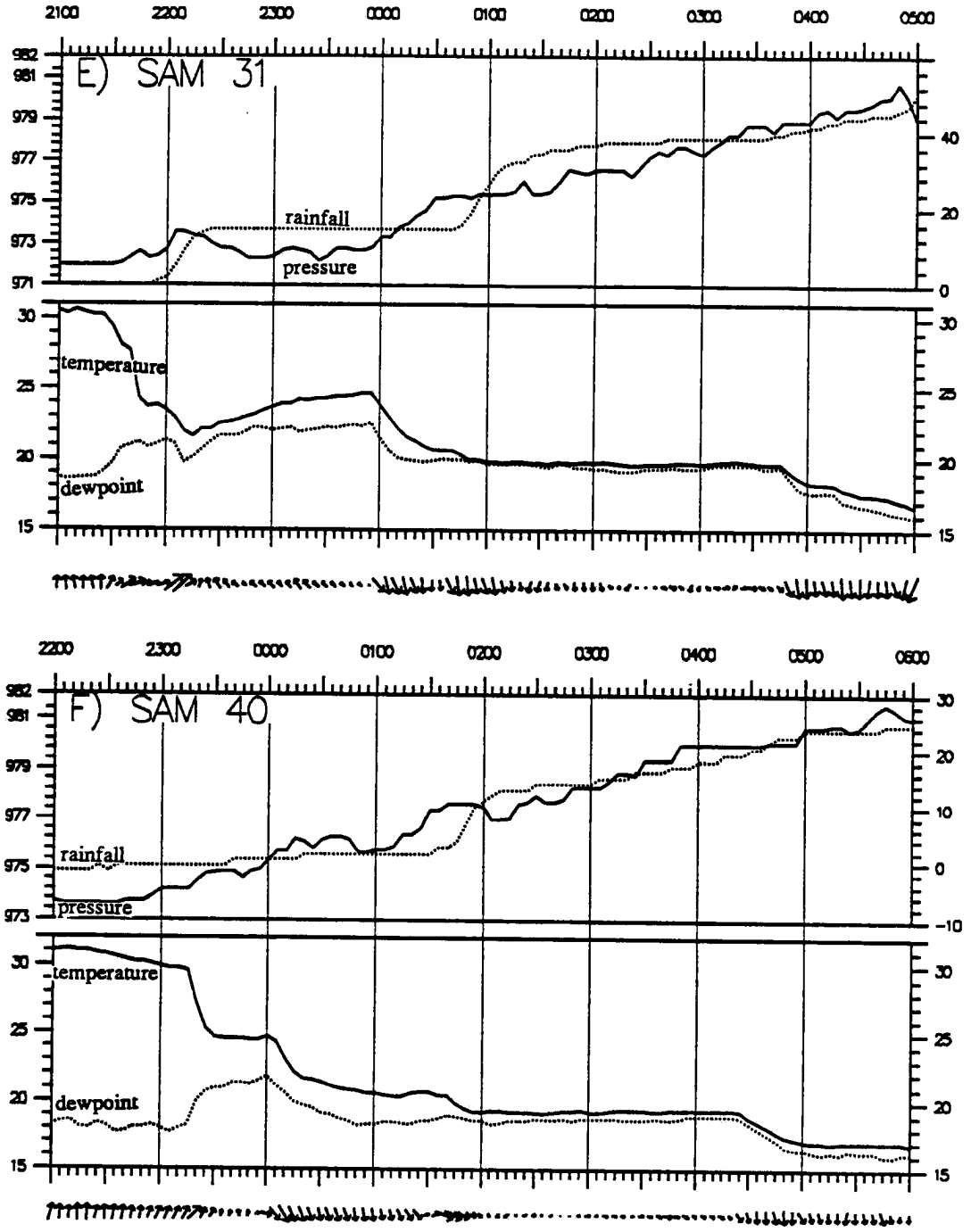

Fig. 3.19: Continued.

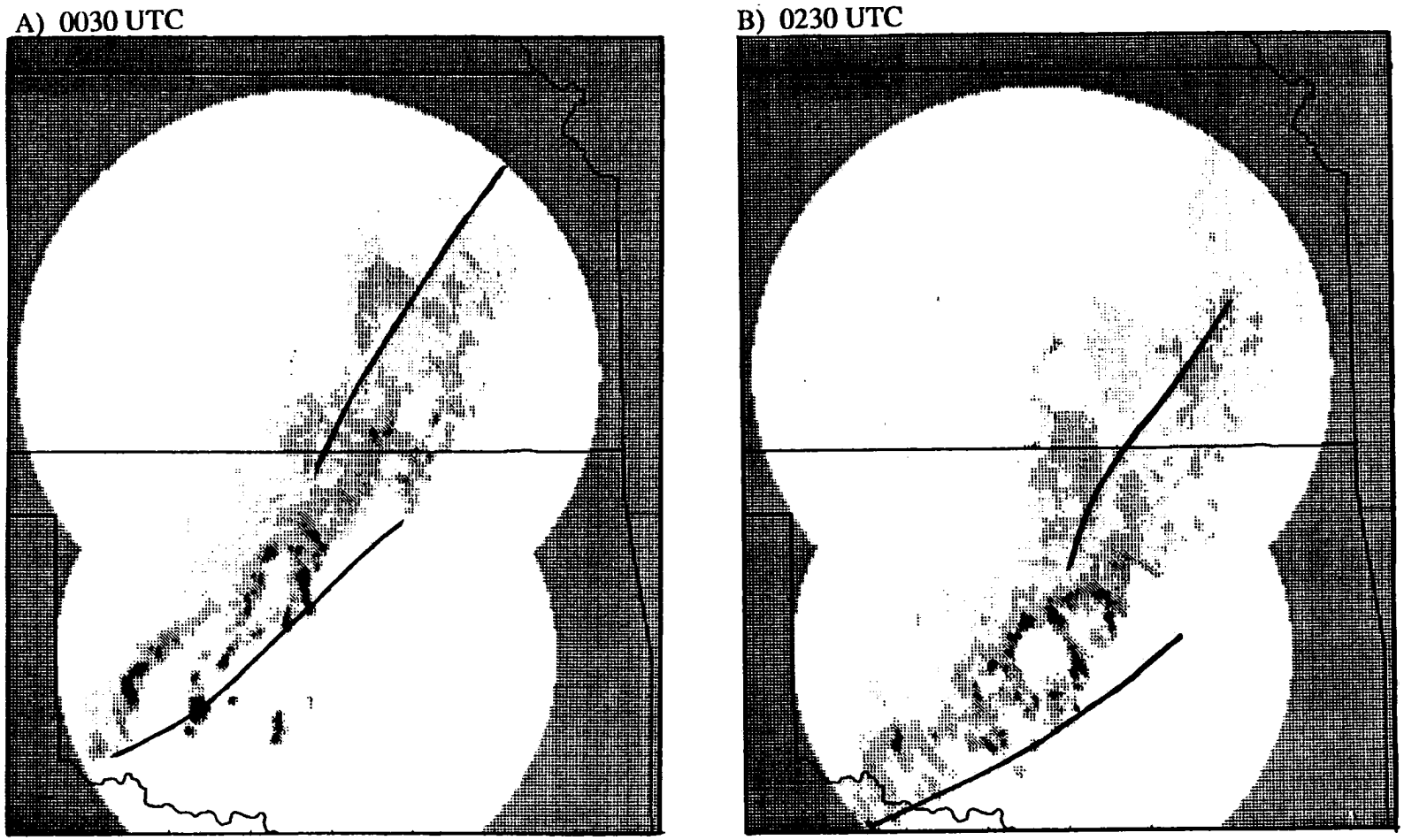

Fig. 3.20: Same as Fig. 3.9 except at a) 0030 UTC, 27 June; b) 0230 UTC, 27 June; and c) 0530 UTC, 27 June.

C) 0530 UTC

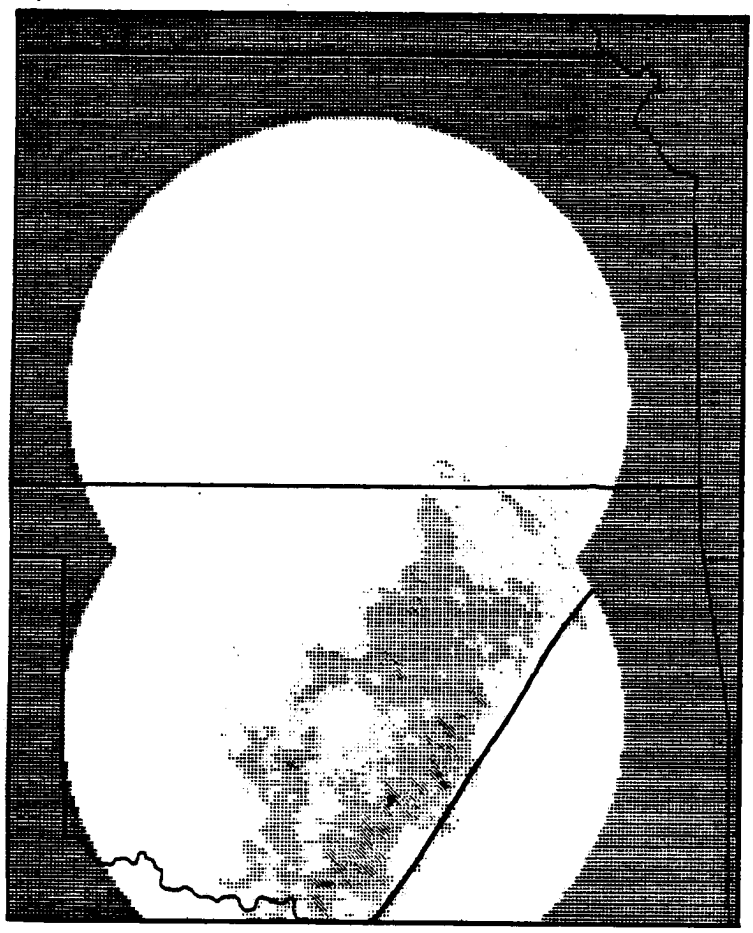

Fig. 3.20: Continued.

evident. The dissipation of the system was also evident from the satellite images (Fig. 3.3), as discussed in section 3.1.

As the front began to move out of the surface network, the two different frontal signatures discussed earlier (Section 3.2.3) were still evident (Fig. 3.21). In the north, the front was characterized by small drops in temperature and dewpoint and a wind shift from light and variable to northwesterly at 8 - 10 m s^{-1}. In the south, the front was marked by large drops in temperature, noticeable (but not large) drops in dewpoint, and a wind shift from southwesterly at 0 - 5 m s^{-1} to northerly at 7 - 10 m s^{-1}. These two sections of the front did not seem to join. In fact, the southern part of the front apparently extended northeastward (ahead of the northern part of the front) as the strong prefrontal outflow boundary.

3.3 Summary of observations

The main points of this chapter are reiterated below:

• The main feature of the synoptic scale situation before the system began was a front moving into a low-to-moderate CAPE, low-to-moderate shear environment, with a band of low to middle level clouds ahead of it remaining from previous convection. The area was in the right entrance region of an upper-tropospheric jet streak.

• The early convection in this MCS developed ahead of the front and moved in a north-northeasterly direction, paralleling the front. Eventually, the convection became more general in the PRE-STORM area and formed a rather disorganized squall line. The convection was never strong, nor long-lived, nor well-organized, and was not followed by a well-defined stratiform region.

• Even though the convection was not strong and the system did not resemble the "classic" squall line in terms of the horizontal structure, in the vertical cross sections, the

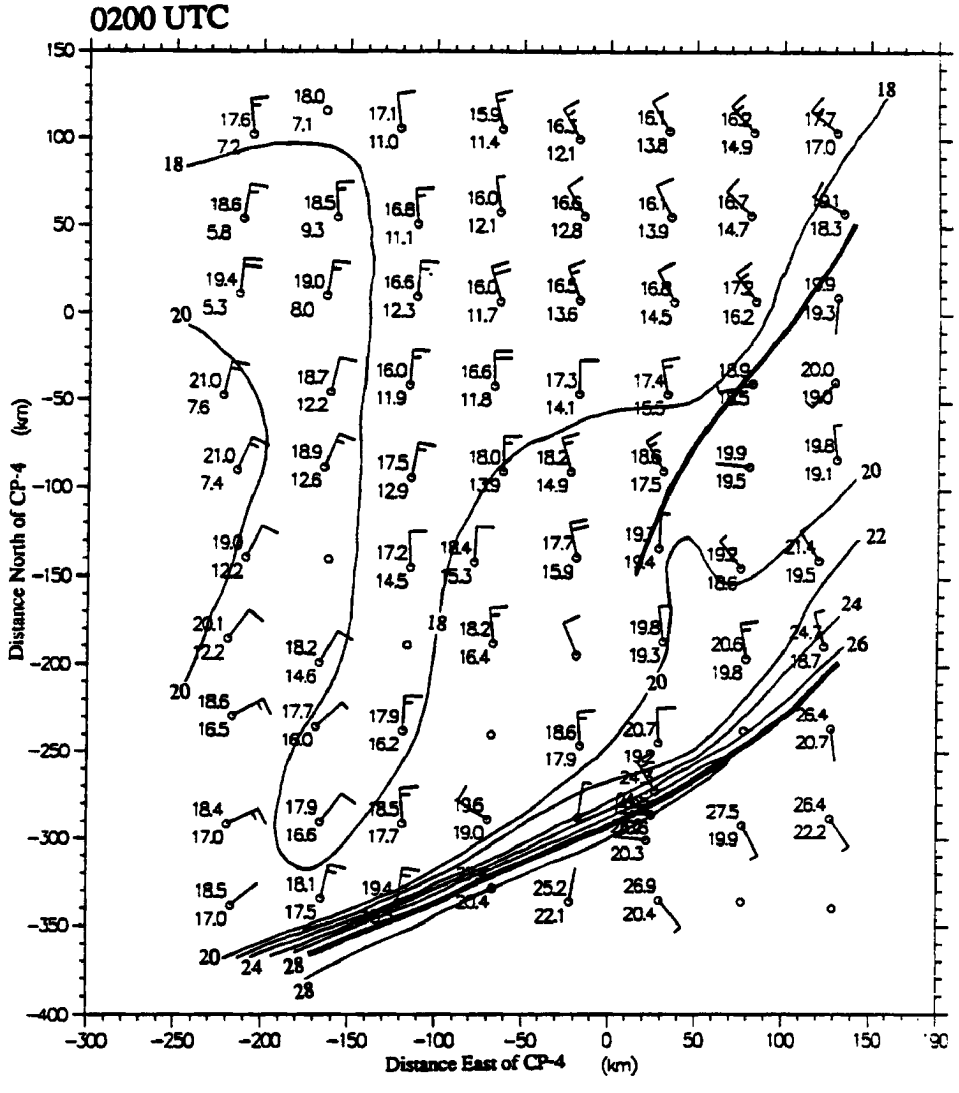

Fig. 3.21: Same as Fig. 3.4, except at 0200 UTC, 27 June.

system had the same line-normal flow structure often seen in the more organized squall lines. This observation suggests that the flow structure may be more common than just the "classic" squall lines.

• Convection modified the prefrontal environment such that the front, at first quite distinct, later became rather difficult to find.

• As the front became ill-defined, outflow boundaries became the dominant feature in the surface observations in Kansas. These boundaries produced a large temperature gradient 100 - 200 km ahead of the front.

Chapter Four

SIMULATIONS OF THE 26 - 27 JUNE 1985 PRE-STORM MCS

The goal of the modelling phase of this study was to simulate the 26 - 27 June 1985 PRE-STORM MCS in an attempt to expand the mesoscale analyses with details that could not be obtained from the observations. The model used in this study was the Regional Atmospheric Modelling System (RAMS), developed at Colorado State University. Original plans were to first simulate the system on a large domain with a resolution of 75 km, initializing the model with the synoptic-scale observations, and to eventually nest down to such a scale that convective parameterization would not be needed, but convection could be simulated using explicit microphysical processes. Unfortunately, this goal proved to be impracticable, as discussed in Section 4.4, below. However, the simulations on the 75 and 25 km scales did produce some interesting results. But since the original goals of this study included explicit resolution of convection, two-dimensional simulations with full microphysics were attempted. These simulations, however, were unsuccessful.

In Section 4.1 of this chapter, RAMS and the options selected for this study are briefly described. In Section 4.2, the results of the three-dimensional simulations are presented and discussed. In Section 4.3, the two-dimensional simulations are discussed. A summary of the modelling study is presented in Section 4.4.

4.1 The Regional Atmospheric Modelling System (RAMS)

The Regional Atmospheric Modelling System is a result of the merger of a hydrostatic mesoscale model (Pielke, 1974; Mahrer and Pielke, 1977) and a non-hydrostatic cloud

model (Tripoli and Cotton, 1982, 1989a,b). A more extensive description of RAMS may be found in Tremback (1990). Some of the options selected for the simulations discussed in this thesis are listed here:

- The non-hydrostatic version was selected.
- A simplified Kuo-type convective parameterization (Kuo, 1974; Tremback, 1990) was used to parameterize the subgrid-scale effects of convection. Since information on the convective parameterization scheme is important for the discussion to follow, it is described in more detail below.
- The "supersaturation condensed" microphysics option was selected. This option allows for the production of cloud water and the associated latent heating by resolvable-scale motions, but does not allow for precipitation. No ice effects were included.
- The radiation parameterization of Chen and Cotton (1983) was selected for both long-wave and short-wave radiation.
- The surface layer and soil model of Tremback and Kessler (1985) was selected as a bottom boundary condition, with a constant soil type of clay loam.
- The Klemp/Wilhelmson (1987a,b) lateral boundary conditions were selected.
- A solid wall was placed at 16.5 km as a top boundary condition.

The convective parameterization scheme (Tremback, 1990) provides the convective heating and moistening profiles for the model. The profile of convective heating, Q_1, is based on potential temperature profiles calculated for updrafts and downdrafts. The updraft potential temperature profile is defined as the potential temperature of the moist adiabat of the source-level air lifted to its lifting condensation level (LCL). The downdraft potential temperature profile is somewhat arbitrarily defined as follows: The downdraft is assumed to start at the θ_e minimum of the column, where its potential temperature is that of the environment. At cloud base, the potential temperature of the downdraft is taken to be 2 K colder than that of the environment; and at the surface, 5 K colder than that of the

environment. The Q_1 profile is then calculated as the difference between the environmental potential temperature profile and a weighted average of the updraft and downdraft profiles. The profile of convective moistening, Q_2, is based on the resolved vertical flux of water vapor through the LCL, *i.e.*, the rate at which the resolvable scale supplies moisture to a column. A precipitation efficiency, based empirically on the environmental shear, determines what fraction of the supplied moisture moistens the column. The remainder of the moisture falls out as convective precipitation and its latent heat warms the column. The convective parameterization scheme is activated if a positive vertical velocity threshold is exceeded at cloud base. In these simulations, a threshold of 0.009 m s^{-1} was used.

This study employed nested grids, which are shown with the terrain in Fig. 4.1. The coarse grid had a resolution of 75 x 75 km in the horizontal, with 60 points in the x-direction and 45 points in the y-direction. The coarse-grid domain thus covered an area of 4425 x 3300 km, which included most of the continental United States. The nested grid had a resolution of 25 x 25 km in the horizontal (a 3:1 nesting ratio), with 65 points in the x-direction and 62 points in the y-direction. The fine grid thus had dimensions of 1600 x 1525 km and was positioned so as to include the PRE-STORM area. The vertical grid spacing was the same for both coarse and fine grids: a total of 27 points in the vertical with a 300 m spacing at the surface stretching to 750 m at the top of the model domain (16.5 km). There were an additional 11 soil gridpoints for the surface layer and soil model.

4.2 Three-dimensional simulations of the 26 - 27 June PRE-STORM MCS

The three-dimensional simulations for this study are discussed in this section. First, the initial conditions are discussed. Second, the results of the coarse-grid simulations,

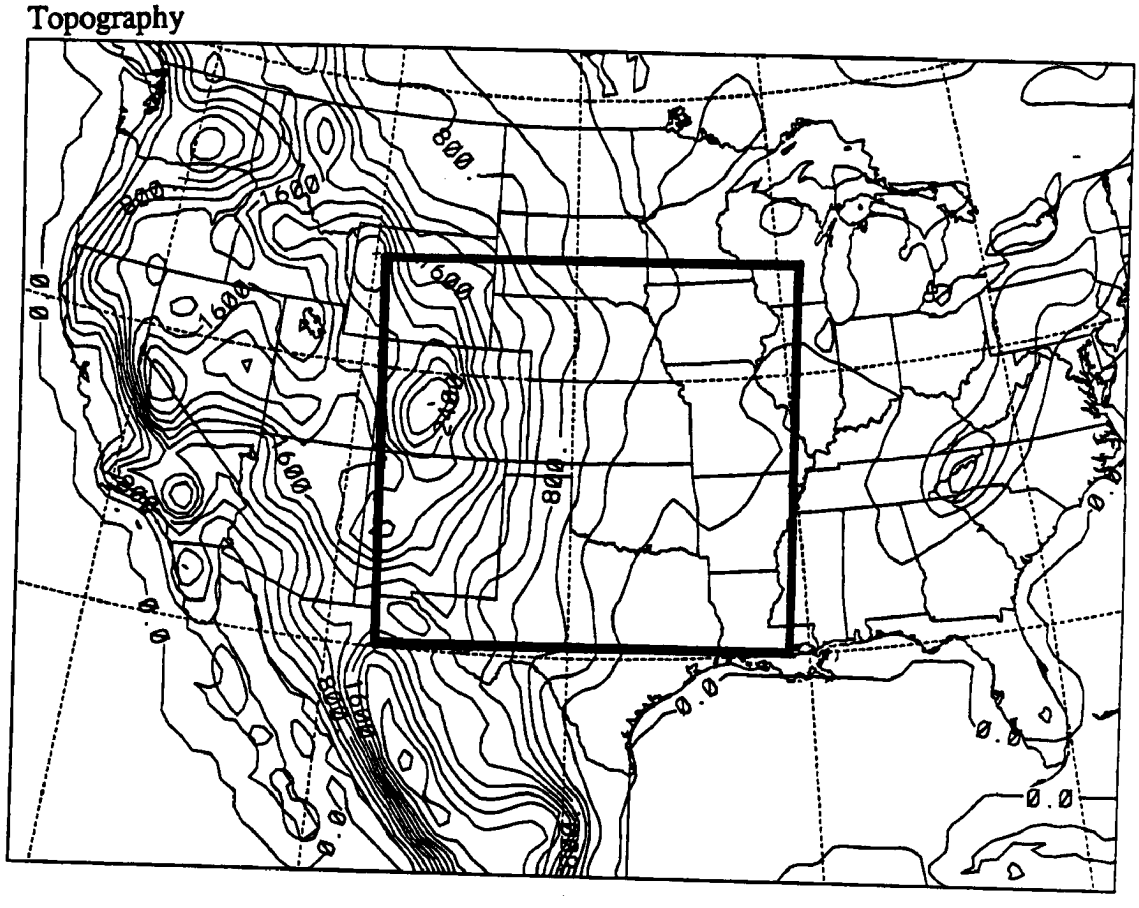

Fig. 4.1: The coarse-grid model domain, with the topography used in the simulations (contour interval of 200 m). The heavy inner rectangle outlines the fine-grid model domain.

performed without the nest, are examined. Finally, the results of the fine-grid simulations are examined and compared to selected PRE-STORM observations.

4.2.1 Initial conditions

The model was initialized with the standard surface and upper-air observations from 1200 UTC, 26 June 1985. The National Meteorological Center's spectral analysis on pressure surfaces (with 2.5° resolution) was first vertically interpolated to isentropic surfaces, and then enhanced to include the surface and rawinsonde observations. The enhanced fields were then interpolated to the model grid. The initial low-level wind field for the simulations is shown in Fig. 4.2. Superimposed on the wind field are the wind-shift line in the model field (heavy solid line) and the location of the front as analyzed by the National Meteorological Center (heavy dashed line). Note that if the front is defined as the wind-shift line in the model fields, the front in the simulation started out with a displacement of up to 100 km from the observed frontal position. This displacement is not large considering that the grid spacing of the model was 75 km. In the PRE-STORM area, however, the front in the initialization was quite close to the observed frontal location.

4.2.2 The coarse-grid three-dimensional simulation

For the coarse-grid simulation, the model was initialized with the 1200 UTC fields described above and run for 12 h of model time. The coarse-grid simulation reproduced the general features of the synoptic-scale situation, and developed convection in some of the right areas. For example, Fig. 4.3 shows the simulated low-level (146 m) wind field after 6 and 12 h. Also shown is the wind-shift position predicted by the model (heavy solid line) and the location of the observed surface front as analyzed by the National Meteorological Center (heavy dashed line). Even after 12 h, the errors in the frontal

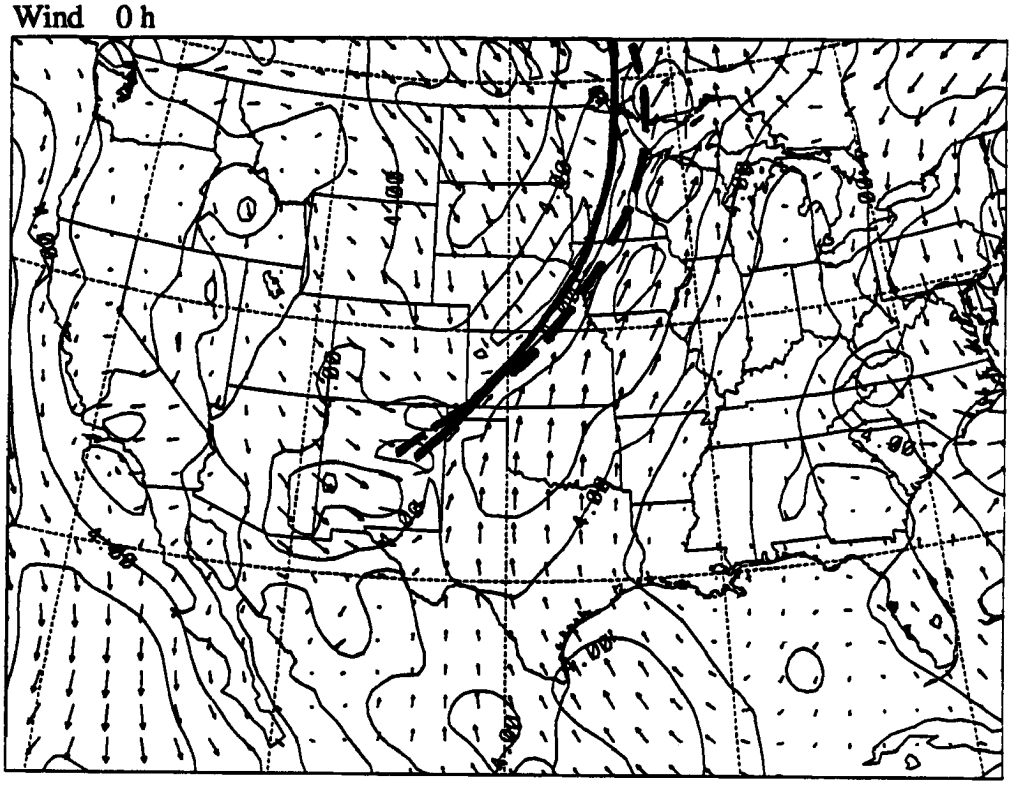

Fig. 4.2: The initial low-level (146 m) wind field on the coarse grid. Heavy solid line shows the location of the wind-shift line. Heavy dashed line shows the location of the surface front as analyzed by the National Meteorological Center. Wind speed is contoured with a 2 m s^{-1} contour interval.

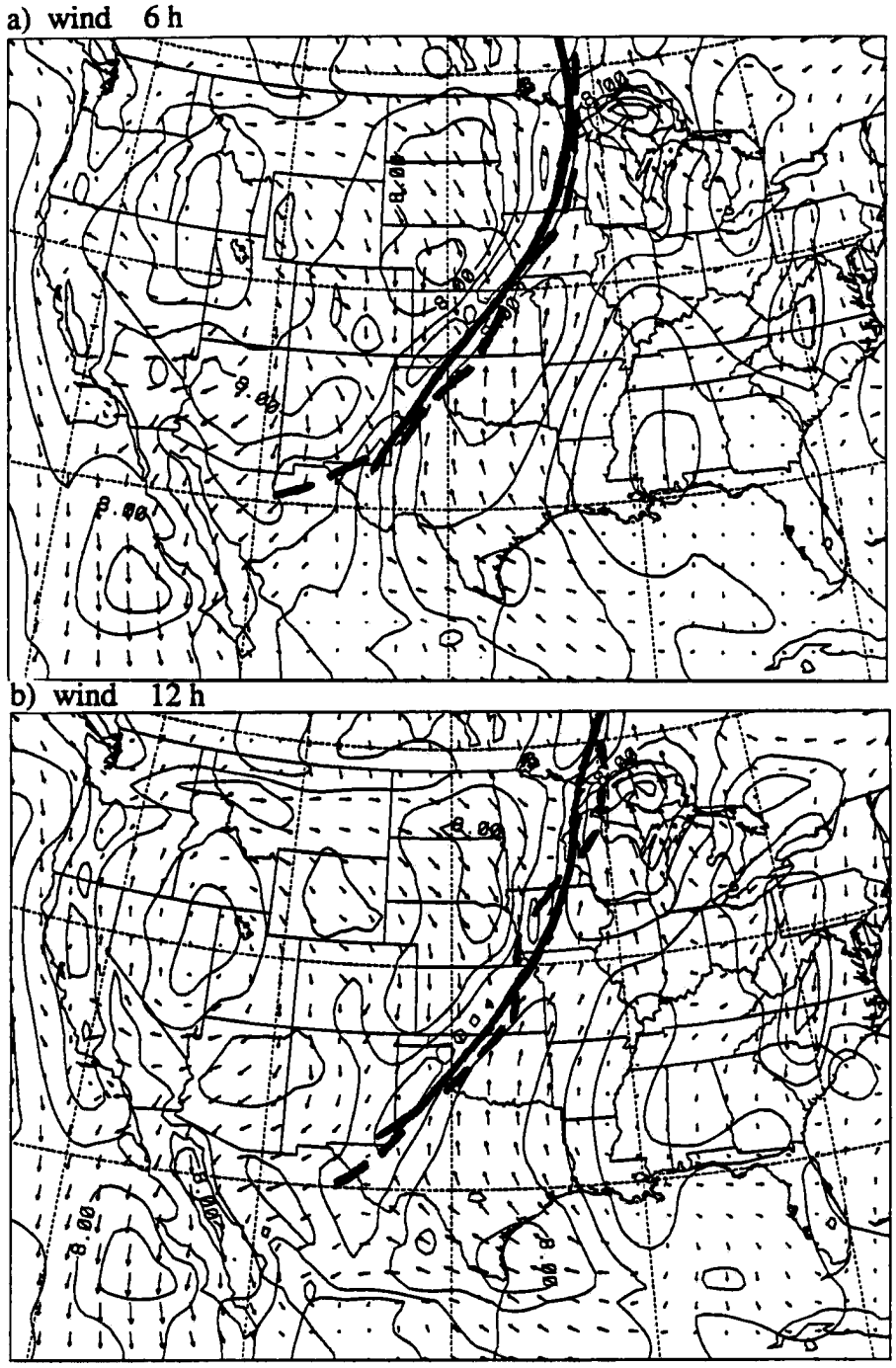

Fig. 4.3: The low-level (146) wind field in the coarse-grid simulation a) after 6 h of model time; b) after 12 h of model time. Heavy solid line show the position of the front in the model fields. Heavy dashed line shows the position of the surface front as analyzed by the National Meteorological Center. Wind speed is contoured with a 2 m s^{-1} contour interval.

location were no greater than in the initialization – no greater than approximately 100 km – and were generally within the resolution of the simulation. In other respects as well, the model results compared well to the observations. Compare, for example, the model wind field at 5153 m (about 540 mb) after 12 h (Fig. 4.4a) and at 11156 m (about 230 mb) after 12 h (Fig. 4.4b) to the 500 and 200 mb observations taken at 0000 UTC, 27 June (Fig. 3.2b and d). The model simulated well the tilt of the trough with height and the slow movement of upper-level features, as well as the location and magnitude of the jet streak.

The model field of convective precipitation rate (from the convective precipitation scheme) had some similarities to observations, but the model did have problems simulating convection on this scale. Compare, for example, the model field of convective precipitation rate after 6 h (Fig. 4.5a), to the NMC national radar summary at the corresponding time, 1735 UTC (Fig. 4.6a). The model predicted the location of the convection with some accuracy in the Kansas area, with values of convective precipitation rate up to about 0.9 mm h^{-1}, where the radar summary showed a line of level 5 echoes along the front. The model was also able to reproduce some of the observed convection in Iowa and southern Minnesota. However, the local maxima of convective precipitation rate in Wisconsin and Illinois had no counterpart in the NMC radar summary, and although the satellite image corresponding to this time (Fig. 3.3b) shows some convection in Northern Mexico, it was not as extensive as depicted in the model. Even where the model did predict convection with some accuracy, the area of parameterized convection was usually considerably more widespread than the area of observed deep convection. For example, the narrow band of level 3 and 5 echoes observed in Kansas and Oklahoma became a much wider band of precipitation in the simulations. After 12 h (Fig. 4.5b; compare to Fig. 4.6b), the model model results looked much as they did after 6 h. The maximum of the convective precipitation rate in the Kansas-Oklahoma area was about 0.6 mm h^{-1}, even less than it was at 6 h. The radar summary, however, shows a line of convective echoes much more extensive than 6 h earlier. While the model produced a band of convection in

a) 5153 m

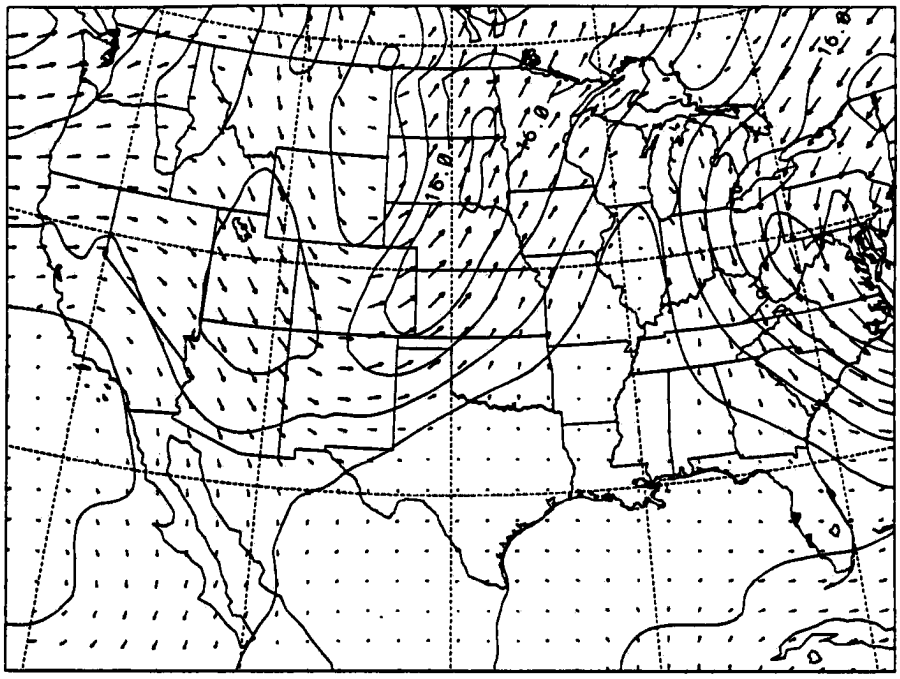

b) 11156 m

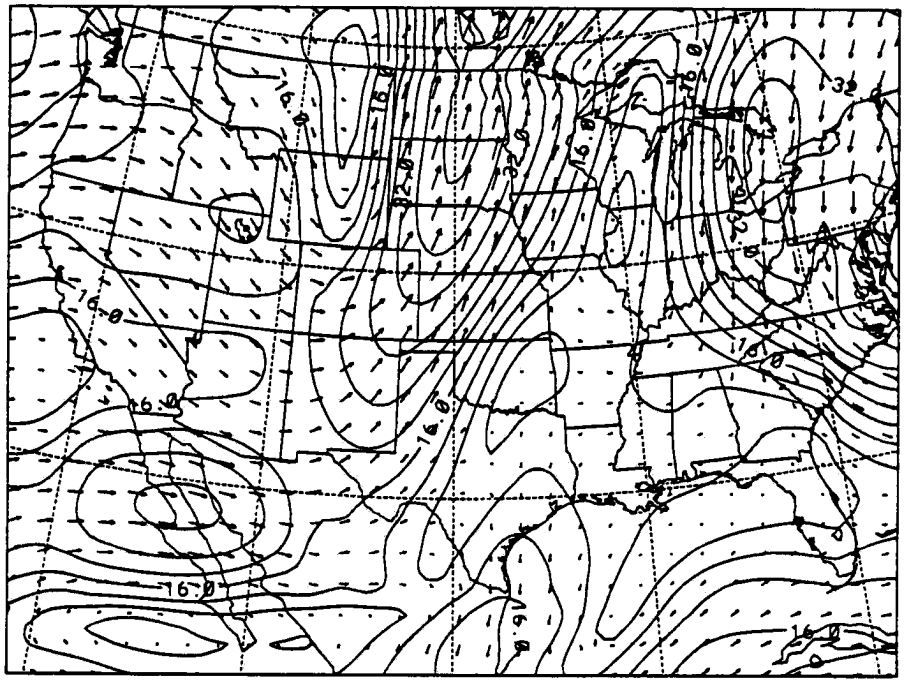

Fig. 4.4: Coarse-grid wind field a) at 5153 m (about 540 mb) and b) at 11156 m (about 240 mb) after 12 h of model time. Contour interval for wind speed is 4 m s^{-1}.

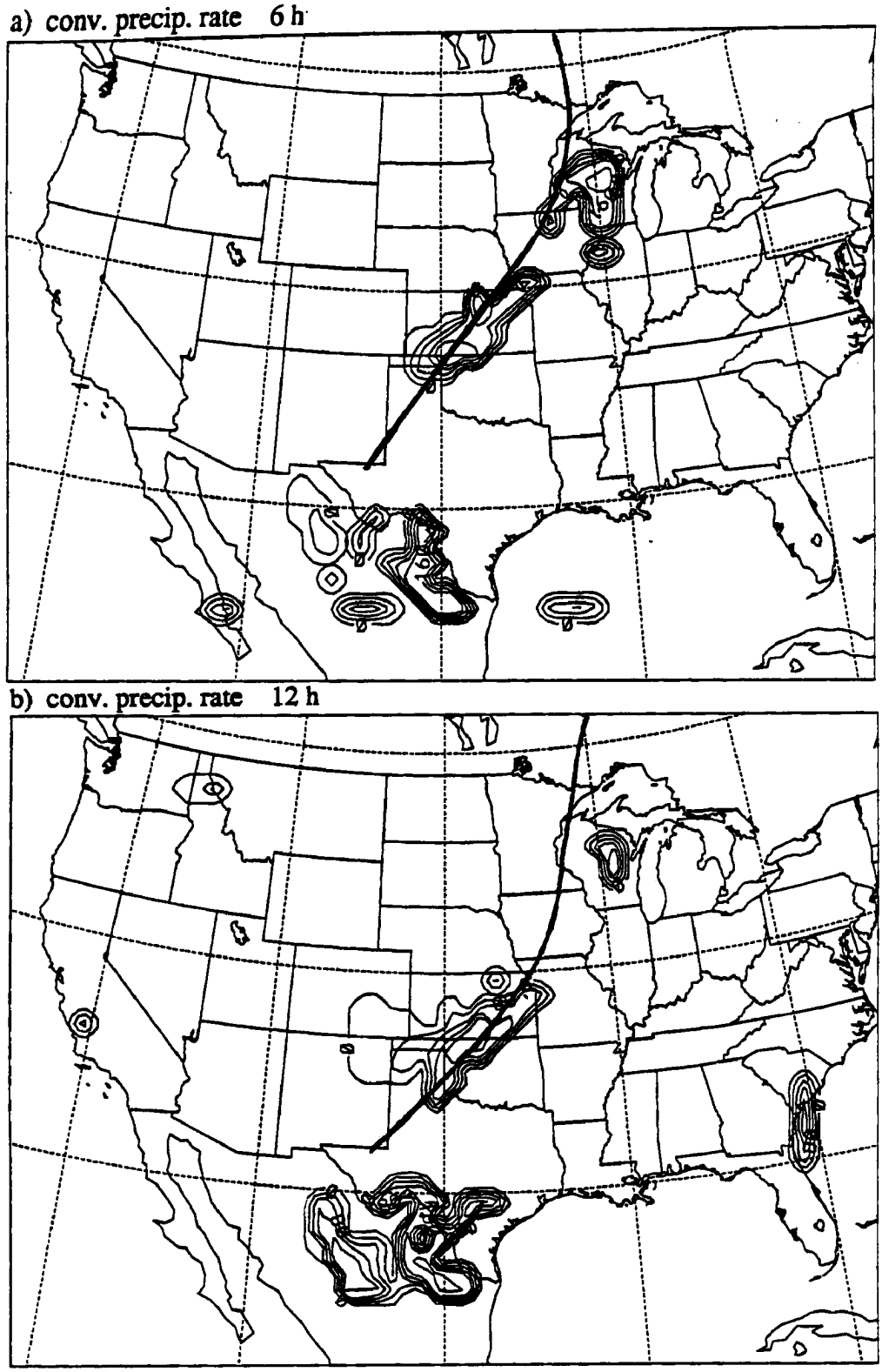

Fig. 4.5: Coarse-grid field of convective precipitation rate a) after 6 h; b) after 12 h. Heavy solid line shows location of front in the model output. Contour interval is 4 x 10^{-5} mm s^{-1} (0.144 mm h^{-1}).

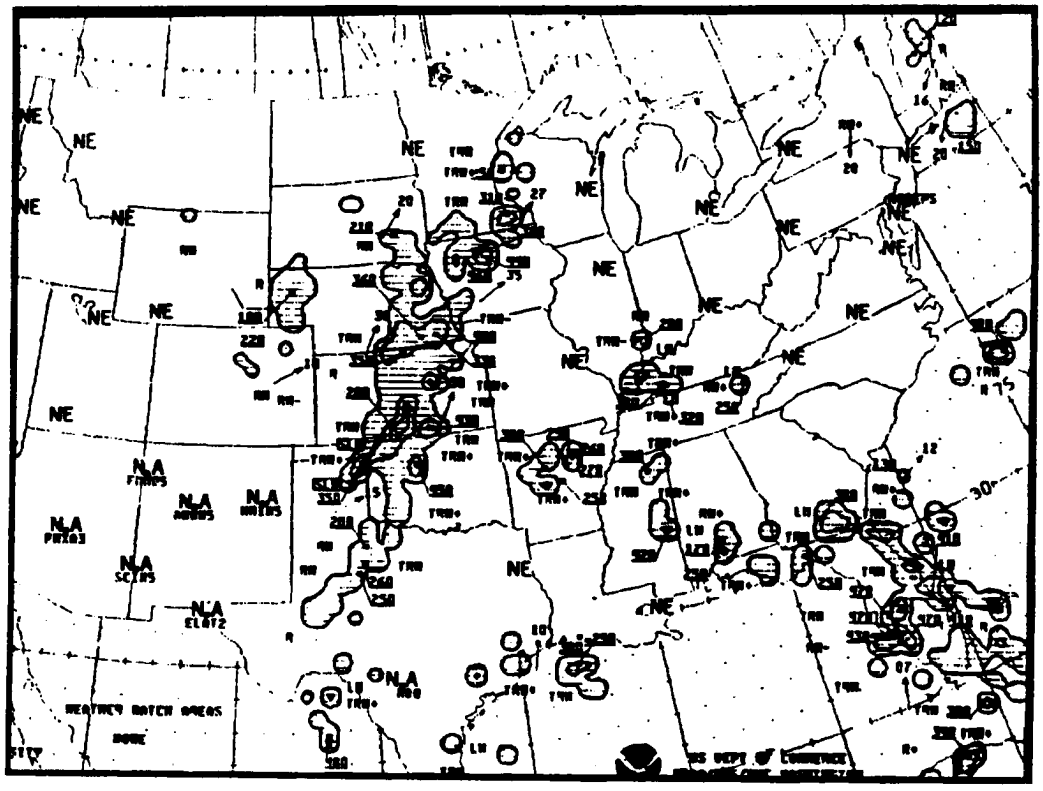

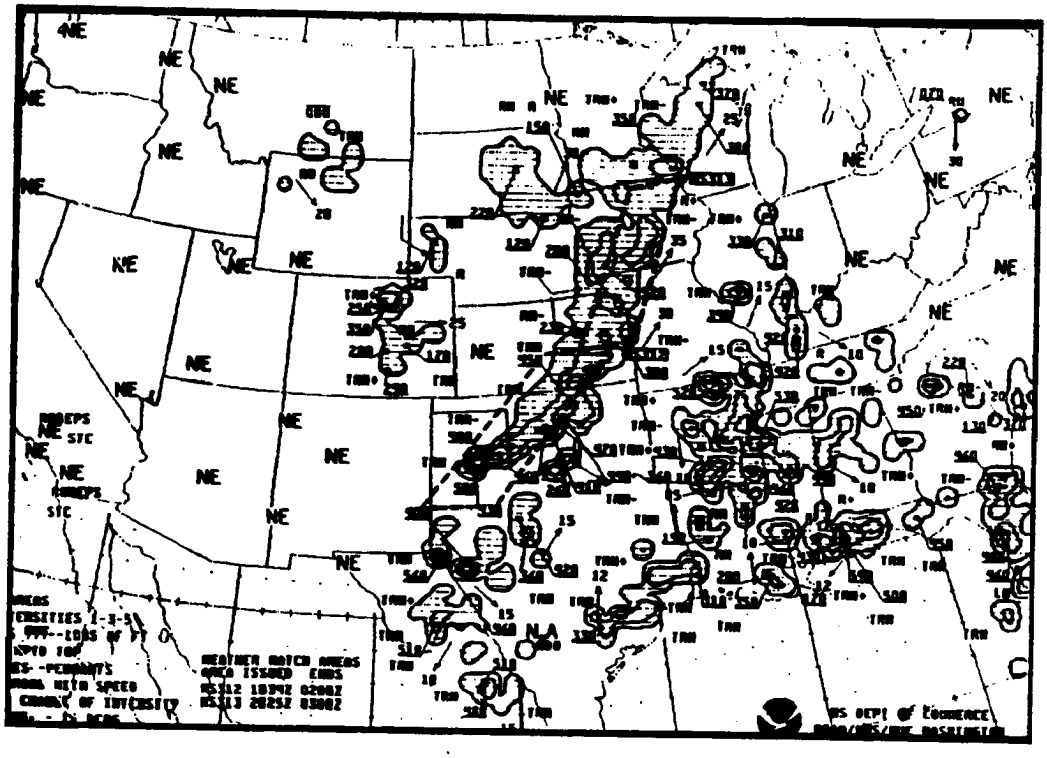

Figure 4.6: NMC national radar summary a) at 1735 UTC, 26 June 1985; b) at 2335 UTC, 26 June 1985.

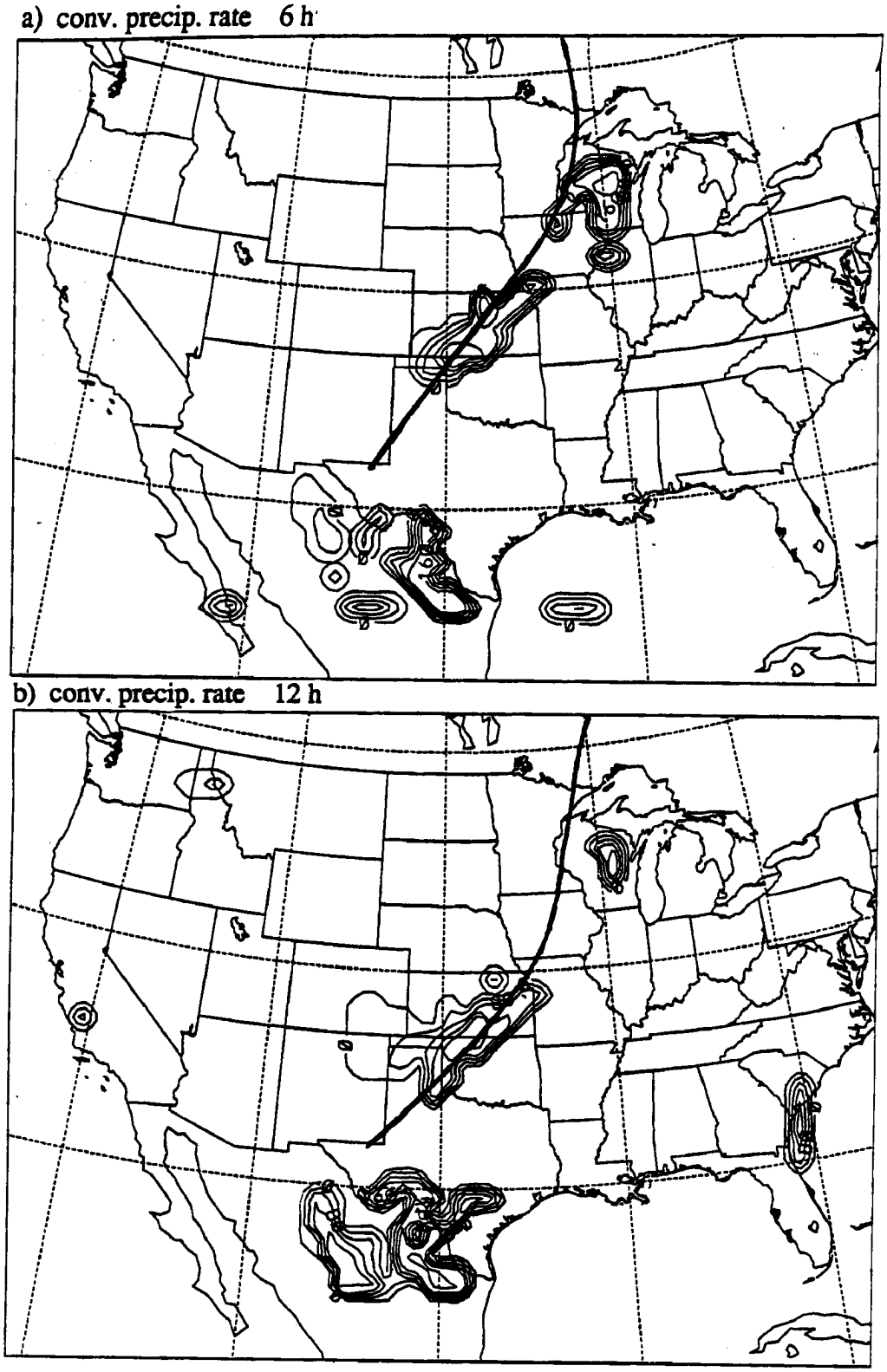

Fig. 4.5: Coarse-grid field of convective precipitation rate a) after 6 h; b) after 12 h. Heavy solid line shows location of front in the model output. Contour interval is 4 x 10^{-5} mm s^{-1} (0.144 mm h^{-1}).

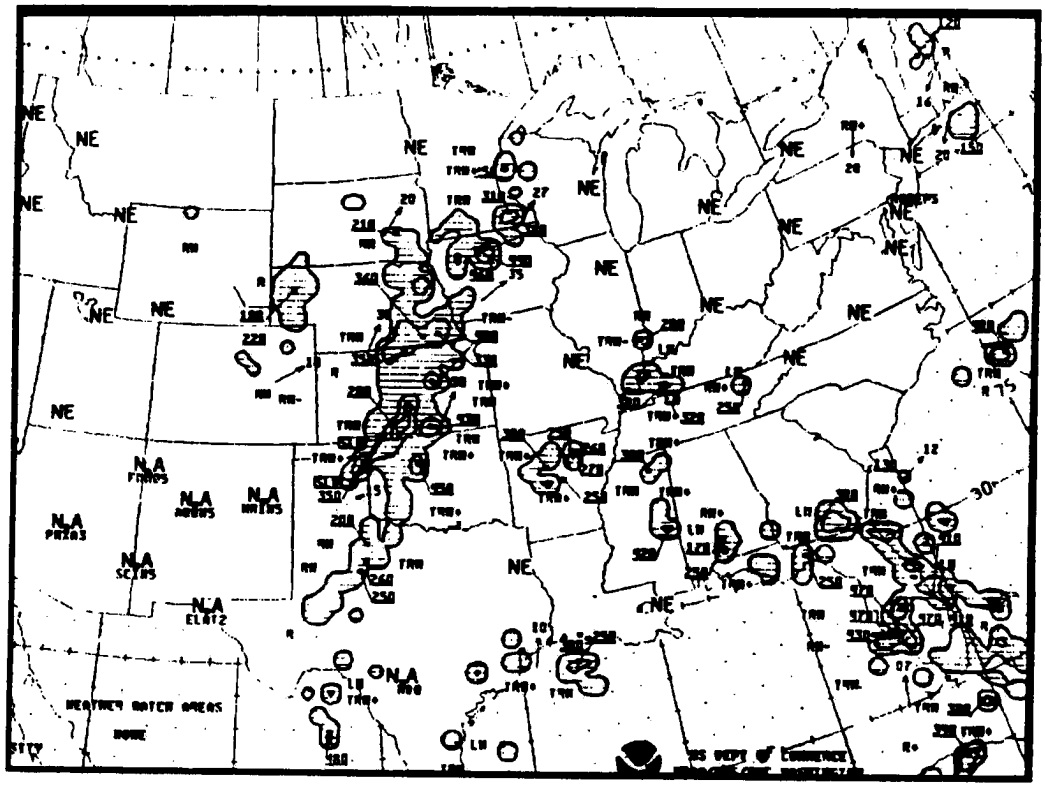

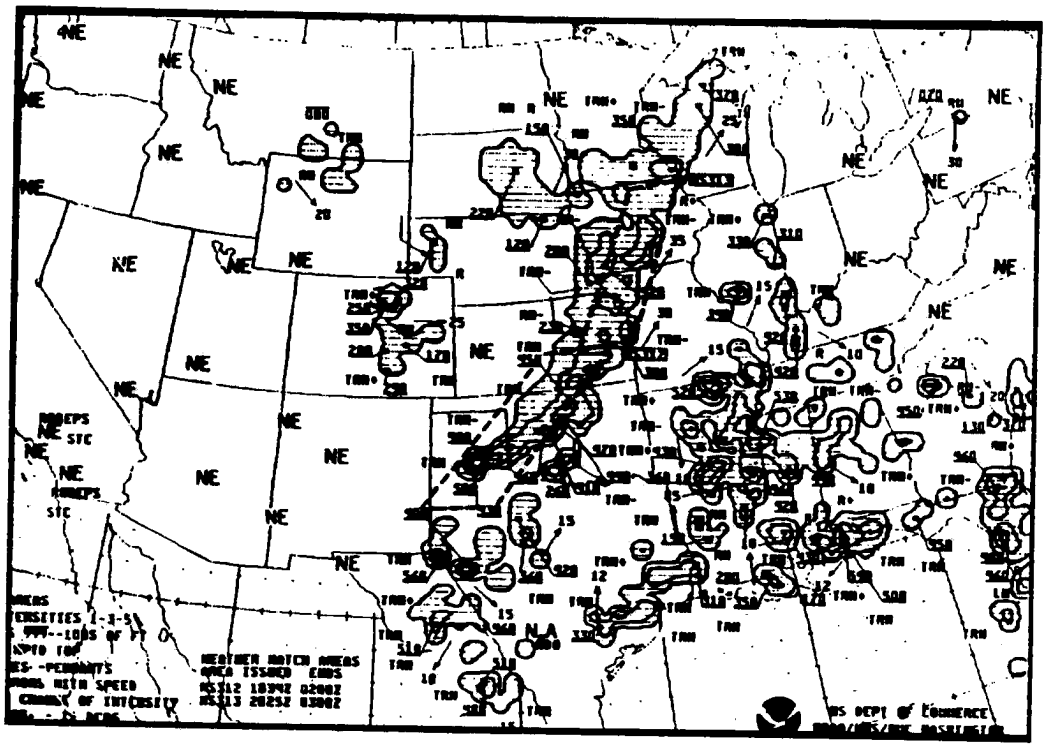

Figure 4.6: NMC national radar summary a) at 1735 UTC, 26 June 1985; b) at 2335 UTC, 26 June 1985.

approximately the right area, in the region of Oklahoma and Kansas, again it was much more spread out than the observed convection. The model did not develop much other convection shown by the radar summary along other parts of the front, or what was apparently "air-mass" convection in the southeastern United States.

Perhaps the most important factor affecting the simulation of the convection on the coarse grid was the resolution of the model. The model apparently had some difficulty resolving frontal convergence on a grid with spacing of 75 km. Sensitivity runs in which the minimum vertical velocity needed to initiate convection was varied indicated that even with a threshold as low as 0.001 m s^{-1}, convection would not occur in many places along the front. Similarly, the low-level (146 m) vertical velocity field (Fig. 4.7) shows only minimal upward motion along the front. These results suggest that the low-level convergence was too small to induce sufficient vertical velocities along the front to activate the convective parameterization scheme in many places. This conclusion is supported by the success of the fine-grid simulations in developing a more significant line of convection along the front (as discussed in the next section). The spreading out of the convective lines in the simulation as compared to the observations may be another effect of the resolution. Considering the resolution of the model, this spreading out of the convection is not unreasonable.

4.2.3 The fine-grid three-dimensional simulations

With the anticipation that a finer resolution would resolve convergence well enough to better initiate convection along the front, the fine grid was added and the model restarted from the 1200 UTC initialization, to run for 13 h. A second simulation was performed with the nested grid, but with the convective parameterization scheme deactivated. The first of these simulations, the one which included the convective parameterization scheme, shall

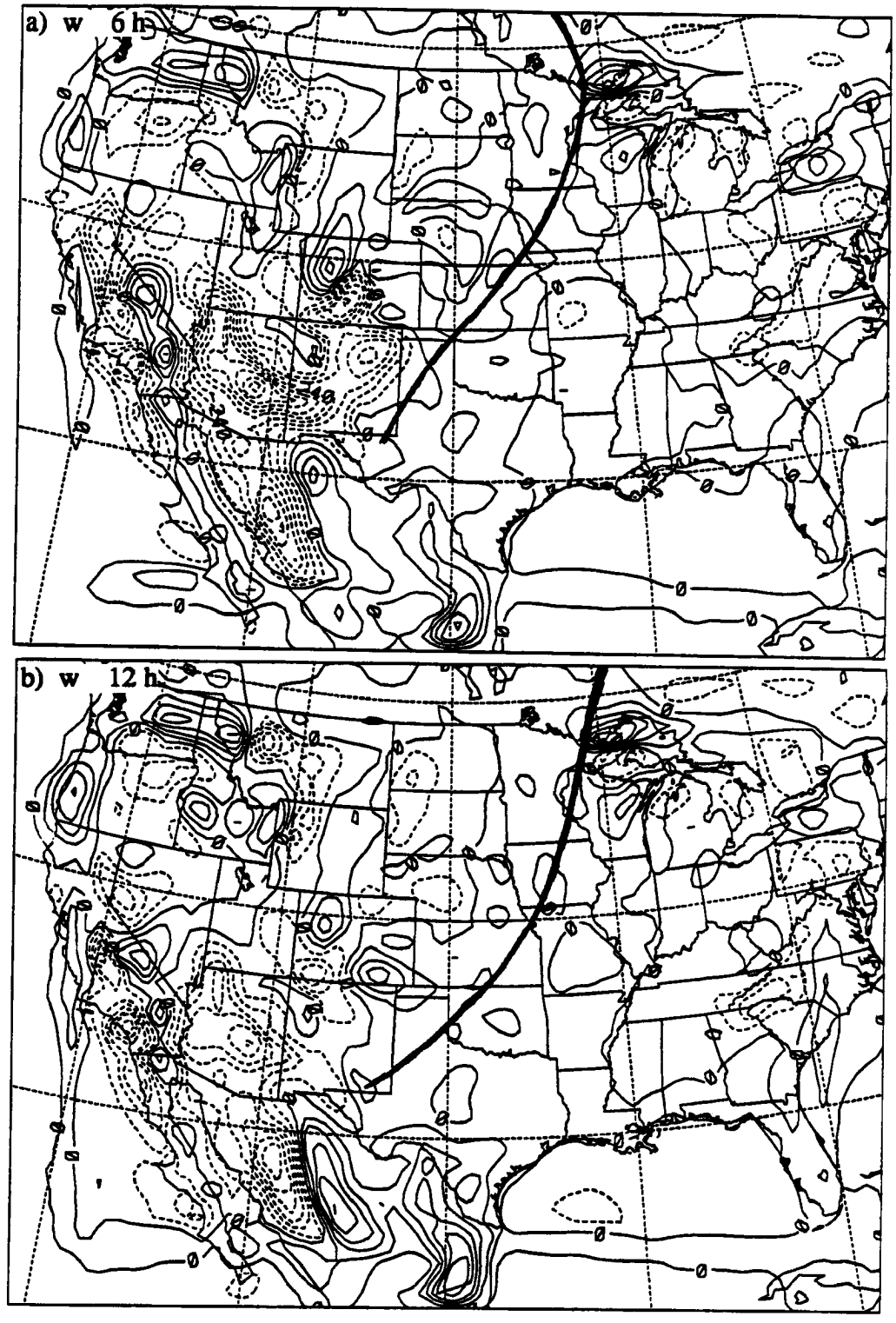

Fig.4.7: The low-level (146 m) vertical velocity field from the coarse grid simulation a) after 6 h; b) after 12 h. Contour interval is 0.006 m s^{-1}.

be referred to as the CP (Convective Parameterization) simulation. The second simulation shall be referred to as the NO-CP (No Convective Parameterization) simulation.

4.2.3.1 Results from the CP simulation

The CP simulation on the 25 km grid captured the gross features of the MCS, but many of the observed features were not simulated. The results are not unreasonable, again considering the resolution of the simulation, and considering the fact that explicit microphysics was not activated. Plots of several of the model fields at the 146 m level are shown in Figs. 4.8 through 4.12. Both the simulated location (solid line) and the observed location of the front as inferred from the PRE-STORM observations (dashed line) are shown in Fig. 4.8. Throughout the simulation, the location of the simulated front was quite close to the observed location. By 10 h, the simulated system had even begun to develop a prefrontal boundary, similar to the development of the gust front from the observed convection. Although the timing of the development of the prefrontal boundary in the simulations did not compare well to observations (the observations show that the outflow boundary was becoming well developed by 2000 UTC, Fig. 3.13d; the prefrontal boundary in the model did not develop until 10 h into the simulation, Fig. 4.8c, corresponding to the time 2200 UTC), the location of the prefrontal boundary was at times close to the observed location of the gust front (*e.g.* Fig. 4.8d). The prefrontal boundary in the simulations was marked in low-level (146 m) plots by a line of confluence, but not a large wind shift (Fig. 4.8d, in contrast to the observations which showed a sharp wind shift, *e.g.* Fig 3.18b); a line of updrafts (Fig 4.9d); a line of convection (Fig. 4.10d); and a gradient of potential temperature (Fig. 4.11). The prefrontal boundary in the simulation was at no time marked by a pressure trough: the pressure trough was always located at the front (Fig. 4.12).

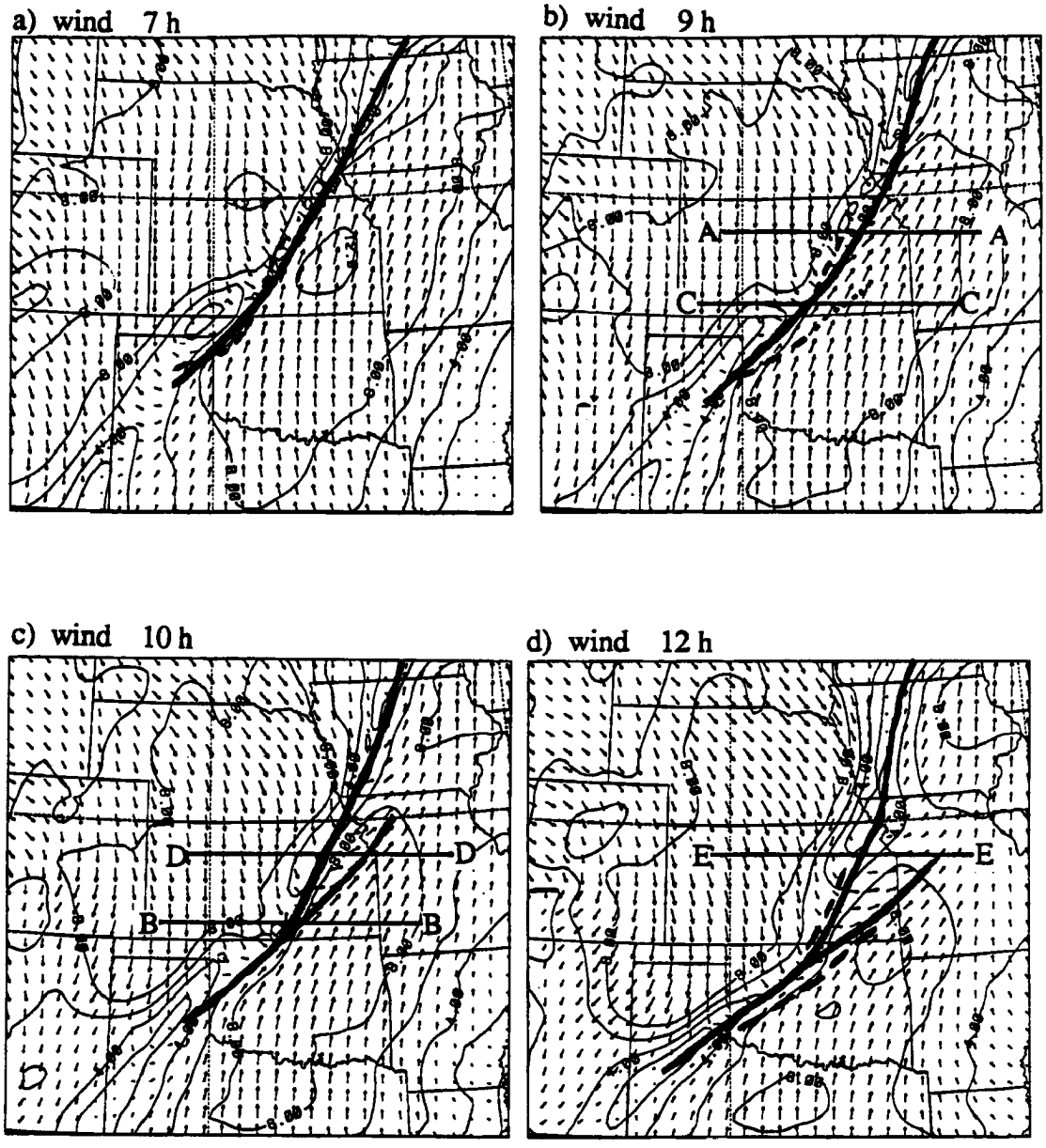

Fig. 4.8: Low-level (146 m) wind field for the CP simulation a) after 7 h; b) after 9 h; c) after 10 h; and d) after 12 h. Contour interval for wind speed is 2 m s^{-1}. Heavy solid line indicates position of front in the model fields. Heavy dashed line indicates position of the observed front as inferred from the PRE-STORM surface observations.

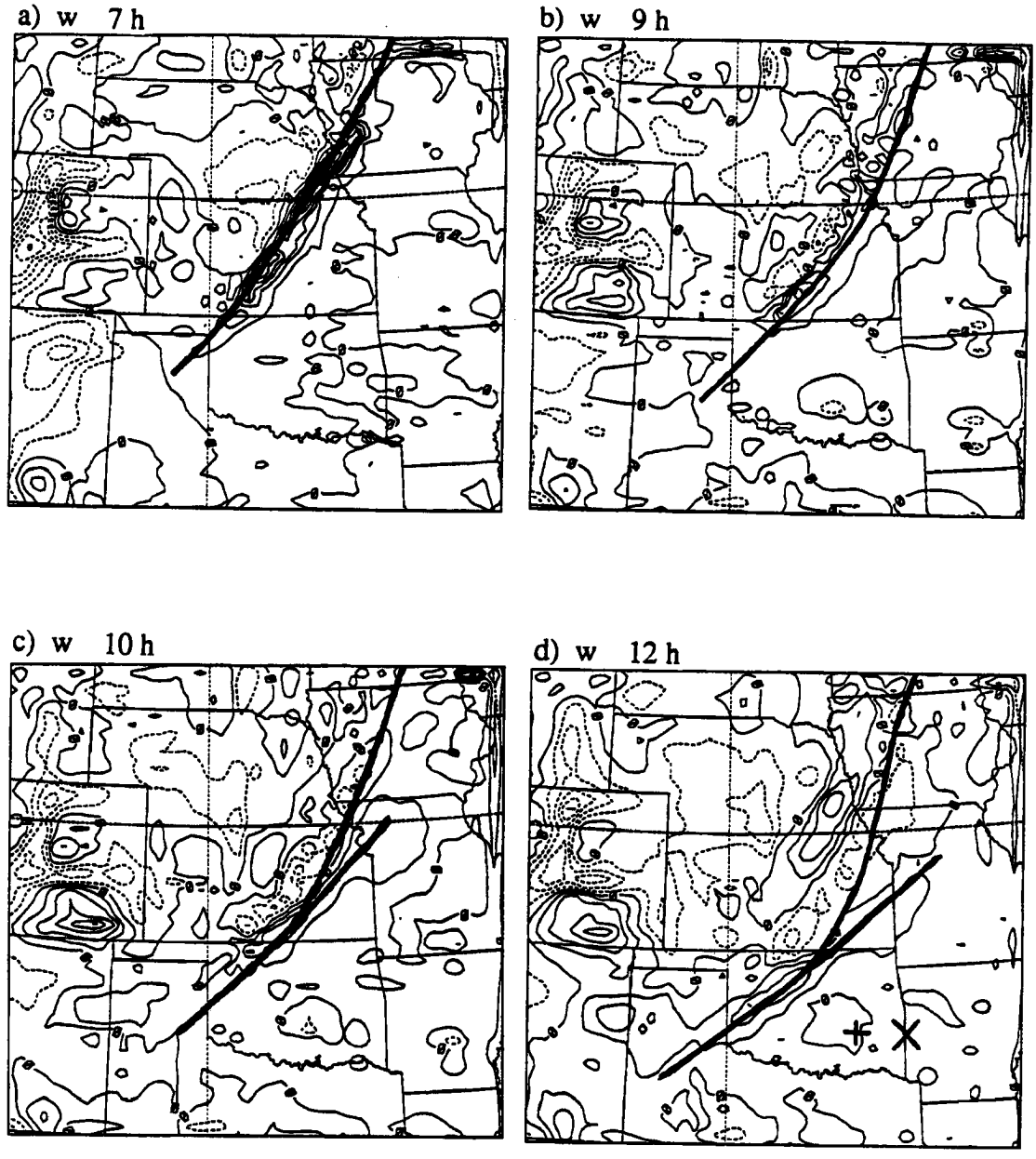

Fig. 4.9: Vertical velocity fields in the CP simulation, a) at 146 m after 7 h; b) at 146 m after 9 h; c) at 146 m after 10 h; d) at 146 m after 12 h; e) at 5153 m after 12 h; and f) at 11156 m after 12 h. Contour interval is 0.01 m s^{-1}, for a, b, c, and d; and 0.03 m s^{-1} for e and f. Heavy solid line indicates position of front as inferred from the model output fields.

e) w 12 h

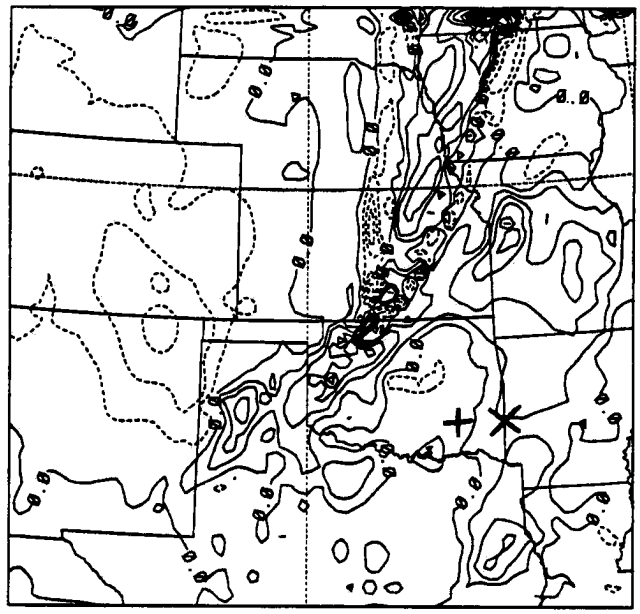

f) w 12 h

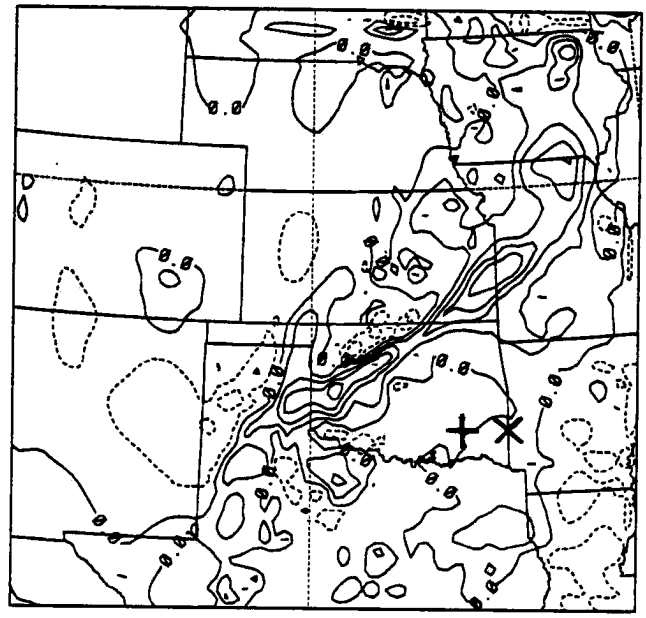

Fig. 4.9: Continued.

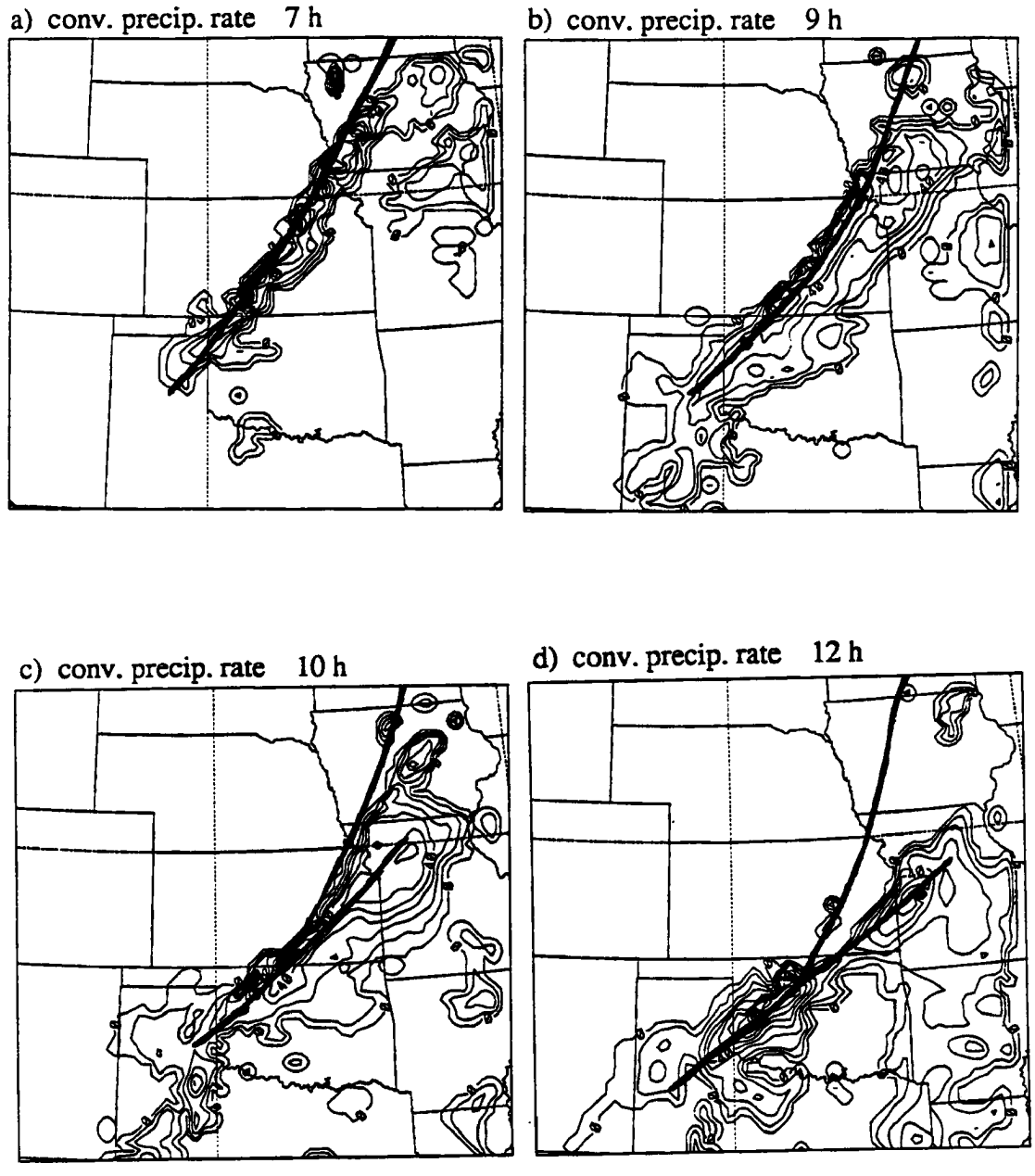

Fig. 4.10: Fields of convective precipitation rate (mm s^{-1}) from the CP simulation a) after 7 h; b) after 9 h; c) after 10 h; and d) after 12 h. Contour interval is 0.0001 mm s^{-1} (0.36 mm h^{-1}). Heavy solid line indicates location of front as inferred from model output.

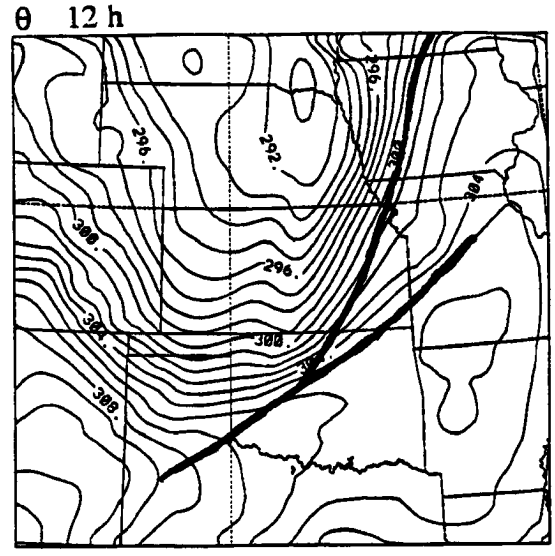

Fig. 4.11: Low-level (146 m) field of potential temperature (K) in the CP simulation after 12 h of model time. Contour interval is 1 K. Heavy solid line indicates location of front as inferred from model output.

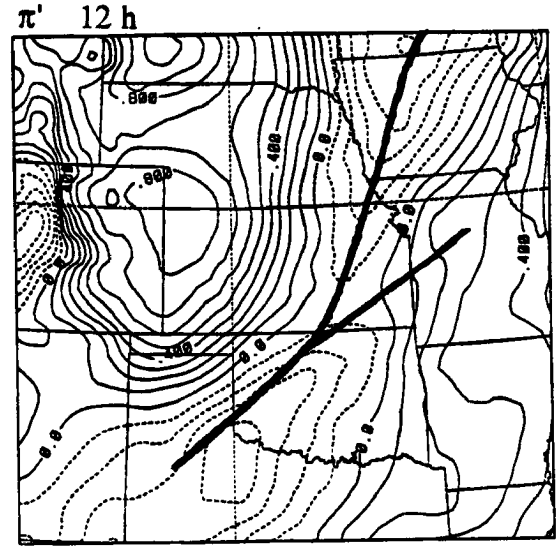

Fig. 4.12: Low-level (146 m) field of perturbation Exner function in the CP simulation after 12 h of model time. Contour interval is 0.1 J kg^{-1} K^{-1}. Heavy solid line indicates location of front as inferred from model output.

The low-level field of vertical velocity (Fig. 4.9) shows a line of updrafts along the front, followed by a region of subsidence, until 9 h. By 10 h, when the prefrontal boundary was first evident, and at 12 h (Fig. 4.9c,d), the line of updrafts was oriented along that prefrontal boundary rather than the front. This line of updrafts was followed by a line of low-level subsidence, which coincided with the frontal location, and a second band of upward motion.

The w fields at middle and upper tropospheric levels (Fig. 4.9e, f) suggest that the deepest and greatest vertical velocities (with magnitudes of up to 18 cm s^{-1} and extending above 200 mb) were associated with convection. The subsidence above the surface front, however, did not extend above middle levels.

The field of convective precipitation rate (Fig. 4.10) indicates the extent and intensity of the parameterized convection. By 7h, some of the prefrontal convection had developed, as well as a fairly narrow line of convection along the front. As the simulation progressed, the line of convection grew wider but not significantly more intense. The maximum precipitation rates in the model output at each hour showed little variation; the maximum rates generally stayed between 3 and 4.5 mm h^{-1}. By 9 h, the most intense convection was occurring along the front, with a sharp gradient in convective precipitation rate behind the front, and a much smoother gradient ahead of the front. By 10 and 12 h, the convection was occurring along and ahead of the prefrontal boundary, while the front behind the boundary experienced little or no convection.

The model output of convective precipitation rate (Fig. 4.10) may be qualitatively compared to the WSR-57 observations of precipitation (Figs. 3.9 and 3.14). Overall, the area of precipitating convection predicted by the model was much more widespread than the precipitation observed by radar. There was no sign of smaller-scale bands of convection in the simulation, as were noted in the observations (*e.g.* Fig. 3.9c). Such bands should not be expected in these simulations, however, as the bands were observed on a scale less than the model resolution, and were therefore too small to be resolved by the model. In a

manner similar to the observed behavior of the convection, the model did predict that the convection would move out ahead of the front in Kansas (*e.g.* Fig. 4.10c and d). While the WSR-57 reflectivity data did show some prefrontal convection occurring within 100 - 150 km of the front (*e.g.* Fig. 3.9d), the model predicted convective precipitation to distances of more than 300 km ahead of the front (Fig. 4.10d). And while the observations showed convection weakening by 0000 UTC, 27 June (Fig. 3.14d), model output at the corresponding time (12 h, Fig. 4.10d) showed no such tendency.

The model field of accumulated precipitation may also be compared more quantitatively to the PRE-STORM surface rainfall observations. This field also confirms that the simulation developed convection over a much more extensive area than observed. However, the maxima of the simulated convective rainfall was less than observed. For example, the observations from 2100 - 2200 UTC, 27 June (Fig. 4.13), showed that precipitation had occurred during that hour in a 200 km wide band, most of which experienced less than 5 mm of rain during that hour. A few stations experienced greater than 10 mm of rain, and one station recorded nearly 30 mm of rain. During the corresponding period in the simulation (9 - 10 h, Fig. 4.14), on the other hand, precipitation had accumulated over a much greater area but the maximum accumulation had reached only 3 mm in a small area.

Total rainfall for the simulation (corresponding to the period from 1200 UTC, 26 June, to 0000 UTC, 27 June) is shown in Fig. 4.15. As compared to the observed rainfall for that same period (Fig. 4.16), much more rain was produced in the simulation than in the observed system. However, maximum accumulations in the simulation were only just above 11 mm, whereas one observed station reported over 100 mm of rain, and another reported nearly 70 mm of rain. These differences, like the differences in the one-hour comparison above, apparently resulted from the fact that the model did not resolve the convective scale.

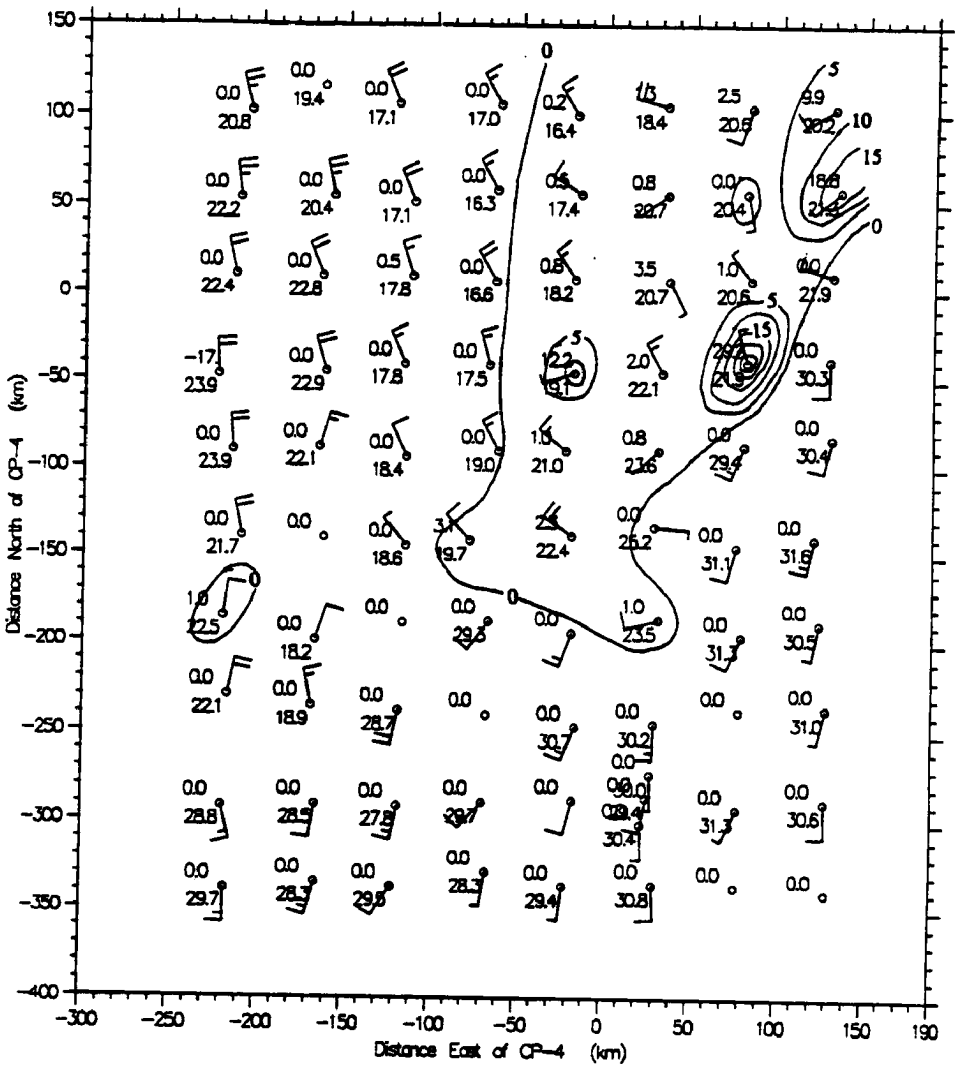

Fig. 4.13: Accumulated precipitation (mm) from the PRE-STORM surface observations over the 1 h preceding 2200 UTC. Contour interval is 5 mm.

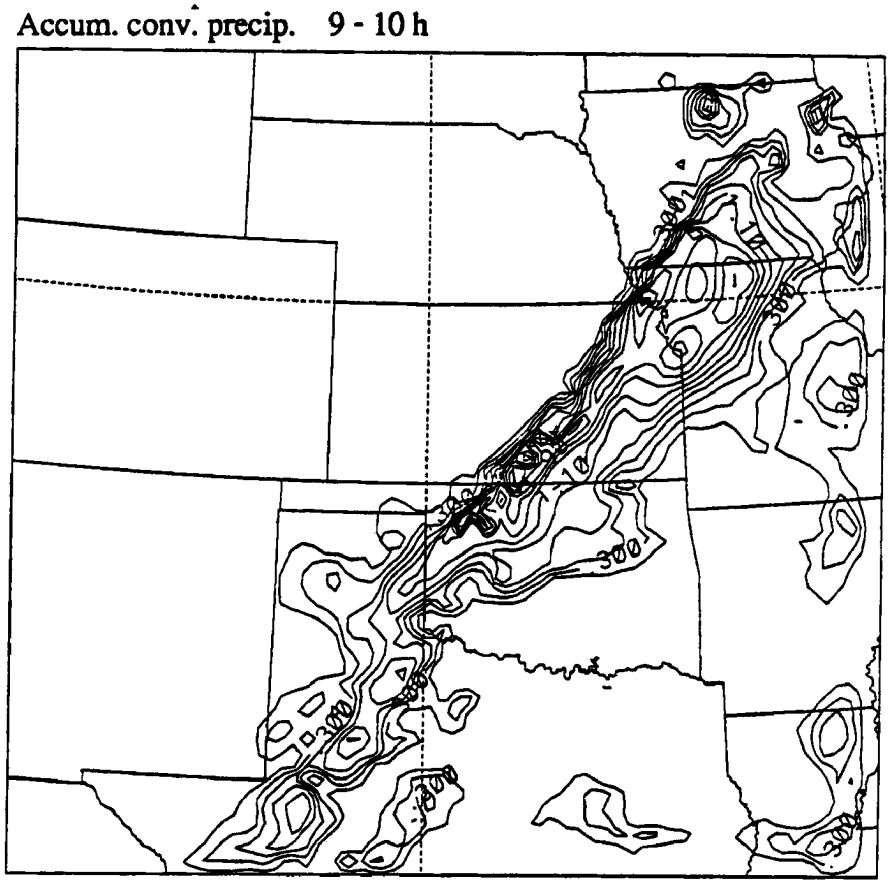

Fig. 4.14: Accumulated convective precipitation (mm) in the CP simulation over the 1 h preceding 10 h. Data are contoured from 0.1 mm, with contour interval of 0.2 mm.

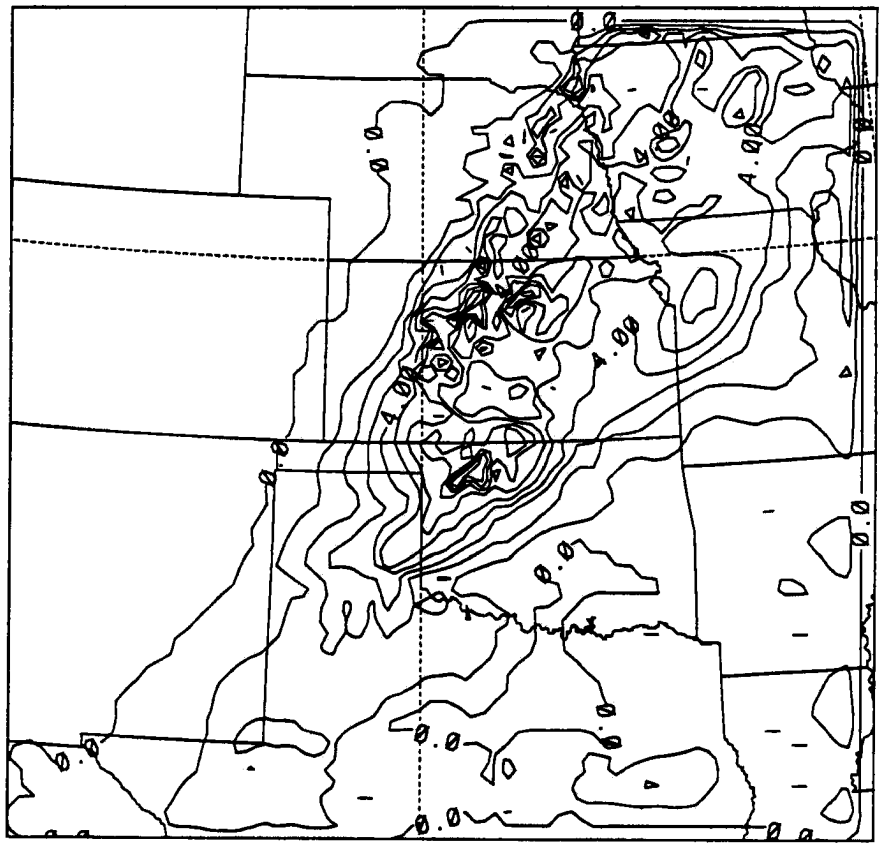

Fig. 4.15: Accumulated convective precipitation (mm) in the CP simulation over the first 12 h of the simulation. Data are contoured with an interval of 1 mm.

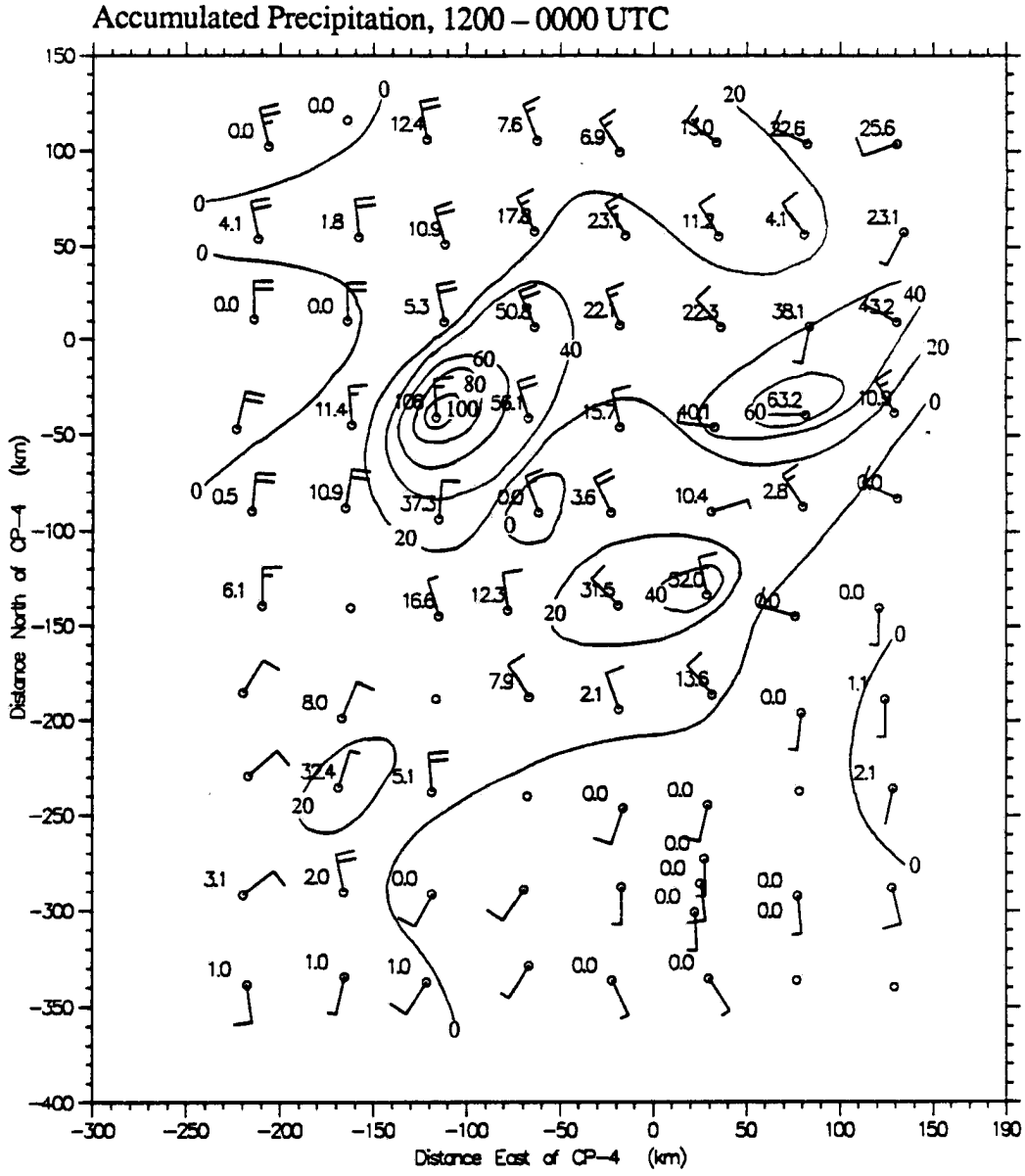

Fig. 4.16: Accumulated precipitation (mm) from the PRE-STORM surface observations between 1200 UTC, 26 June; and 0000 UTC, 27 June. Contour interval is 20 mm. Winds are at 0000 UTC, 27 June.

Vertical cross sections taken through the front at several places and several times during the CP simulation (Fig. 4.17; as noted in Fig. 4.8) show the differences between the vertical structure of the vertical velocity in the area where the prefrontal boundary had developed ahead of the front, and the areas above the front alone. The cross sections which intersected the front, but not the prefrontal boundary (Fig. 4.17a,b,c) show that an updraft with velocities of about 15 - 20 cm s^{-1} was consistently located above the frontal boundary, centered at a height of about 8 - 10 km AGL. This updraft was apparently the result of upper-level heating from the convective parameterization, as the extent of the updraft is quite similar to the extent of the convection. The cross sections which intersected both the prefrontal boundary and the front (Fig. 4.17d,e), however, indicated a different structure: Above the front was a region of subsidence usually about 5 km deep. Ahead of the front, above the prefrontal boundary and extending often several hundred kilometers to the east was a region of ascent centered at about 9 km AGL, similar to the ascent seen above the front in other cross sections. This ascent is apparently an effect of the convection as well, as again the extent of the updraft is quite similar to the extent of the convection.

4.2.3.2 Results from the NO-CP simulation

The NO-CP simulation was run with the convective parameterization turned off. Moisture was included only as a passive tracer. Thus, convection, clouds of any sort, any form of precipitation, and latent heating and cooling due to evaporation and condensation were all eliminated from the NO-CP simulation. The results of this simulation after 12 h show a well-defined front in the dynamic and thermodynamic fields (Fig. 4.18). Fig. 4.18 shows the location of the front as predicted in the CP simulation as well as the front in the NO-CP simulation. Although at times the front in the NO-CP simulation lagged the front in the CP simulation by as much as 100 km, the frontal locations from the two simulations coincided closely north of central Kansas. There was no sign of the prefrontal boundary in

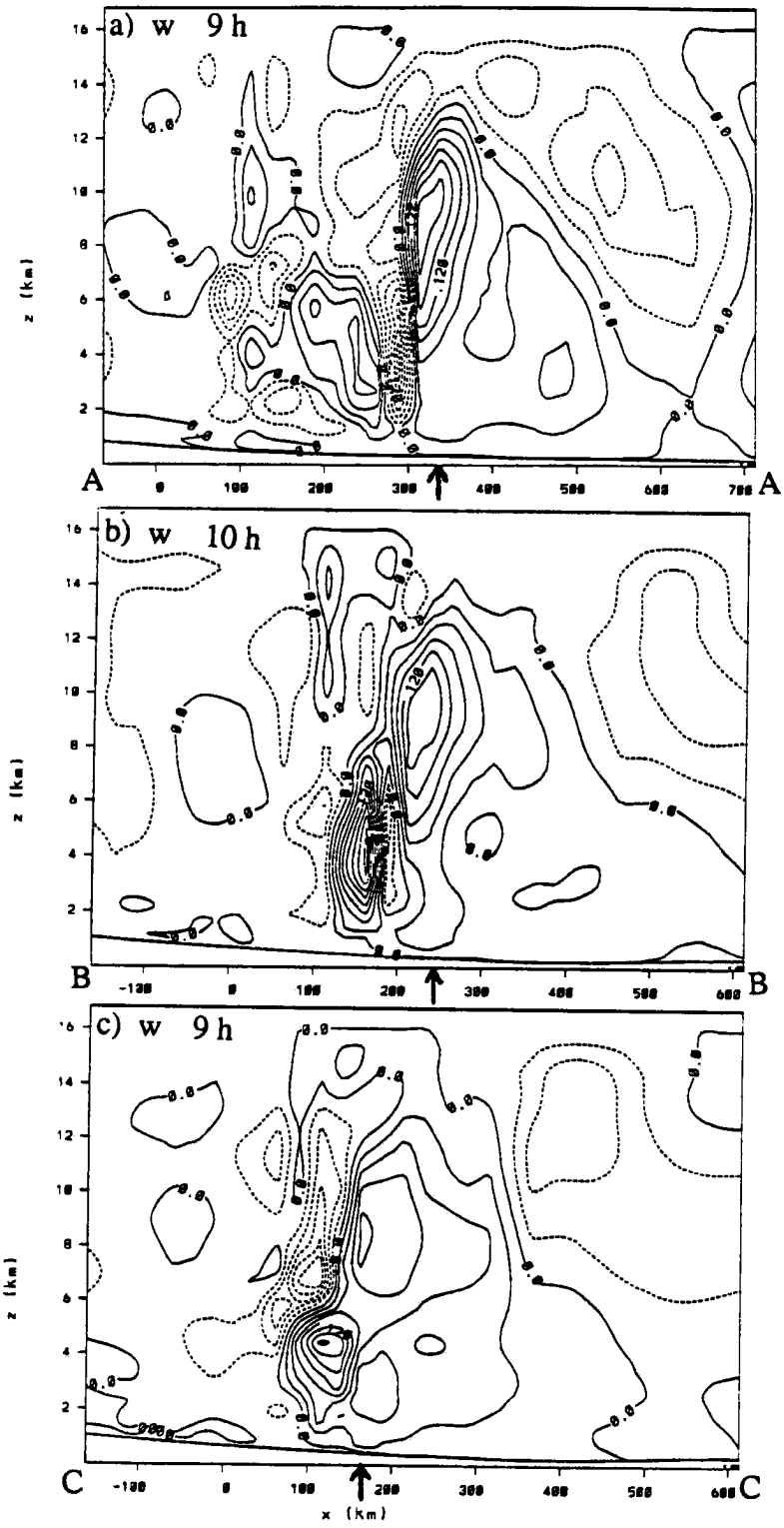

Fig. 4.17: Vertical cross sections of vertical velocity in the CP simulation along the lines indicated in Fig. 4.8. a) along line AA; b) along line BB; c) along line CC; d) along line DD; and e) along line EE. Contour interval is 0.03 m s^{-1}.

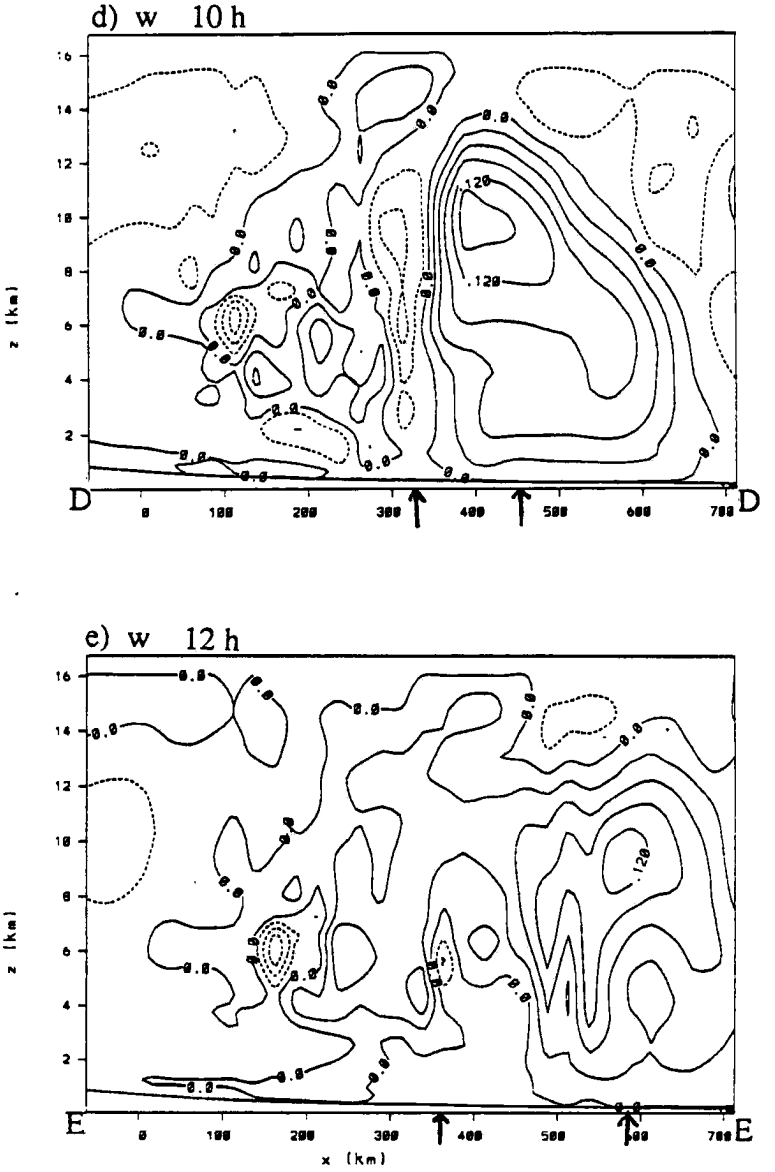

Fig. 4.17: Continued.

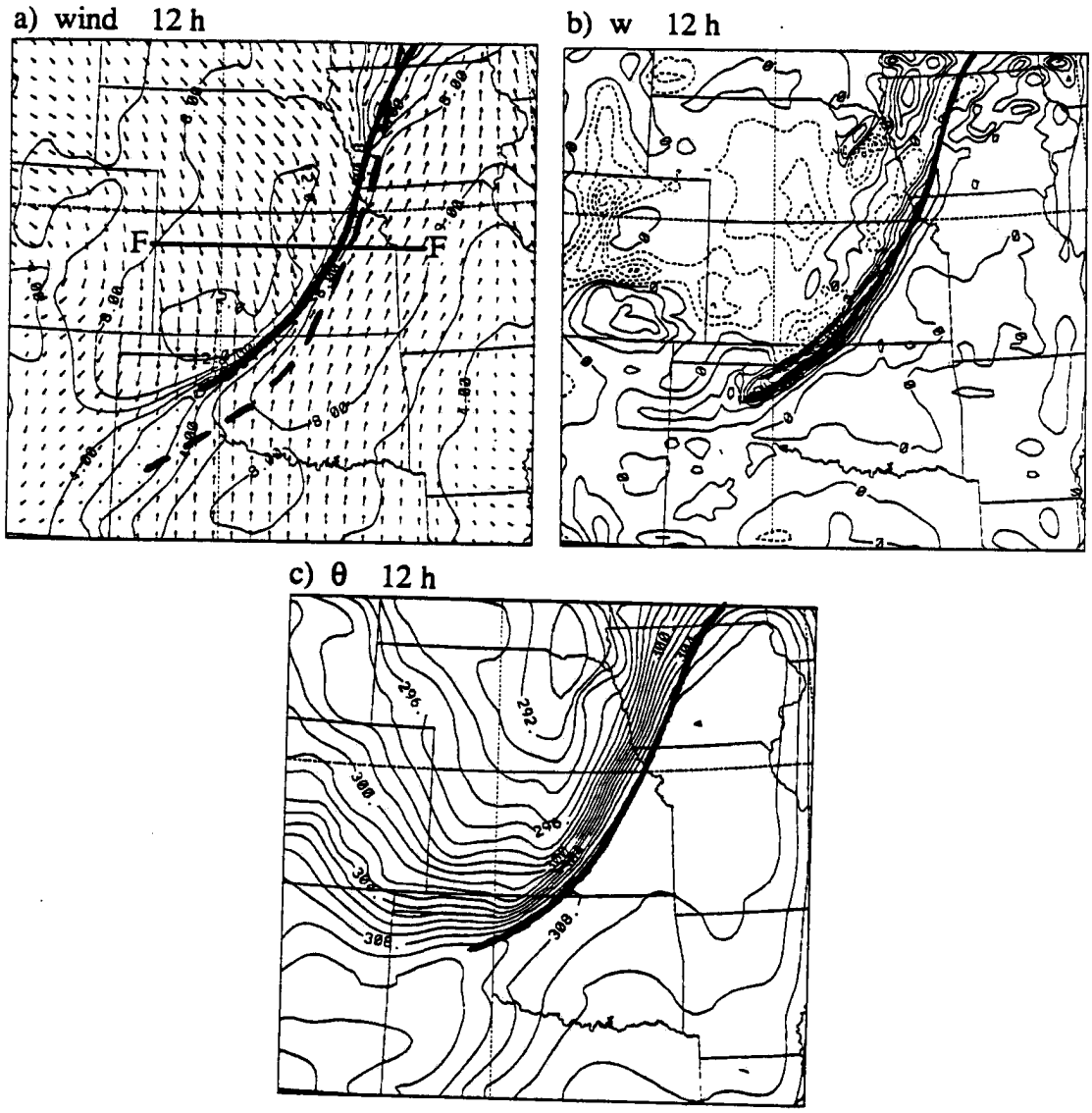

Fig. 4.18: Low-level (146 m) fields from the NO-CP simulation after 12 h of model time: a) Horizontal wind vectors and speed (m s^{-1}, contour interval is 2 m s^{-1}); b) Vertical velocity (m s^{-1}, contour interval is 0.01 m s^{-1}); and c) Potential temperature (K, contour interval is 1 K). Heavy solid line shows location of front as inferred from the model fields. Heavy dashed line in a) shows location of front from the CP simulation. Line FF in a shows location of the cross section in Fig. 4.20.

this simulation, as there was in the CP simulation. This absence of such a boundary in the NO-CP simulation suggests that the prefrontal boundary was a result of the parameterized convection in the CP simulation.

Vertical velocities (Fig. 4.19) at various levels in the NO-CP simulation indicate low-level lifting (with magnitudes of up to 9 cm s^{-1}) immediately above the surface front, probably due directly to the frontal lifting. In general throughout the troposphere, the vertical velocities were positive in the region ahead of the front and negative in the region behind the front. However, in the lower troposphere, there were negative vertical velocities ahead of the front where in the CP simulation, convection was occurring. The ascent was strongest in the upper troposphere, with magnitudes greater than 3 cm s^{-1}. This pattern is consistent with the expected vertical velocity field associated with a jet streak. An X-Z cross section through the front along line FF of Fig. 4.19 (Fig. 4.20) illustrates the same situation.

This cross section supports the conclusion that the deepest, strongest lifting in the CP simulation was due to the parameterized convection. In the NO-CP simulation, no deep, strong lifting was present in the frontal or prefrontal areas. However, the broader, regional scale ascent ahead of the surface front, particularly at upper levels, suggests that jet-streak circulations (Section 1.1, Fig. 1.2) may have played a role in sustaining convection. This reasoning is supported by the work of Dudhia and Moncrieff (1987), who in a number of three-dimensional simulations of tropical convection, determined that large-scale lifting on the order of 1 - 2 cm s^{-1} was essential to enhance updrafts and maintain the development of new cells.

The general region of prefrontal ascent in this case has been noted observationally by Trier *et al.* (1991). In an analysis of data from pre-system soundings in the southern part of the PRE-STORM network, Trier *et al.* noted an average vertical velocity (ω) of -4 to -8 $\mu b\ s^{-1}$. Their observed velocity is much greater than the results from a vertical profile in the NO-CP simulation in the same area (marked by a (+) in Fig. 4.19), which had

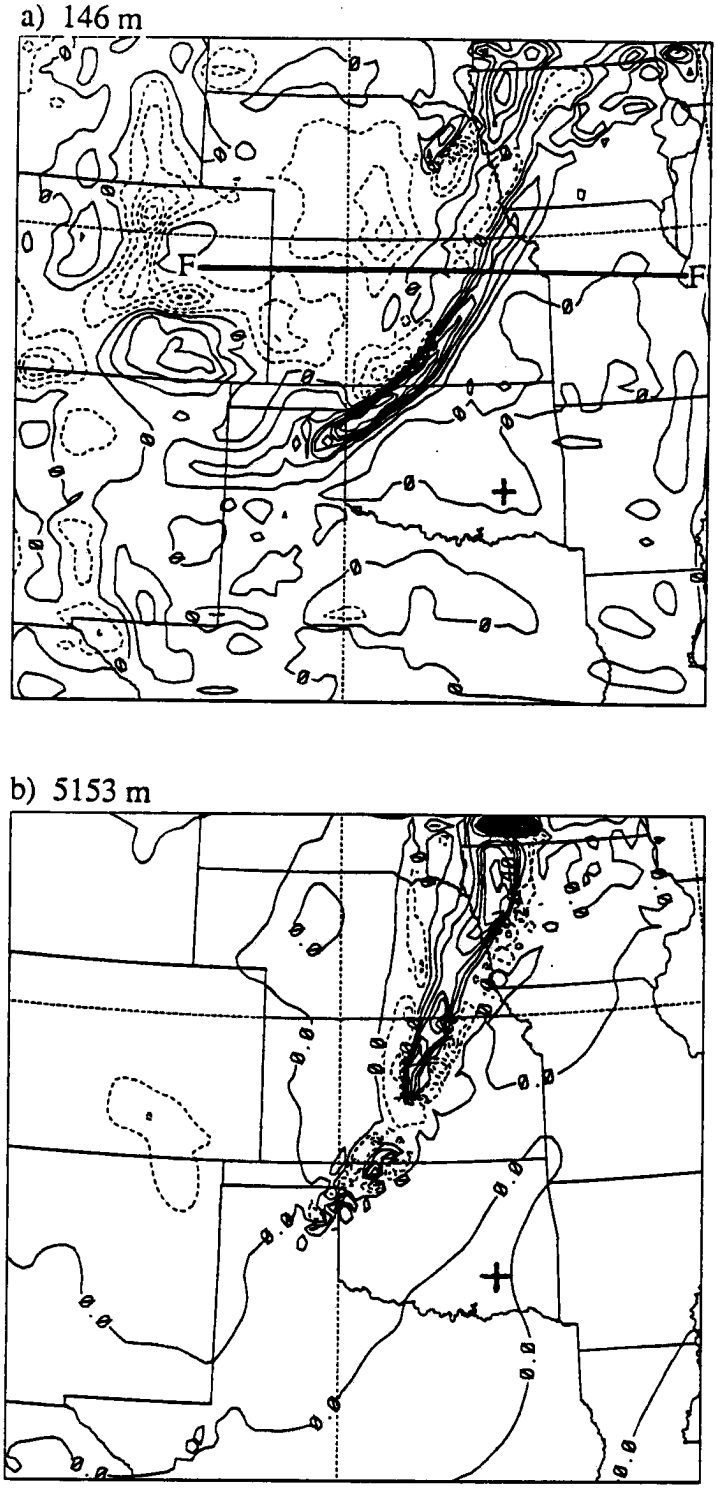

Fig. 4.19: Vertical velocity fields from the NO-CP simulation after 12 h at a) 146 m, b) 5153 m, and c) 11156 m. Contour interval is 0.01 m s^{-1} in a and c; and 0.06 m s^{-1} in b.

c) 11156 m

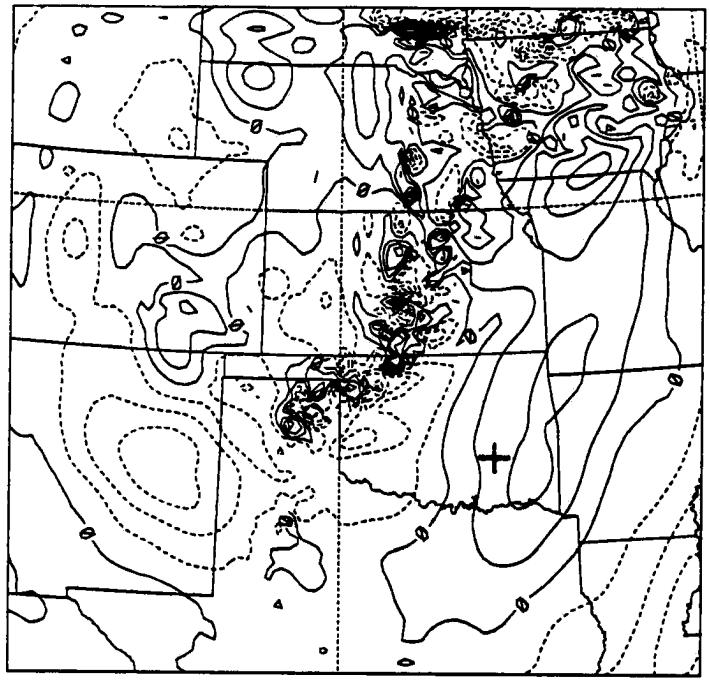

Fig. 4.19: Continued.

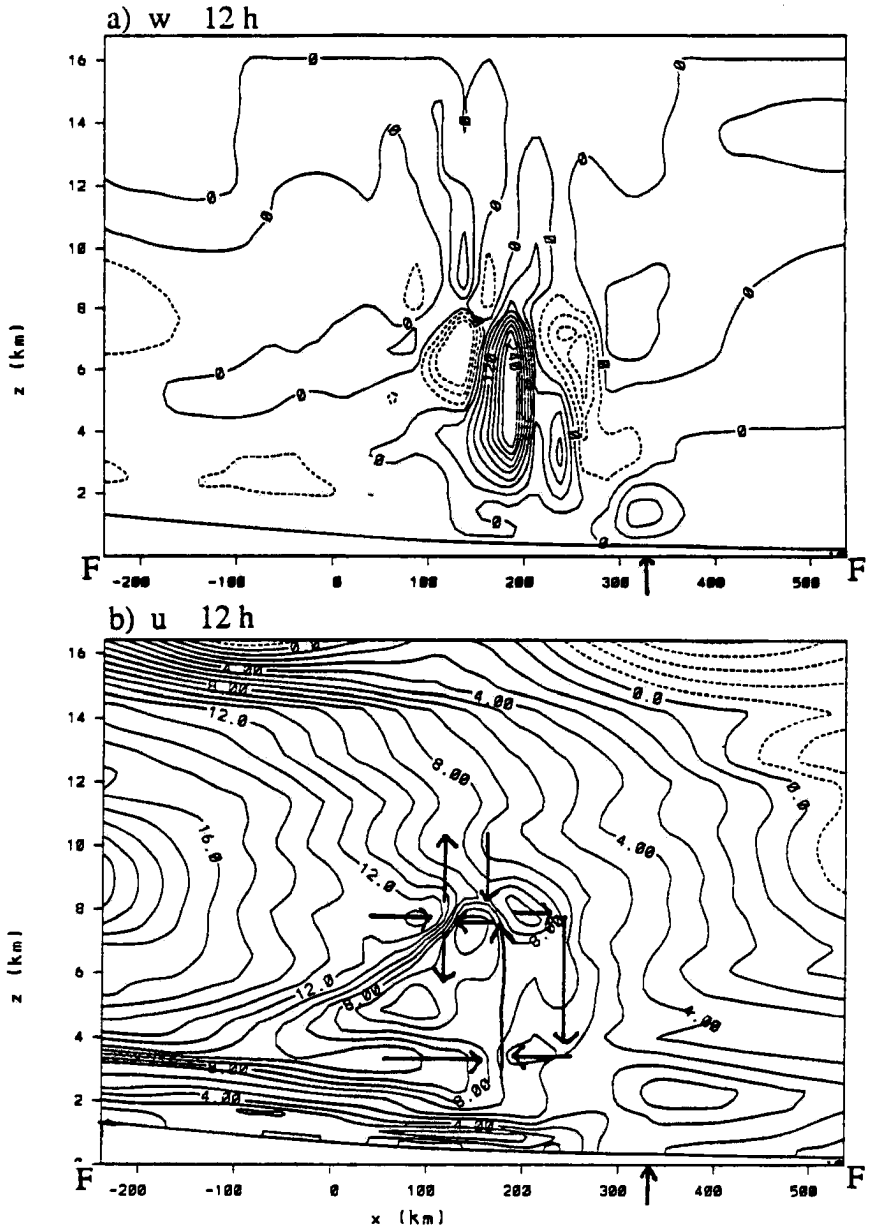

Fig. 4.20: X-Z cross section of vertical velocity in the NO-CP simulation along line FF of Fig. 4.19. a) w, contour interval is 0.03 m s^{-1}; b) u-velocity, contour interval is 1 m s^{-1}. Arrows in b indicate the sense of vertical velocity and convergence associated with the gravity wave. Arrows at bottom of a and b indicate location of surface front.

lifting of approximately -1 μb s^{-1}. In the CP simulation, again in the same place (marked by (+) in Fig. 4.9d,e,f), the vertical velocity profile is dominated by downward motion of approximately 0.3 to 0.5 μb s^{-1}. This area, however, was between two regions of convection, so it is not surprising to find the profile dominated by subsidence. Just to the east (marked by (X) in Fig. 4.9d,e,f), where convection was occurring in the simulation, the profile indicated lifting throughout the troposphere, with vertical velocity approximately -0.5 to -2 μb s^{-1}. Trier *et al.* also noted an area of prefrontal cirrus, which indicates the presence of upper level lifting. They attribute the prefrontal region of ascent to geostrophically forced frontal circulations.

The greatest rate of ascent in Fig. 4.20 is seen not ahead of or at the front, but about 150 km behind the front. In a band behind the front at middle levels (also noticeable in Fig. 4.19b), vertical velocities reached a maximum of approximately 36 cm s^{-1}. This strong ascent did not extend down into the post-frontal air mass, but was located above the frontal inversion. Comparison of the vertical velocity field (Fig. 4.20) to the u-velocity field (Fig. 4.21) shows that this band of ascent had some characteristics of a gravity wave, particularly the pattern of horizontal convergence and divergence and associated vertical motions. The band of ascend was originally located directly over the front, but appeared to propagate to the east more slowly than the front, which may account for its post-frontal location. In the CP simulation, there was no such obvious feature in the vertical velocity field.

4.2.3.3 Discussion of the fine-grid three-dimensional simulations

The development of a prefrontal boundary in the CP simulation was particularly interesting because it was similar to the small-scale observations of a gust front from the convective system. The cause of this boundary in the model output seems to be related to the presence of the convection, as it did not occur in the NO-CP simulation. The

boundary may have been a result of the downdrafts caused by low-level cooling from the convective parameterization scheme, and thus perhaps a rough representation of an outflow boundary. One of the marks of the prefrontal boundary, for example, was a potential temperature gradient (Fig. 4.11), which may have been a result of the low-level cooling from the convective parameterization scheme. However, there is only a little evidence suggesting that the model reproduced an outflow boundary.

One possible reason that the prefrontal convection in the CP simulation was so extensive is that the vertical-velocity threshold above which the convective parameterization scheme would be activated was set at too low a value. While a value of 0.009 m s^{-1} may have worked well for the coarse grid simulations, a higher threshold might be more appropriate for the fine grid, as convergence and the resulting vertical motion would be better resolved. If a higher threshold were selected, prefrontal convection might be less extensive. Another possible reason is that lateral boundary effects may have contaminated the vertical velocity field. As the convection moved closer to the right boundary of the nested grid, the convection became more extensive within 400 km of the right boundary of the fine-grid domain. Effects of the resolution also would have affected the extent of the convection. A simulation with grid spacing of 25 km would have certainly spread the convection out more than observed, in the same way that the convection was spread out in the coarse-grid simulations.

Initial plans were to nest down further. However, the recent research of Cram *et al.* (1991a,b) suggested that simulations with an additional nest were not likely to be successful. Cram *et al.* attempted to simulate a squall line with a resolution of 5 km and explicit microphysics, but found that the convergence on the 5 km scale was not strong enough to explicitly initiate convection, and that the resolution of 5 km seemed too large to explicitly simulate microphysical processes successfully. As an additional 3:1 nest in the study reported in this thesis would bring the resolution down to approximately 8 km, there

was no reason to believe that those simulations would be any more successful than those of Cram *et al.* on the 5 km scale.

4.3 Two-dimensional simulations

Because the initial goals of this study included simulating smaller scales of the MCS, and because it became evident that adding another nest to the simulations would likely be unsuccessful, a number of two-dimensional simulations with explicit microphysics were attempted. By their very nature, the two-dimensional simulations were much further removed from the observations than the three-dimensional ones. However, it was hoped that these simulations would reproduce some of the observed features of the convection.

For these simulations, the model was configured similar to the three-dimensional configuration, except that the convective parameterization was not activated and full microphysics was selected. The horizontal grid spacing was 1.5 km, vertical grid spacing was 150 m at the surface, stretching to 750 m high in the troposphere. The simulations were initialized with horizontally homogeneous conditions from one of the soundings taken ahead of the system. At first, the 1800 sounding from CNU was tried; when those simulations produced no convection, a sounding with higher CAPE, the 2100 sounding from FSB, was tried. To the horizontally homogeneous fields, a cold pool was added in an attempt to simulate the frontal convergence, and an upper-level jet into the plane of the simulation was added. The simulations did not produce anything resembling a long-lived convective system, but rather produced one convective cell which lasted for approximately one hour. This cell seemed to behave in much the same way as the deeper region of ascent which occurred in the NO-CP simulation: it quickly became decoupled from the surface lifting of the cold pool and was apparently cut off from the boundary-layer air as the cold pool advanced beneath the ascending air.

One reason that these simulations failed may be that this was a low-CAPE situation, and as such, the two-dimensional simulations could not provide enough convergence to support deep convection. A second reason may be that the upper-level lifting from the jet streak circulations, inferred from the analysis and seen in three-dimensional simulations, was absent from these simulations, so there was no upper-level upward motion to support deep convection. The upper-level support apparently existed in the three-dimensional simulations, as evidenced by the results from the NO-CP simulation (Fig. 4.20).

4.4 Summary of modelling study

The CSU-RAMS model was used to perform a nested-grid simulation of the 26 - 27 June 1985 PRE-STORM MCS. In several ways, the fine-grid CP simulation matched the observations fairly closely:

- The location and movement of the simulated front and upper-level features were quite close to the observed frontal location and movement.
- The general prefrontal nature of the convection in the northern half of the domain and the frontal nature of the convection in the southern half was reproduced in the CP simulation.
- The development of a prefrontal boundary in about the same place as the observed thunderstorm outflow boundary was noticed in the CP simulation. However, this boundary probably cannot be conclusively interpreted as an outflow boundary, but was perhaps a result of convergence associated with the deep convection directly above.
- A region of ascent ahead of the front, which was inferred from the observations of a jet streak and observed more directly by Trier *et al.* (1991), was was noted in the results of the simulation.

In other respects, however, the model did not simulate the system well. For example, the simulated convection in Kansas initially occurred along the front, and subsequently propagated ahead of the front. The observed convection, on the other hand, initially occurred ahead of the front in Kansas. The parameterization of convection also seemed to be a particularly weak element in the CP simulation. The convection was much more extensive in the model than in the observations, possibly because of an inappropriate selection of a threshold parameter, or possibly simply because of the coarse resolution.

Two-dimensional simulations were attempted, but were unsuccessful in developing a convective system. The failure is probably due to a number of factors, among them: convergence that may have been too weak to sustain even one convective cell for long; and a lack of upper-level support for the convection from the jet-streak circulations.

Despite the problems, the three-dimensional simulations of this case were encouraging in that essential features of a relatively weak, disorganized system were successfully simulated. Although Zhang *et al.* (1988) were quite successful in their attempt to simulate many details of the 10 - 11 June 1985 PRE-STORM squall line with a nested-grid model and a resolution of 25 km, they suggest that their success was facilitated by sufficiently strong forcing on the synoptic scale in that case. Similarly, the case of Cram *et al.* (1991a,b) was strongly forced by surface frontal convergence. In addition, both Zhang *et al.* and Cram *et al.* included explicit microphysical processes in their simulations. The forcing was apparently weaker in the 26 - 27 June case, which could in part account for some of the difficulty the model had in simulating this MCS. But the fact that the model did simulate such behavior as the prefrontal convection in the presence of larger-scale lifting suggests that some weaker systems can be effectively modelled from the synoptic scale forcing.

Chapter Five

SUMMARY

A case study of a Mesoscale Convective System was performed and several simulations of the system were attempted. The observed system occurred ahead of a shallow cold front in an environment of weak to moderate shear (up to about 4.5 x 10^{-3} s^{-1}) and weak to moderate CAPE (about 600 - 1200 J kg^{-1}), in the right entrance region of an upper-tropospheric jet streak. The observed system had only weak to moderate convection (ahead of the front in Kansas; along the front in Oklahoma) and weak linear organization. As the system evolved and the front began to dissipate, a thunderstorm outflow boundary from the convection became a dominant feature of the surface observations.

As compared to a conceptual model of an ordinary squall line (Houze *et al.* 1989), the 26 - 27 June 1985 PRE-STORM system was poorly organized. The system did not have a well-defined convective line or stratiform region. However, vertical cross sections of horizontal velocity normal to the line as observed by Doppler radar revealed a familiar layered flow structure, including the familiar rear inflow jet.

Nested-grid simulations were performed, with the fine-grid having a horizontal grid-spacing of 25 km. One of the simulations (the CP simulation) included a Kuo-type convective parameterization scheme and "supersaturation condensed" microphysics, a second simulation (the NO-CP simulation) excluded both features. Both simulations accurately predicted the movement of the front through the PRE-STORM network. The CP simulation developed convection initially along the front, but the convection in the northern half of the fine-grid domain (north of central Kansas) then moved out ahead of the front while the convection in the south remained along the front.

The CP simulation developed a prefrontal boundary, which may have been a rough representation of the observed thunderstorm outflow boundary. However, the evidence to support this speculation is not convincing. The prefrontal boundary may have been a result of convection and prefrontal convergence, rather than the cause.

It does not appear that the convection in the model propagated ahead of the front as a gravity wave, in contrast to the case of Cram *et al.* (1991b). Larger-scale prefrontal lifting, possibly due to jet-streak circulations, was apparently an important feature for the maintenance and propagation of the MCS. Two-dimensional simulations, which were unsuccessful, also suggest the importance of larger-scale support (which was absent in the two-dimensional simulations) for the convection.

5.1 Suggestions for future research

There are a number of directions which future research on this particular MCS could take. More detailed analyses of upper-air winds, possibly incorporating wind profiler data, could be used to determine vertical velocity over the PRE-STORM region. These analyses might provide more evidence for the possible effect of the jet-streak circulations. Results could also be compared to the model output field of vertical velocity to further evaluate the model results. The Doppler radar analyses could be continued, including some dual-Doppler analyses, perhaps to explore the development of the thunderstorm outflow.

The modelling portion of this study could also be extended. Most importantly, sensitivity studies should be incorporated into any further modelling studies of this system. Any number of such studies could be performed, but perhaps the most useful ones would test the sensitivity of the convective parameterization scheme to various parameters such as the vertical velocity threshold discussed in Chapter 4. Other convective parameterization schemes, particularly schemes developed specifically for the 5 - 10 km scale (*e.g.* Weissbluth, 1991), could be tested with an additional nest. Other studies could be

performed to test the sensitivity to of the simulations to grid size, domain size, boundary conditions, radiation, soil moisture, and many other factors.

Ideally, a full microphysics simulation of an entire MCS would be performed with no nesting on a grid with resolution of 1 km or less. Such a simulation might provide much insight into the behavior of the convection, thunderstorm outflows, as well as larger-scale features of the system. As computer power increases, supercomputer time becomes less expensive, and atmospheric modelling techniques improve, such simulations will likely be performed. Until then, however, nested grids and convective parameterization schemes will be necessary.

REFERENCES

Anthes, R. A., and D. Keyser, 1979: Tests of a fine-mesh model over Europe and the United States. *Mon. Wea. Rev.*, **107**, 963-984.

Augustine, J. A., and E. J. Zipser, 1987: The use of wind profilers in a mesoscale experiment. *Bull. Amer. Meteor. Soc.*, **68**, 4-17.

Battan, L. J., 1973: *Radar Observation of the Atmosphere*. University of Chicago Press, 324 pp.

Bluestein, H. B., and M. H. Jain, 1985: Formation of mesoscale lines of precipitation: Severe squall lines in Oklahoma during the spring. *J. Atmos. Sci.*, **42**, 1711-1732.

Chen, C., and W. R. Cotton, 1983: A one-dimensional simulation of the stratocumulus-capped mixed layer. *Boundary-Layer Meteorol.*, **25**, 289-321.

Chen, S., and W. R. Cotton, 1988: The sensitivity of a simulated extratropical mesoscale convective system to longwave radiation and ice-phase microphysics. *J. Atmos. Sci.*, **45**, 3897-3910.

Cotton, W. R., and R. A. Anthes, 1989: *Storm and Cloud Dynamics*. Academic Press, 883 pp.

Cram, J. M., R. A. Pielke and W. R. Cotton, 1991a: Numerical simulation and analysis of a prefrontal squall line. Part I: Observations and basic simulation results. *J. Atmos. Sci.*, (in press).

____, ____ and ____, 1991b: Numerical simulation and analysis of a prefrontal squall line. Part II: Propagation of the squall line as an internal gravity wave. *J. Atmos. Sci.*, (in press).

Cunning, J. B., 1986: The Oklahoma-Kansas preliminary regional experiment for STORM-central. *Bull. Amer. Meteor. Soc.*, **67**, 1478-1486.

Dudhia, J., and M. W. Moncrieff, 1987: A numerical simulation of quasi-stationary tropical convection bands. *Quart. J. R. Met. Soc.*, **113**, 929-967.

____, and ____, 1989: A three-dimensional numerical study of an Oklahoma squall line containing right-flank supercells. *J. Atmos. Sci.*, **46**, 3363-3391.

Fovell, R. G., and Y. Ogura, 1988: Numerical simulation of a midlatitude squall line in two dimensions. *J. Atmos. Sci.*, **45**, 3846-3879.

Fritsch, J. M., and C. F. Chappell, 1980: Numerical prediction of convectively driven mesoscale pressure systems. Part I: Convective parameterization. *J. Atmos. Sci.*, **37**, 1722-1733.

____, R. J. Kane and C. R. Chelius, 1986: The contribution of mesoscale convective weather systems to the warm season precipitation in the United States. *J. Climate and Appl. Meteor.*, **25**, 1333-1345.

Fujita, T. T., 1955: Results of detailed synoptic studies of squall lines. *Tellus*, **7**, 405-436.

Gamache, J. F., and R. A. Houze, Jr., 1982: Mesoscale air motions associated with a tropical squall line. *Mon. Wea. Rev.*, **110**, 118-135.

____, and R. A. Houze, Jr., 1983: Water budget of a mesoscale convective system associated with a tropical squall line. *J. Atmos. Sci.*, **70**, 1835-1850.

Hane, C. E., 1973: The squall line thunderstorm: Numerical experimentation. *J. Atmos. Sci.*, **30**, 1672-1690.

Heymsfield, G. M., and S. Schotz, 1985: Structure and evolution of a severe squall line over Oklahoma. *Mon. Wea. Rev.*, **113**, 1563-1589.

Houze, R. A., Jr., 1977: Structure and dynamics of a tropical squall-line system. *Mon. Wea. Rev.*, **105**, 1540-1567.

____, and P. V. Hobbs, 1982: Organization and structure of precipitating cloud systems. *Advances in Geophysics*, Vol. 24, Academic Press, 225-315.

____, and E. N. Rappaport, 1984: Air motions and precipitation structure of an early summer squall line over the Eastern Atlantic. *J. Atmos. Sci.*, **41**, 553-574.

____, B. F. Smull and P. Dodge, 1990: Mesoscale organization of springtime rainstorms in Oklahoma. *Mon. Wea. Rev.*, **118**, 613-654.

____, S. A. Rutledge, M. I. Biggerstaff and B. F. Smull, 1989: Interpretation of Doppler weather radar displays of midlatitude mesoscale convective systems. *Bull. Amer. Meteor. Soc.*, **70**, 608-619.

Johnson, R. H., and P. J. Hamilton, 1988: The relationship of surface pressure features to the precipitation and airflow structure of an intense midlatitude squall line. *Mon. Wea. Rev.*, **116**, 1444-1472.

Keyser, D., and M. A. Shapiro, 1986: A review of the structure and dynamics of upper-level frontal zones. *Mon. Wea. Rev.*, **114**, 452-499.

Kuo, H. L., 1974: Further studies of the parameterization of the influence of cumulus convection on large-scale flow. *J. Atmos. Sci.*, **41**, 1232-1240.

Lafore, J. P., and M. W. Moncrieff, 1989: A numerical investigation of the organization and interaction of the convective and stratiform regions of tropical squall lines. *J. Atmos. Sci.*, **46**, 521-544.

Leary, C. A., and E. N. Rappaport, 1987: The life cycle and internal structure of a mesoscale convective complex. *Mon. Wea. Rev.*, **115**, 1503-1527.

Maddox, R. A., 1980: Mesoscale convective complexes. *Bull. Amer. Meteor. Soc.*, **61**, 1374-1387.

Mahrer, Y., and R. A. Pielke, 1977: A numerical study of the airflow over irregular terrain. *Beitrage zur Physik der Atmosphere*, **50**, 98-113.

McAnelly, R. L., and W. R. Cotton, 1990: Dual-Doppler analysis of the maturing stage of the "random convection" MCC of 4 June 1985 in PRE-STORM. *Preprints, Fourth Conference on Mesoscale Processes*, Boulder, Colorado, Amer. Meteor. Soc.

Mohr, C. G., and L. J. Miller, 1983: CEDRIC--a software package for Cartesian space editing, synthesis and display of radar fields under interactive control. Twenty-first Conference on Radar Meteorology, Edmonton, Alta., Canada. Boston: American Meteorological Society. AMS Reprints, pp. 559-574.

____, ____, and R. L. Vaughan, 1979: An economical procedure for Cartesian interpolation and display of reflectivity factor data in three-dimensional space. *J. Appl. Meteor.*, **18**, 661-670.

NCAR, 1984: The National STORM Program: STORM-Central Phase. Prepared by the National Center for Atmospheric Research, Boulder, Colorado, in consultation with the Interagency Team for STORM-Central.

Newton, C. W., 1950: Structure and mechanism of the prefrontal squall line. *J. Meteor.*, **7**, 210-222.

____, C. W., 1966: Circulations in large sheared cumulonimbus. *Tellus*, **18**, 699-712.

Ogura, Y., and M. T. Liou, 1980: The structure of a midlatitude squall line: A case study. *J. Atmos. Sci.*, **37**, 553-567.

____, and ____, 1984: The evolution of an observed cold front. Part II: Mesoscale dynamics. *J. Atmos. Sci.*, **41**, 1669-1703.

Oye, R. and R. Carbone, 1981: Interactive Doppler Editing Software. Twentieth Conference on Radar Meteorology, Boston. American Meteorological Society. AMS Reprints, pp 683-689.

Pielke, R. A., 1974: A three-dimensional numerical model of the sea breezes over south Florida. *Mon. Wea. Rev.*, **102**, 115-139.

Rotunno, R., J. B. Klemp and M. L. Weisman, 1988: A theory for strong, long-lived squall lines. *J. Atmos. Sci.*, **45**, 463-485.

Rutledge, S. A., 1986: A diagnostic numerical study of the stratiform region associated with a tropical squall line. *J. Atmos. Sci.*, **43**, 1337-1358.

____, and P. V. Hobbs, 1983: The mesoscale and microscale structure and organization of clouds and precipitation in midlatitude cyclones. Part VIII: A model for the "seeder-feeder" process in warm-frontal rainbands. *J. Atmos. Sci.*, **40**, 1185-1206.

____, and R. A. Houze, Jr., 1987: A diagnostic modeling study of the trailing stratiform region of a midlatitude squall line., *J. Atmos. Sci.*, **44**, 2640-2656.

____, ____, M. I. Biggerstaff and T. J. Matejka, 1988: The Oklahoma-Kansas mesoscale convective system of 10-11 June 1985: Precipitation structure and single-Doppler analysis. *Mon. Wea. Rev.*, **116**, 1409-1430.

Schmidt, J. M., and W. R. Cotton, 1989: A High Plains squall line associated with severe surface winds. *J. Atmos. Sci.*, **40**, 281-302.

____, and ____, 1990: Interactions between upper and lower tropospheric gravity waves on squall line structure and maintenance. *J. Atmos. Sci.*, **47**, 1205-1222.

Smull, B. F., and R. A. Houze, Jr., 1985: A midlatitude squall line with a trailing region of stratiform rain: Radar and satellite observations. *Mon. Wea. Rev.*, **113**, 117-133.

____, and ____, 1987a: Dual-Doppler radar analysis of a midlatitude squall line with a trailing region of stratiform rain. *J. Atmos. Sci.*, **44**, 2128-2148.

____, and ____, 1987b: Rear inflow in squall lines with trailing stratiform precipitation. *Mon. Wea. Rev.*, **115**, 2869-2889.

Srivastava, R. C., T. J. Matejka and T. J. Lorello, 1986: Doppler radar study of the trailing anvil region associated with a squall line. *J. Atmos. Sci.*, **43**, 356-377.

Takeda, T., 1971: Numerical simulation of a precipitating convective cloud: The formation of a long-lasting cloud. *J. Atmos. Sci.*, **28**, 350-376.

Thorpe, A. J., M. J. Miller and M. W. Moncrieff, 1982: Two-dimensional convection in non-constant shear: A model of mid-latitude squall lines. *Quart. J. R. Met. Soc.*, **108**, 739-762.

Tremback, C. J., 1990: Numerical simulation of a mesoscale convective complex: Model development and numerical results. Ph.D. dissertation, Atmos. Sci. Paper No. 465, Colorado State University, Dept. of Atmospheric Science, Fort Collins, CO 80523.

____, and R. Kessler, 1985: A surface temperature and moisture parameterization for use in mesoscale numerical models. Preprints, 7th Conference on Numerical Weather Prediction, 17-20 June 1985, Montreal, Canada, AMS.

Trier, S. B., D. B. Parsons, and J. H. E. Clark, 1991: Environment and evolution of a cold-frontal Mesoscale Convective System. *Mon. Wea. Rev.*, **119**, 2429-2455.

Tripoli, G. J., and W. R. Cotton, 1982: The Colorado State University three-dimensional cloud/mesoscale model - 1982. Part I: General theoretical framework and sensitivity experiments. *J. de Rech. Atmos.*, **16**, 185-219.

____, and ____, 1989a: Numerical study of an observed orogenic mesoscale convective system. Part 1: Simulated genesis and comparison with observations. *Mon. Wea. Rev.*, **117**, 273-304.

____, and ____, 1989b: Numerical study of an observed orogenic mesoscale convective system. Part 2: Analysis of governing dynamics. *Mon. Wea. Rev.*, **117**, 305-328.

Uccellini, L. W., and D. R. Johnson, 1979: The coupling of upper and lower tropopspheric jet streaks and implications for the development of severe convective storms. *Mon. Wea. Rev.*, **107**, 682-703.

Wakimoto, R. M., 1982: The life cycle of thunderstorm gust fronts as viewed with Doppler radar and rawinsonde data. *Mon. Wea. Rev.*, **110**, 1060-1082.

Weisman, M. L., and J. B. Klemp, 1982: The dependence of numerically simulated convective storms on vertical wind shear and buoyancy. *Mon. Wea. Rev.*, **110**, 504-520.

Weissbluth, M. J., 1991: Convective parameterization in mesoscale models. Ph.D. Dissertation, Colorado State University, Dept. of Atmospheric Science, Fort Collins, CO 80523. 211 pp.

Wetzel, P. J., W. R. Cotton and R. L. McAnelly, 1983: A long-lived mesoscale convective complex. Part II: Evolution and structure of the mature complex. *Mon. Wea. Rev.*, **111**, 1919-1937.

Zhang, D.-L., K. Gao and D. P. Parsons, 1989: Numerical simulation of an intense squall line during 10-11 June 1985 PRE-STORM. Part I: Model verification. *Mon. Wea. Rev.*, **117**, 960-994.

Zipser, E. J., 1969: The role of organized unsaturated convective downdrafts in the structure and rapid decay of an equatorial disturbance. *J. Appl. Meteor.*, **8**, 799-814.

___, 1977: Mesoscale and convective-scale downdrafts as distinct components of squall-line structure. *Mon. Wea. Rev.*, **105**, 1568-1589.